BLACK HOLE ELECTROMAGNETIC OBSERVATIONS AS TESTS OF GENERAL RELATIVITY: QUADRATIC GRAVITY

by

Dimitry Ayzenberg

A dissertation submitted in partial fulfillment
of the requirements for the degree

of

Doctor of Philosophy

in

Physics

MONTANA STATE UNIVERSITY
Bozeman, Montana

April, 2017

DEDICATION

To my mom and dad, Anna and Gennady.

Dad, you passed away before I really got to know you, but I'd like to think your love of science, technology, and mystery – that you left behind in the form of an ample sci-fi novel collection – helped guide me to where I am today.

Mom, there is no one in my life who has guided and influenced me more than you. I know I don't thank you enough and there's no way I could thank you enough, but I hope this shows you how important you are to me. In particular, I want to thank you for always telling me to not compare myself to others. You may only have said it when I tried to get away with less than perfect grades, but it's become a principle I live by.

ACKNOWLEDGEMENTS

None of this would have been possible without my advisor, Nicolás Yunes, who imparted me with the knowledge necessary to succeed as a scientist, and he has my absolute gratitude. I would also like to thank Kent Yagi for always being willing to answer my questions, rudimentary and otherwise, and Neil Cornish for always keeping me on my toes and making sure I understood the most basic and fundamental aspects of a subject.

TABLE OF CONTENTS

TABLE OF CONTENTS – CONTINUED

TABLE OF CONTENTS – CONTINUED

LIST OF TABLES

LIST OF FIGURES

Figure Page

ABSTRACT

The recent detections of gravitational waves from merging black holes by advanced LIGO provide the first tests of General Relativity that probe the non-linear and dynamical nature of gravity. For General Relativity to be properly tested, though, many more observations are necessary. This lack of tests, coupled with several reasons General Relativity may not be the correct description of nature, motivates the study of modified theories of gravity. This dissertation presents the results of four studies on two well-motivated modified gravity theories in the class known as quadratic gravity: dynamical Chern-Simons gravity and Einstein-dilaton-Gauss-Bonnet gravity.

First, I study the stability of quadratic gravity to linear perturbations. If the theory shows instabilities, black holes may not be realized in Nature, and the theory would lack physical motivation. I perform a linear stability analysis, concentrating on dynamical Chern-Simons gravity and Einstein-dilaton-Gauss-Bonnet gravity, and find that these two theories are stable to linear perturbations far from the gravitational source.

Exact analytic solutions for rotating black holes in Einstein-dilaton-Gauss-Bonnet gravity are lacking, and most solutions are either numerical or approximate. I expand on previous work and find a new approximate rotating black hole solution to quadratic order in the spin angular momentum. The properties of this new solution are then studied.

Many modified gravity theories lack exact solutions for rotating black holes and the approximate nature of those solutions may introduce systematic error in any attempts to constrain those theories using black hole observations. I determine the systematic error introduced by using an approximate black hole solution in General Relativity in the context of continuum spectrum and black hole shadow observations. I find that for small enough values of the spin angular momentum, the systematic error introduced is negligible compared to current sources of observational error.

Finally, I study if it is possible to place better-than-current constraints on dynamical Chern-Simons gravity and Einstein-dilaton-Gauss-Bonnet gravity using black hole continuum spectrum observations. I find that while dynamical Chern-Simons gravity cannot be better constrained, with next generation telescopes it may be possible to place better constraints on Einstein-dilaton-Gauss-Bonnet gravity.

1

INTRODUCTION

"A hole is nothing, and if it is black we can't even see it. Ought we to get excited over an invisible nothing?

"Yes – if that black hole represents the most extreme state of matter possible, if it represents the possible end of the universe, if it represents the possible beginning of the universe, if it represents new physical laws and new methods for circumventing what had previously been considered absolute limitations."

–Isaac Asimov, *The Collapsing Universe: The Story of Black Holes* (1973)

1.1 Preamble

In 1784, well before Einstein's seminal 1915 paper *Die Feldgleichungen der Gravitation* (The Field Equations of Gravitation) [1], John Michell proposed the existence of what he called "dark stars": stars with a large enough gravitational pull to prevent light from escaping. During this time period light was believed to be made up of "corpuscles" (small particles) that had a finite velocity. If a star was massive enough to have an escape velocity larger than the velocity of light, no light would be able to escape from the surface of the star and it would appear dark. Michell suggested that these objects could in principle be observed through the motions of a companion star, if such a system existed. While the details underlying the idea are incorrect, it is undeniable that the general notion of Michell's dark stars are what we today term black holes (BH) and that Michell was indeed correct in how we might detect and study them.

The story of BHs in General Relativity (GR) begins soon after Einstein's noted paper, but Einstein's work is a necessary starting point. Einstein's theory of GR states that the three spatial dimensions and the time dimension form a "spacetime continuum" that is dynamically determined by distributions of energy (this of course includes rest-mass energy). Einstein described the interaction between energy and spacetime through a set of coupled non-linear partial differential equations that are now called the Einstein field equations. Within GR, gravity is an effect of spacetime being curved by energy and makes predictions that are different from Newtonian gravity. For example, in his original work Einstein showed that GR could explain the perihelion precession of Mercury, i.e. the rotation of an elliptical orbit such that the furthest point in the orbit is not in the same position on sequential orbits, which was a long-standing problem as it could not be explained with Newton's equations alone.

Just a few months after Einstein's paper, Karl Schwarzschild provided the first exact solution to the Einstein field equations, describing the gravitational field of a non-rotating spherical mass [2]. The properties of Schwarzschild's solution were studied in depth over the next few decades, in particular the two singularities that appear in the solutions: a point singularity at the origin and a surface singularity at what is now called the Schwarzschild radius. In 1924, work by Arthur Eddington showed the latter singularity was an unphysical coordinate singularity [3], although this fact wasn't recognized until 1933 by Georges Lemaître [4]. The identification of the Schwarzschild surface as an event horizon, a surface within which no causal influences can cross to the outside world, was done by David Finkelstein in 1958 [5]. In the following decade an explosion of progress in the study of these extreme objects occurred, which included Roy Kerr finding the exact solution for a rotating BH [6] and the actual coining of the term "black hole".

The first strong evidence for the existence of BHs came in 1971 with the discovery of Cygnus X-1 [7]. Today, there are over two dozen known and candidate stellar mass ($\sim 1- \sim 10^3$ solar masses) BHs [8] and it is commonly accepted that nearly every galaxy contains a supermassive ($\gtrsim 10^5$ solar masses) BH at its center [9]. Most stellar mass black holes are believed to be the remnants of the most massive stars after they have succumbed to gravitational collapse. The remaining stellar mass BHs likely originate from the gravitational collapse of neutron stars due to collision with or accretion from a companion, though some models also predict the formation of such black holes due to density perturbations of the medium in the early universe [10]. While the formation of supermassive BHs is still debated, it is commonly accepted that they grow through the accretion of matter and mergers with other BHs. Supermassive BHs are the most massive objects in the universe, some reaching masses on the order of 10^{10} solar masses, and are at the centers of active galactic nuclei, the most luminous persistent sources of electromagnetic radiation in the universe.

The extreme nature of BHs, as conveyed in the quote at the beginning of this chapter, makes them prime resources for understanding the fundamental physics of the universe. The study of BHs spans a large portion of the physics space, from the mathematical studies of the properties of BH solutions to the design and implementation of new telescopes and detectors, and from the search for a theory of quantum gravity to the modeling of orbits. As such, it is unreasonable to cover all aspects of BHs in this dissertation, or in any single body of work for that matter. With that in mind, the rest of this Introduction will focus on the aspects relevant to the work presented in subsequent chapters.

The remainder of this Introduction will briefly discuss the background necessary for understanding the later chapters. First, I summarize the different BH EM

observations and go into more detail on the observations studied in my work. The next section gives a very brief introduction to modified gravity theories and summarizes QG and why it is an interesting theory to study. Connecting the two prior areas of study, a brief summary of tests of GR is given, focusing on the tests relevant to this work. I close the Introduction with an overview of the remaining chapters.

1.2 Black Hole Electromagnetic Observations

Since BHs are electromagnetically invisible, EM observations attempt to indirectly study BHs through their influence on matter and radiation. Generally, this matter and radiation is in the form of an accretion disk and the radiation produced from the disk. Accretion disks are disk shaped structures of gas and dust commonly found in orbit around young stars, neutron stars, and black holes [11]. Angular momentum in the disk is transported outwards, through a mechanism that is still debated, leading to gas and dust accreting, or falling, onto the surface or through the event horizon of the massive central object. While the gas is still within the disk, gravitational and viscous forces heat the gas, which in turn radiates electromagnetically. During quiescent states, accretion disk radiation is dominated by the thermal component with contributions from inverse Compton scattering and possibly synchrotron emission [12]. These disks can also flare, which can alter the spectrum significantly for brief or long periods of time [13,14]. Much about accretion disks is still not understood, but they can in principle be used to observe and study BHs.

The formation of accretion disks around stellar mass BHs is fairly well understood. The majority of massive stars are found in binary systems [15]. Some of these systems evolve to become a binary containing a massive star and a BH. If the orbital separation of the system is small enough and the star is no more massive

than a few solar masses, the star can overflow its Roche lobe, the region around the star within which gas is gravitationally bound to the star. When the star overflows its Roche lobe gas will flow from the star towards the BH. For more massive stars the gas is transferred to the BH through the stellar wind of the star [16]. Through conservation of angular momentum the gas does not fall directly towards the BH and instead enters into an orbit around the BH. The orbiting gas builds up over time and eventually forms a structure large enough to be considered an accretion disk. This process is not static for binaries with a lower mass star, in fact turning on and off over time, as the star and the orbit will evolve over time. The evolution of the accretion disk formation process as well as the structure of the accretion disk itself is thought to lead to flaring activity and other variation in the electromagnetic emission in stellar mass black hole accretion disks [17, 18].

As all known supermassive BHs are at the centers of galaxies, there is a large source of dust and gas available for an accretion disk to form. Accretion disks around supermassive BHs can, in principle, be described with the same physics as those found around stellar mass BHs [11]. The significant differences in scale, though, lead to differences in how the accretion disk and BH can be studied. Accretion disks around supermassive BHs evolve on timescales longer than these objects have been observed due to the significant scale difference between stellar mass and supermassive BHs [16]. This means all current observations of supermassive BH accretion disks have only seen each disk in one stage of its evolution, which allows us to study each individual stage in much more detail than possible with stellar mass BH accretion disks. Some supermassive BH accretion disks can also be extremely luminous, e.g. active galactic nuclei are centers of galaxies that exceed the luminosity of the rest of the galaxy in at least some portion of the EM spectrum and are thought to result from the interaction of the central supermassive BH and the accretion disk around it [19]. The higher

luminosity allows one to observe structure in accretion disks not easily seen in those around stellar mass black holes, such as coronae, electron clouds that enshroud the disk and are much hotter than the rest of the accretion disk [16].

Before moving on to the BH EM observations themselves, it is important to understand the processes behind which the gas in accretion disks is heated and radiates electromagnetically. Gas particles within the disk on average follow approximately Keplerian orbits around the BH. This means that particles at smaller radii have larger angular velocities, and the disk can be thought of as radial layers of rotating rings that have increasing angular velocity as radius decreases. Any system with material moving at different angular velocities at different radii is said to have *differential rotation*. Due to the thermal and turbulent motion of the particles there is interaction between these differentially rotating layers, which in turn leads to viscous torques between the layers. This viscous torque transfers angular momentum outwards, but also heats up the inner layers [20]. The thermal radiation from the hot gas dominates the radiation from an accretion disk during quiescent states, but there are contributions from Compton scattering and possibly synchrotron emission, if the disk has a significant magnetic field [12]. If the disk has a hot corona, there may also be spectral lines in the emission caused by reflection of photons from the corona off of the colder, non-ionized parts of the disk [16].

There are a number of different BH EM observations, some better understood than others (see [16] for a review). The BH continuum spectrum is simply the thermal spectrum produced by an accretion disk around a BH. The Kα iron line is the most prominent line seen in BH accretion disks and is produced when a hot corona illuminates the colder accretion disk. Quasi-periodic oscillations are commonly found in the flux of stellar mass BHs, but there is no consensus on the mechanism behind these oscillations. Similarly, the mechanism behind BH jets is not completely

understood, but the more popular models have the spin angular momentum of the BH playing an important role. The BH shadow is a dark region on an image of an illuminated BH caused by the fact that any light entering the event horizon of a BH cannot escape. The shadow, more so than any other BH EM observation, is the least influenced by the properties of the accretion disk and is almost solely dependent on the properties of the BH.

This work focuses on continuum spectrum observations and black hole shadow observations as these are the best understood and the least contaminated by the properties of the accretion disk. The continuum spectrum is dominated by the innermost part of the accretion disk, as this is the region that is hottest and, in turn, most luminous. There is a fair amount of evidence that the innermost part of the disk can be reasonably approximated to be the innermost stable circular orbit (ISCO) of the BH [16, 21–26], which is only dependent on the properties of the BH. Even with this evidence there is still a fair amount of uncertainty in the correct accretion disk model [27]. Of prime importance for the continuum spectrum is the uncertainty in the location of the innermost radius of the disk. Some accretion disk models, simulations, and observations have an inner radius that is not at the ISCO [28–32]. If the inner edge is not at the ISCO, the location of the inner edge becomes an extra parameter in the continuum spectrum observation that will be degenerate with the properties of the BH. This degeneracy is currently treated as a systematic error in BH parameter extraction from continuum spectrum observations, although the magnitude of the error is not well known [8]. The BH shadow, ideally, is an observation that depends purely on the properties of the BH. In reality, a shadow observation can be imperfect and/or obscured due to the accretion disk. This issue can be dealt with through image reconstruction techniques or by removing the regions of the BH shadow image that are obscured by the disk [33].

Black hole continuum spectrum observations up to this point in time have been primarily used to determine the spin angular momentum of stellar mass BHs. The peak of the thermal spectrum is determined by the ISCO radius, and since the ISCO depends on the mass and spin of the BH so does the spectrum peak. For example, a smaller mass BH has a smaller ISCO radius and particles orbiting near the ISCO radius will have a higher temperature due to viscous heating. For stellar mass BHs this peak is in the soft X-Ray band at around 2-3 keV, while supermassive BHs, since they are much more massive and have a wider range of masses, peak roughly within an order of magnitude or two of the optical band ($\sim$1 eV) [16]. Continuum spectrum observations are very difficult in the case of supermassive BHs because gas and dust more readily scatters and absorbs light in and around the optical band than light in the X-Ray band. Thus, most work with the BH continuum spectrum focuses on stellar mass BHs.

Continuum spectrum observations of stellar mass BHs are made using X-Ray telescopes such as the Rossi X-Ray Timing Explorer, the Chandra X-Ray Observatory, XMM-Newton, and NuSTAR. With these observations the spins of roughly 10 BHs have been estimated to date [8, 16]. To make these estimates the observed spectra, usually composed of on the order of 10 data points across the relevant frequency range, are fit with continuum spectrum models. The continuum spectrum depends on the BH mass and spin as well as the inclination angle, i.e. the angle between the line of sight and the spin angular momentum of the BH with the assumption that the angular momentum of the accretion disk is in the same direction or opposite to that of the BH. In fitting the data there is some degeneracy between these parameters, but the BH mass and inclination angle can be determined through observations and modeling of the orbit of the binary. The remaining uncertainty in the estimated spins comes from observational error, i.e. statistical error (e.g. finite accuracy of telescopes),

instrumental error (e.g. inaccuracies in calibration of telescopes), and environmental error (e.g. scattering and absorption by gas and dust), and systematic error due to the lack of knowledge of the correct model for the accretion disks. Using next generation telescopes, such as eXTP [34] and a Hitomi successor [35], the observational error is expected to improve by at least an order of magnitude. With this improvement and better accretion disk models, it may be possible to use continuum spectrum observations to not only determine the properties of many more BHs much more accurately, but to also test GR and place constraints on modified gravity theories.

While the continuum spectrum observation is more suited for studying stellar mass BHs, observations of the BH shadow are more suited for studying supermassive BHs. This is due to the size of the shadow, which is only slightly larger than the size of the BH event horizon. The radius of the event horizon of a stellar mass BH is on the order of 10 km, while for a supermassive BH the event horizon can have a radius ranging from 10^5 to 10^{10} km. The closest stellar mass BH known is V616 Monocerotis [36] at a distance of about 3000 light-years away. Observing the shadow of V616 Mono is equivalent to observing a single bacteria cell on the moon. On the other hand, the closest supermassive BH is Sagittarius A*, the supermassive BH at the center of our galaxy, at a distance of about 26,000 light-years and a mass of about 4×10^6 solar masses [37]. Observing its shadow would be like observing a grapefruit on the moon, and while this feat is still a difficult undertaking it is certainly much more attainable than attempting to observe the shadows of stellar mass BHs. Two other prime candidates for BH shadow observations are the supermassive BHs at the centers of the galaxies M87 [38] and NGC 1600 [39]. Both of these BHs are more distant than Sagittarius A*, but their masses are proportionately larger, making their shadows roughly as difficult to observe.

The first observations of a BH shadow are expected to come out of the 2017 observing run of The Event Horizon Telescope (EHT) [40]. EHT is a worldwide collaboration that includes ten different telescopes around the world using the very-long-baseline interferometry (VLBI) observation method to achieve an observing resolution of about 10 μas or smaller (roughly equivalent to a golf ball on the moon). The telescopes that form the collaboration are radio telescopes that observe in the millimeter and submillimeter wavelengths. Most of the telescopes are large single aperture telescopes (10 m in diameter or more), such as the Large Millimetre Telescope (LMT), but a few are arrays of equivalent or smaller telescopes, such as the Atacama Large Millimeter/submillimeter Array (ALMA). EHT currently makes observations at the 1.3 mm wavelength, which reduces scattering by gas and dust and allows for the high angular resolution. VLBI is an interferometry method commonly used in radio astronomy that allows for telescopes at locations around the world to be treated as a single large telescope with a diameter equal to the maximum separation between the individual telescopes [41]. EHT has been making observations for close to a decade, but the observing run this year, after upgrades made to several of the telescopes and more telescopes joining the collaboration, has reached a resolution high enough to produce an image of the shadow. The primary observing targets are Sagittarius A* and the M87 supermassive BH. With observations of the shadow of these BHs, EHT should be able to determine their properties and possibly test GR as well.

1.3 Modified Gravity Theories

Einstein's theory of General Relativity has stood up to scrutiny for over a century, so one may reasonably ask why so much time and effort is spent on studying possible modifications to GR or even completely new theories of gravity. The primary reason for such studies is that there is no reason to prefer GR over other theories

that also reproduce current observations [42]. All theories of gravity answer two questions: "How does matter move in the presence of a gravitational field?" and "How is the gravitational field generated in the presence of matter?". In Newtonian dynamics, the first question is answered by Newton's Second Law and the second question is answered by Poisson's equation. In GR, the former is answered through the equivalence principle, which, simply stated, is the principle that one cannot tell the difference between a reference frame at rest and one freely-falling in a gravitational field. The equivalence principle encodes Lorentz invariance as well as the generally accepted belief that there is no preferred position or reference frame in the universe. The equivalence principle is discussed in more detail later on in this section. The latter question is answered in GR through Einstein's field equations. While Einstein's field equations are an elegant solution to the problem of gravity, there is no fundamental reason why they should be preferred over any other set of equations that describe gravity.

A second compelling reason for studying other theories of gravity is that we know GR breaks down in the limit of very strong gravitational fields [42]. GR is a classical theory, in that it does not incorporate the fundamental principles of quantum mechanics, and when treated as a complete theory it leads to predictions of singularities in two important scenarios. In the first, gravitational collapse of gas and dust, as seen at the end of the lives of massive stars when the fusion processes in the cores can no longer produce enough energy to counteract gravitational forces, ends in the formation of a black hole with a singularity at its center [43]. In the second scenario, the Friedmann equations [44], which describe a homogenous and isotropic universe in the context of GR, when evolved backwards in time lead to a singularity at the beginning of time, known as the Big Bang. These singularities are unphysical, and since they occur in scenarios that are of prime importance for understanding

the universe, they are the central focus of many studies in GR and other theories of gravity. Many modified gravity theories are motivated by attempts to resolve these issues, as well as other open questions in physics (e.g. the nature of dark energy and dark matter), or are approximations of more fundamental theories, such as string theory [45, 46].

Since modified gravity theories are developed for a wide range of reasons, one can expect there to be a wide range of modified gravity theories. In general, these theories can be categorized by which fundamental aspects of GR they violate [47]. For example, in variable G theories Newton's gravitational constant is promoted to a function of the spacetime [48]. This in turn means the laws of gravity are dependent on spacetime position, which violates the equivalence principle. There are a number of variable G theories and, in fact, the earliest attempts at modifying GR involved a modification of the gravitational constant [49]. Another class of theories that is well studied are massive graviton theories, i.e. theories that predict a massive force carrier for gravity as opposed to a massless one as assumed in GR [50]. Since gravitons are massive in these theories the gravitational interaction would propagate at smaller than light speed. This implies that in massive graviton theories there would be a delay (possibly detectable) between EM and gravitational signals that are emitted simultaneously at some source. There are many more theories that modify GR and each of them are interesting in their own right, but they are far too numerous to discuss in detail within this dissertation.

In this work I will focus on a particular class of modified gravity theories called quadratic gravity, and more specifically two theories within the class: dynamical Chern-Simons (dCS) gravity and Einstein-dilaton-Gauss-Bonnet (EdGB) gravity. Quadratic gravity theories modify GR by introducing a dynamical scalar field that couples to curvature squared terms. DCS gravity and EdGB gravity, in particular,

introduce a scalar field that couples to a curvature invariant, i.e. a scalar that is a measure of the curvature of spacetime and does not depend on the choice of coordinates. The invariants in dCS gravity and EdGB gravity are also topological invariants, i.e. they do not change under homeomorphisms, transformations that preserve the topological properties of a manifold (a space that locally resembles Euclidean space), such as whether the boundary conditions of the manifold are periodic or the number of holes in the manifold. The scalar field in dCS gravity couples to the Pontryagin invariant, while in EdGB gravity the scalar field couples to the Gauss-Bonnet invariant. The Pontryagin invariant is related to the first Pontryagin number and the Gauss-Bonnet invariant is related to the Euler characteristic [51], where the former is a way to describe how a manifold loops back on itself and the latter is a way to describe the shape and structure of a manifold. The motivation for such modifications to GR comes from similar terms that appear in low-energy expansions of more fundamental theories such as string theory [52,53], theories of inflation [54], and loop quantum gravity [55, 56]. Since QG comes from low-energy expansions it must be treated as an *effective field theory*, i.e. only valid up to some cut-off energy [57,58]. If not treated as effective, instabilities will be generated dynamically [59], rendering the theory ill-posed.

EdGB gravity and dCS gravity both violate the strong equivalence principle (SEP) *spontaneously* [48], i.e. the violation appears in the solutions of the theories and not at the level of the action describing the theories. The equivalence principle, described in simple terms at the beginning of this section, comes in three forms with an increasing strength in the claims made. The weak equivalence principle (WEP), also known as the Galilean equivalence principle, states that the mass of an object is proportional to its weight. Another way to state the WEP is that the trajectory of a freely falling *test* body, i.e. one not influenced by other forces and small enough to

not be affected by tidal gravitational forces (caused by varying gravitational forces across a body), is independent of the internal structure and composition of the body. The Einstein equivalence principle (EEP) combines the WEP and the statement that within a freely falling laboratory any *local* (i.e. not dependent on or influenced by anything external to the laboratory and small enough to not be affected by tidal forces) non-gravitational experiment is independent of the velocity (local Lorentz invariance (LLI)) and position (local position invariance (LPI)) of the laboratory. The EEP is the equivalence principle referred to at the beginning of this section and is central to modern gravitational theory, since one can make a strong argument that gravity is caused by curved spacetime if the EEP is valid (see [60] for a discussion on the subject). Both the WEP and the EEP are fairly well tested on scales present in the solar system [60], the WEP more so as tests of local velocity and position invariance are more difficult.

The SEP extends the claims of the WEP and the EEP. Under the SEP, the WEP applies to both test bodies and self-gravitating bodies, i.e. bodies that are held together by internal gravitational forces rather than any other internal forces. The SEP further adds to the EEP by also applying LLI and LPI to gravitational experiments. Since the SEP distinguishes itself from the WEP and the EEP by including self-gravitating bodies and gravitational experiments it becomes sequentially more difficult to test. This difficulty arises because it is more difficult to perform experiments on self-gravitating bodies (like the moon) than on small test bodies and gravitational experiments require high precision instruments due to the small relative strength of gravity as compared to the EM and nuclear forces. With that difficulty in mind, tests on the solar system scale have been performed [60], as well as some tests in regimes of higher gravitational field and spacetime curvature than found in the solar system [47, 61–64].

In EdGB gravity and dCS gravity, self-gravitating bodies, such as neutron stars and BHs, induce a scalar field that depends on the composition and internal structure of the bodies (in dCS gravity these bodies must be rotating to induce a scalar field). Test bodies will, in principle, also induce a scalar field, but the scalar field will be negligible because the gravitational curvature created by the test body, which sources the scalar field, will be very small. In a system with at least two self-gravitating bodies in orbit the scalar fields of the bodies will interact, in a similar manner to the magnetic dipole-dipole interaction [65,66]. From this interaction arises a scalar force, which influences the motion of bodies. Thus, in EdGb gravity and dCS gravity, the composition and internal structure of freely falling self-gravitating bodies (through the induced scalar field) affect the motion of the bodies, in turn violating the SEP.

As well as violating the SEP, dCS gravity spontaneously violates parity invariance. Parity invariance can be thought of as a lack of preference for a right-handed or left-handed coordinate system, i.e. physics is the same regardless of which coordinate system is used. A theory that obeys parity invariance is said to have even-parity, while one that does not has odd-parity. The odd-parity structure of dCS gravity means that any modifications arise only if there is a directional preference, e.g. Schwarzschild is a solution in dCS gravity as it is spherically symmetric, but the Kerr BH metric is not as it is axially symmetric with a preferred direction in the form of the spin angular momentum. Parity invariance in gravity is very difficult to test as it requires a system that causes a gravitational effect with a directional preference that is of comparable strength with the even-parity gravitational effects of the system. Spinning BHs, particularly rapidly spinning BHs, are well suited for these tests as the gravitational effects of the spin are in principle observable near the BH [16, 42].

1.4 Tests of General Relativity

In some sense, tests of GR have been going on since the famous observation of gravitational light deflection by Arthur Eddington in the 1919 solar eclipse. Since then the motivation behind tests of GR has not changed: to determine whether GR is the correct description for gravity. The focus of these tests, though, has shifted from observations on gravitational curvature and strength scales common in the solar system to scales common near compact objects, like neutron stars and BHs. Tests within the solar system and using observations of widely separated neutron stars have consistently reconfirmed that GR is correct on those scales, but tests on scales near extreme objects have only begun very recently. The first tests in the *extreme gravity* regime, i.e. the regime where the non-linear and dynamical nature of gravity becomes important, were provided by advanced LIGO (aLIGO) [47, 67]. On two separate occasions in 2016, the LIGO Scientific Collaboration and Virgo Collaboration announced the detection of gravitational waves, i.e. oscillations in the curvature of spacetime, produced by binary black hole mergers [68, 69]. Over the next decade or so, aLIGO will be joined by other gravitational wave detectors, such as advanced VIRGO [70], KAGRA [71] and pulsar timing arrays [72], as well as EM detectors that observe neutron stars and BHs, such as NICER [73] and EHT [40]. All of these devices will help test General Relativity in a regime of gravity that has just begun to be explored.

There are a number of different types of modified gravity theories with a plethora of modifications and violations of GR, so one expects there to be a proportionate amount of possible tests of GR [42, 60]. Observations of the orbital evolution of binary pulsars probe the effect of gravity on the orbital dynamics of compact objects, and have already been used to test GR [74]. Gravitational wave signals are modified

in different ways depending on the type of departure from GR [75]. As discussed previously, EM radiation originating from accretion disks near BHs is influenced by the properties of the BH. If these properties include an effect due to a modified gravity theory, that is something that can in principle be measured. Some modified theories of gravity can alter the evolution of the early universe [76], which may be observable in the cosmic microwave background, i.e. the oldest EM radiation from when the universe first became transparent to light, and in the structure of the universe today.

As both the BH continuum spectrum and BH shadow are strongly dependent on the spacetime describing the BH, they make for excellent observations to use for testing GR. As discussed previously, the continuum spectrum is dominated by the location of the ISCO, which is dependent on the properties of the BH. Modified gravity theories can also alter the location of the ISCO from that expected in GR and, in turn, change the observed spectrum [42]. Modifications to GR can also have an effect on the redshift of light caused by the BH, which will also have an impact on the spectrum. In GR, BH shadows have a shape that is determined by the spin of the BH and the inclination angle (BH mass simply scales the size of the shadow). A modified gravity theory can modify the shape of the BH shadow if BHs in the theory are not described with the Kerr metric. With observations at high enough resolutions, the shape of the shadow can be measured and used to test GR and constrain modified gravity theories [16].

As with all tests of GR, and all observations in general, some complications arise in placing constraints on modified theories of gravity due to sources of error in the continuum spectrum and BH shadow observations. Accretion disks are still not well understood, and while the continuum spectrum observation is strongly dependent on the properties of the BH, there is still some influence from the properties of the disk. Systematic error is introduced due to our imperfect knowledge of the correct model

for accretion disks, which limits the ability of using the continuum spectrum to test GR. The BH shadow is ideally free of any influence from the disk, but in reality the variability of the disk can muddy the image of the shadow. Flaring structures and non-uniformity in luminosity of the disk can distort the shape of the shadow and limit its usefulness in studying the BH. Techniques have been developed and will be used to combat these issues [77], but their effectiveness waits to be seen.

1.5 Summary of This Work

Prior to studying a theory in the context of testing GR with BH EM observations it is important to show that BH solutions within the theory are stable to perturbations, otherwise they would not be realized in Nature. Until 2013, linear perturbation analyses had only been carried out in dCS gravity in the context of gravitational waves [78, 79] and Schwarzschild BHs [80–83]. The study performed in Chapter 2 expands on this previous work by performing a linear stability analysis of QG of all perturbation modes on generic backgrounds, concentrating on dCS gravity and EdGB gravity. In particular, the results show that non-rotating and rotating BH solutions in these theories are stable to linear perturbations far from the BH.

In the universe there is a tendency for objects to rotate, which is a consequence of nothing in the universe being perfectly spherically symmetric. This is no less true for BHs and one expects BHs to have some spin angular momentum. Thus, to study BHs it is necessary to have a metric that includes spin. In GR, the solution for an axially symmetric, rotating BH is known as the Kerr metric, as opposed to the spherically symmetric Schwarzschild metric. In QG theories it is not obvious how to find exact analytic solutions, and so most BH solutions that have been found to this point are either numerical or approximate. The approximate nature of the latter solutions is two-fold: a small-coupling approximation, as these theories must

be treated as *effective*, and a slow-rotation approximation, which is only necessary in practice to be able to attain a solution. Due to its parity-violating nature, dCS gravity has the Schwarzschild BH as a solution [84], while EdGB gravity does not and instead has a modified solution found in [85]. BH solutions to linear-order-in-spin were found for dCS gravity and EdGB gravity in [86] and a quadratic-order-in-spin solution was found for dCS gravity in [57]. Chapter 3 uses the same method outlined in [57] to find a quadratic-order-in-spin solution in EdGB gravity and studies the properties of the new solution.

When beginning work on testing GR with the continuum spectrum and BH shadow, the question arose of how to deal with the approximate nature of the BH solutions in dCS gravity and EdGB gravity. One has to ask whether the approximate solutions would introduce systematic uncertainty in any attempts to place constraints on these theories. In an attempt to answer this, Chapter 4 presents a study on the uncertainty introduced in extracting physical parameters from EM observations when using an approximate BH solution in GR. The results, while only applicable to approximate solutions in GR or any theory that has the Kerr solution, does suggest that approximate solutions in modified theories of gravity do not introduce significant systematic error.

The penultimate work of this dissertation is presented in Chapter 5, and aims to determine whether or not it is possible to use BH continuum spectrum observations to place constraints on dCS gravity and EdGB gravity and test GR. The continuum spectrum is calculated for rotating BHs in dCS gravity and EdGB gravity, and compared against the spectrum for a Kerr BH in GR. The results show that while current X-Ray telescopes do not have the sensitivity to place better-than-current constraints on either theory, next generation telescopes may be able to place better constraints on EdGB gravity using continuum spectrum observations of BHs at masses

smaller than about 8 solar masses. Better constraints cannot be placed on dCS gravity, even with next generation telescopes, primarily because the non-rotating part of the BH solution is not modified from GR.

In the Conclusion, I will summarize the results detailed throughout this dissertation, discuss the implications of said results, and point to possible future avenues of research.

Throughout, the following conventions are used: the metric signature $(-,+,+,+)$ is used; Latin letters in index lists stand for spacetime indices; parenthesis and brackets in index lists stand for symmetrization and antisymmetrization, respectively, i.e. $A_{(ab)} = (A_{ab} + A_{ba})/2$ and $A_{[ab]} = (A_{ab} - A_{ba})/2$; we use geometric units with $G = c = 1$ (e.g. $1M_\odot$ becomes 1.477 km by multiplying by G/c^2 or 4.93×10^{-6} s by multiplying by G/c^3), except where otherwise noted. Note that the notation and formatting of the original published/submitted works has been slightly modified in an attempt to remain consistent throughout this dissertation.

LINEAR STABILITY ANALYSIS OF DYNAMICAL QUADRATIC GRAVITY

Contribution of Authors and Co-Authors

Manuscript in Chapter 2

Author: Dimitry Ayzenberg

Contributions: Implemented the study design. Wrote first draft of the manuscript.

Co-Author: Dr. Kent Yagi

Contributions: Helped conceive the study design. Provided feedback of analysis and comments on drafts of the manuscript.

Co-Author: Dr. Nicolás Yunes

Contributions: Conceived the study design. Provided feedback of analysis and comments on drafts of the manuscript.

Manuscript Information Page

Dimitry Ayzenberg, Kent Yagi, Nicolás Yunes

Physical Review D

Status of Manuscript:

___Prepared for submission to a peer-reviewed journal

___Officially submitted to a peer-reviewed journal

___Accepted by a peer-reviewed journal

_x_Published in a peer-reviewed journal

Published by the American Physical Society

Published February, 2014, Phys. Rev. D 89, 044023

Abstract

We study the linear stability of dynamical, quadratic gravity, focusing on two particular subclasses (the even parity sector, exemplified by Einstein-dilaton-Gauss-Bonnet gravity, and the odd parity sector, exemplified by dynamical Chern-Simons gravity) in the high-frequency, geometric optics approximation. This analysis is carried out by studying gravitational and scalar modes propagating on spherically-symmetric and axially-symmetric, vacuum solutions of the theory and finding the associated dispersion relations. These relations are solved in two separate cases (the scalar regime and the gravitational wave regime, defined by requiring the ratio of the amplitude of the perturbations to be much greater or smaller than unity) and found in both cases to not lead to exponential growth of the propagating modes, suggesting linearly stability. The modes are found to propagate at subluminal and superluminal speeds, depending on the propagating modes' direction relative to the background geometry, just as in dynamical Chern-Simons gravity.

2.1 Introduction

Ever since its conception in 1915, Einstein's theory of General Relativity (GR) has held up to numerous experimental tests stretching across a wide range of areas. These tests include Solar System observations, such as the perihelion precession of Mercury, as well as binary pulsar observations, such as the orbit period decay of the Hulse-Taylor pulsar [60, 87]. In the next couple of decades, these tests and observations will be extended by data from next-generation gravitational wave (GW) detectors [75,81,88–106] (for a recent review of GR tests with ground-based detectors, see [45]). These observations will extend into the *strong-field* regime of gravity, where the gravitational field is non-linear and dynamical, precisely where tests are currently lacking.

Strong-field tests of gravity have implications to a large range of areas in physics and astrophysics. For example, modified gravity theories that attempt to quantize gravity usually break gravitational parity invariance [52, 53, 55, 56]. Gravitational

parity breaking modifies the geometry of spinning black holes (BHs) [57, 107] and the propagation of GWs in these backgrounds [79, 92, 94, 100, 106]. Constraining such a departure from the Kerr geometry of GR in the strong-field regime will place constraints on the coupling constants of such theories. These constraints are expected to be orders of magnitude stronger than those one can achieve with Solar System observations.

A recently studied class of modified theories is quadratic gravity (QG) [85]. This class departs from GR by adding a dynamical field coupled to all possible curvature squared terms to the Einstein-Hilbert action. The motivation for these modifications comes from similar terms appearing in string theory in a low-energy expansion after compactifying to four-dimensions [52, 53], effective field theories of inflation [54], and loop quantum gravity coupled to fermions [55, 56]. Since QG derives as a low-energy expansion of more fundamental theories, it should be viewed as an *effective field theory*, valid up to a cut-off energy scale above which cubic and higher-order curvature invariants cannot be neglected [57,58]. If one does not treat the theory as effective and exceeds the cutoff, ghosts and other instabilities will be non-linearly generated [59], rendering the theory ill-posed.

Two of the more popular QG theories are dynamical Chern-Simons (dCS) gravity [108] and Einstein-dilaton-Gauss-Bonnet (EdGB) gravity. In the former, the field couples to the Pontryagin invariant, while in the later it couples to the Gauss-Bonnet invariant. Because of this, dCS gravity is a parity-violating theory, and thus, non-spinning BHs are not modified because they are parity-even. Spinning BHs, of course, are not parity-even and do acquire corrections [57, 107, 109]. BHs in generic QG are different from those in GR already at the non-spinning level [85], and of course also at the spinning level [86].

For these QG theories to be physically appealing, the BH solutions described above must be stable to perturbations. An instability would imply that BHs generated in gravitational collapse would actually not be realized in Nature, if the instability timescale is short enough. QG is obviously linearly stable on a flat background, as higher-order derivatives only arise due to the excitation of the scalar field, which is in turn sourced by the Riemann tensor. A more meaningful test is the study of linear perturbations about solutions to QG that have non-trivial curvature. Such a test was performed on dCS gravity on a Schwarzschild background in [80–83]. Similar studies were carried out in the context of gravitational radiation in [78, 79], but a systematic study of all perturbation modes on generic backgrounds was lacking until now.

In this paper, following the classic work of Isaacson's [110], we perform a linear stability analysis on QG in the high-frequency, geometric optics approximation. We concentrate on two particular subclasses of this theory: the even parity sector, exemplified by EdGB gravity, and the odd parity sector, exemplified by dCS gravity. We use the high-frequency, geometric optics approximation because to study how perturbative modes or waves propagate on a given background spacetime, the wavelength of the modes has to be much shorter than the curvature length of the background. If this is not the case, the separation of background and wave is ill-defined [110]. This approximation is sometimes called WKB and is in fact used in many fields, including electromagnetism, quantum mechanics, plasma physics and hydrodynamics.

We here derive general dispersion relations valid for an arbitrary background in modified quadratic gravity, focusing on the even and odd parity sectors. We evaluate these relations on non-spinning [85] and spinning [86] BH backgrounds that are solutions in these theories. In the odd parity case, we extend the results of [82] by considering spinning BH backgrounds. We consider two particular perturbative

regimes: a scalar-dominated and a GW-dominated regime, depending on whether the amplitude of the scalar perturbation is much larger or smaller than the amplitude of the GW perturbation. Our results show that these QG theories are linearly stable in both regimes and for both spherically symmetric and axially symmetric backgrounds in the far field (at distances much farther than the GW wavelength). The speed of coupled gravitational/scalar modes, in the regime where the scalar field perturbation dominates the metric perturbation, is different from that of light, subluminal and superluminal modes, just as in dCS gravity. We argue that this is a generic feature of these theories.

The remainder of this paper presents the mathematical details that back up these results. Section 2.2 gives a brief summary of QG, including the modified field equations. Section 2.3 outlines the linear stability analysis that is performed and computes the perturbed field equations. Section 2.4 finds the dispersion relations needed to analyze the stability of waves within QG and outlines how we study these dispersion relations for a set of examples. Section 2.5 studies the solution of the dispersion relations for non-spinning [85] and spinning [86] BH spacetimes. Section 2.6 concludes by summarizing the results, discussing the implications of said results, and pointing to future possible research.

We will here use the following conventions: we use the metric signature $(-,+,+,+)$; Latin letters in index lists stand for spacetime indices; parenthesis and brackets in index lists stand for symmetrization and antisymmetrization, respectively, i.e. $A_{(ab)} = (A_{ab} + A_{ba})/2$ and $A_{[ab]} = (A_{ab} - A_{ba})/2$; we use geometric units with $G = c = 1$.

2.2 Quadratic Gravity

QG can be described by an action containing all possible quadratic, algebraic curvature scalars with running (i.e. non-constant) couplings [85]

$$S \equiv \int d^4x\sqrt{-g}\left\{\kappa R + \alpha_1 f_1(\vartheta)R^2 + \alpha_2 f_2(\vartheta)R_{ab}R^{ab} + \alpha_3 f_3(\vartheta)R_{abcd}R^{abcd} \right.$$
$$\left. +\alpha_4 f_4(\vartheta)R_{abcd}{}^*R^{abcd} - \frac{\beta}{2}\left[\nabla_a\vartheta\nabla^a\vartheta + 2V(\vartheta)\right] + \mathcal{L}_{\rm mat}\right\}. \tag{2.1}$$

Here, g stands for the determinant of the metric g_{ab}. R, R_{ab}, R_{abcd}, and ${}^*R_{abcd}$ are the Ricci scalar, Ricci tensor, and the Riemann tensor and its dual, respectively, with the latter defined as

$${}^*R^a{}_{bcd} = \frac{1}{2}\varepsilon_{cd}{}^{ef}R^a{}_{bef}\,, \tag{2.2}$$

and ε^{abcd} the Levi-Civita tensor. The quantity $\mathcal{L}_{\rm mat}$ is the external matter Lagrangian, ϑ is a field, $f_i(\vartheta)$ are functionals of this field, (α_i, β) are coupling constants, and $\kappa = 1/(16\pi)$. We assume that all quadratic terms are coupled to the same field. All other quadratic curvature terms are linearly dependent, such as the Weyl tensor squared. Terms proportional to derivatives of the curvature can be integrated by parts to obtain the action shown above.

QG contains some well-studied specific theories. For example, $(\alpha_1, \alpha_2, \alpha_3, \alpha_4) = (\alpha_{\rm EdGB}, -4\alpha_{\rm EdGB}, \alpha_{\rm EdGB}, 0)$ and $(f_1, f_2, f_3, f_4) = (e^\vartheta, e^\vartheta, e^\vartheta, 0)$ correspond to EdGB gravity, where $\alpha_{\rm EdGB}$ is the EdGB coupling constant and ϑ is the dilaton. Another example is $(\alpha_1, \alpha_2, \alpha_3, \alpha_4) = (0, 0, 0, \alpha_{\rm dCS}/4)$ and $(f_1, f_2, f_3, f_4) = (0, 0, 0, \vartheta)$, which corresponds to dCS gravity, where $\alpha_{\rm dCS}$ is the dCS coupling parameter and ϑ is the dCS (axion-like) field. EdGB gravity is constrained most strongly by low-mass X-ray binary observations, $\sqrt{|\alpha_{\rm EdGB}|} < 1.9 \times 10^5$cm [111], which is six orders of magnitude stronger than Solar System bounds [112]. The proposed bound on EdGB with future

GW observations is discussed in [79, 111], where the authors show that space-borne GW interferometers, such as eLISA [113] and DECIGO [114], should be able to place stronger constraint than the bound mentioned above. On the other hand, dCS theory is most strongly constrained from Solar System [115] and table-top experiments [57], $\sqrt{|\alpha_{\rm dCS}|} < 10^{13}$ cm, while again future GW observations will allow much stronger constraints [106].

In dynamical QG $f_i(\vartheta)$ is some function of the dynamical scalar field ϑ, with potential $V(\vartheta)$. We assume ϑ is at the minimum of the potential and thus Taylor expand $f_i(\vartheta) = f_i(0) + f_i'(0)\vartheta + \mathcal{O}(\vartheta^2)$ about small perturbations from the minimum (assumed here to be at zero), where $f_i(0)$ and $f_i'(0)$ are constants. The ϑ-independent terms, proportional to $f_i(0)$, lead to a theory with a minimally coupled field, where the latter does not interact with the curvature invariants. In the dCS and the EdGB cases, these invariants are topological, and the $f_i(0)$ terms do not modify the field equations. Since we will here concentrate on these theories, the $f_i(0)$ are irrelevant and will be neglected. Instead, we concentrate on on the $f_i'(0)$ terms, which can be modeled by letting $f_i(\vartheta) = c_i\vartheta$. Reabsorbing the constants $c_i = f_i'(0)$ into α_i, such that $\alpha_i f_i(\vartheta) \to \alpha_i\vartheta$, the field equations are then [79, 85]

$$G_{ab} + \frac{\alpha_1}{\kappa}\mathcal{H}^{(\vartheta)}_{ab} + \frac{\alpha_2}{\kappa}\mathcal{I}^{(\vartheta)}_{ab} + \frac{\alpha_3}{\kappa}\mathcal{J}^{(\vartheta)}_{ab} + \frac{\alpha_4}{\kappa}\mathcal{K}^{(\vartheta)}_{ab} = \frac{1}{2\kappa}\left(T^{\rm mat}_{ab} + T^{(\vartheta)}_{ab}\right), \tag{2.3}$$

where

$$T^{(\vartheta)}_{ab} = \beta\left[\nabla_a\vartheta\nabla_b\vartheta - \frac{1}{2}g_{ab}\left(\nabla_c\vartheta\nabla^c\vartheta - 2V(\vartheta)\right)\right] \tag{2.4}$$

is the scalar field stress-energy tensor and

$$\begin{aligned}\mathcal{H}^{(\vartheta)}_{ab} \equiv & -4\nabla_{(a}\vartheta\nabla_{b)}R - 2R\nabla_{(a}\nabla_{b)}\vartheta + g_{ab}\left(2R\nabla^c\nabla_c\vartheta + 4\nabla^c\vartheta\nabla_c R\right) \\ & + \vartheta\left[2R_{ab}R - 2\nabla_a\nabla_b R - \frac{1}{2}g_{ab}\left(R^2 - 4\Box R\right)\right],\end{aligned} \tag{2.5}$$

$$\begin{aligned}\mathcal{I}^{(\vartheta)}_{ab} \equiv & -\nabla_{(a}\vartheta\nabla_{b)}R - 2\nabla^c\vartheta\left(\nabla_{(a}R_{b)c} - \nabla_c R_{ab}\right) + R_{ab}\nabla_c\nabla^c\vartheta - 2R_{c(a}\nabla^c\nabla_{b)}\vartheta \\ & + g_{ab}\left(\nabla^c\vartheta\nabla_c R + R^{cd}\nabla_c\nabla_d\vartheta\right) \\ & + \vartheta\left[2R^{cd}R_{acbd} - \nabla_a\nabla_b R + \Box R_{ab} + \frac{1}{2}g_{ab}\left(\Box R - R_{cd}R^{cd}\right)\right],\end{aligned} \tag{2.6}$$

$$\begin{aligned}\mathcal{J}^{(\vartheta)}_{ab} \equiv & -8\nabla^c\vartheta\left(\nabla_{(a}R_{b)c} - \nabla_c R_{ab}\right) + 4R_{acbd}\nabla^c\nabla^d\vartheta \\ & - \vartheta\left[2\left(R_{ab}R - 4R^{cd}R_{acbd} + \nabla_a\nabla_b R - 2\Box R_{ab}\right) - \frac{1}{2}g_{ab}\left(R^2 - 4R_{cd}R^{cd}\right)\right],\end{aligned} \tag{2.7}$$

$$\mathcal{K}^{(\vartheta)}_{ab} \equiv 4\nabla^c\vartheta\varepsilon_c{}^d{}_{e(a}\nabla^e R_{b)d} + 4\nabla_d\nabla_c\vartheta^* R_{(a}{}^c{}_{b)}{}^d. \tag{2.8}$$

Variation of the action with respect to ϑ yields the scalar field equations

$$\beta\Box\vartheta - \beta\frac{dV}{d\vartheta} = -\alpha_1 R^2 - \alpha_2 R_{ab}R^{ab} - \alpha_3 R_{abcd}R^{abcd} - \alpha_4 R_{abcd}{}^* R^{abcd}. \tag{2.9}$$

2.3 Linear Stability Analysis

We study the modified field equations in perturbation theory, decomposing the full, spacetime metric into

$$g_{ab} = \bar{g}_{ab} + \xi' g^M_{ab} + \epsilon h^{\rm GR}_{ab} + \epsilon\xi' h^{\rm QG}_{ab} + \mathcal{O}(\epsilon^2, \xi'^2) \tag{2.10}$$

and the full scalar field into

$$\vartheta = \xi'^{1/2}\bar{\vartheta} + \epsilon\xi'^{1/2}\delta\vartheta + \mathcal{O}(\epsilon^2, \xi'). \tag{2.11}$$

$\bar{g}_{ab}$ is a stationary GR solution, g^M_{ab} is a stationary, QG modification to this solution, and $h^{\rm GR}_{ab}$ and $h^{\rm QG}_{ab}$ are GR and QG perturbations away from these (background) solutions $\bar{g}_{ab} + \xi' g^M_{ab}$. $\bar{\vartheta}$ is a stationary solution to the unperturbed field equations and $\delta\vartheta$ is a small perturbation away from this background field. The book-keeping parameters ϵ and ξ' denote the order of the perturbation and QG effect respectively. In particular, the latter denotes the order in the coupling parameter $\xi \equiv \alpha_i^2/(\beta\kappa)$, which appears frequently in QG theories.

All quantities computed in this paper will depend on g_{ab} and ϑ, such as the Riemann tensor, and thus, they can be also decomposed into

$$A = \sum_{n,m} \epsilon^n \xi'^{m/2} A^{(n,m)}, \tag{2.12}$$

where $A^{(n,m)}$ is assumed independent of ϵ and ξ'. With this decomposition, $\bar{g}_{ab}$, g^M_{ab}, $h^{\rm GR}_{ab}$, $h^{\rm QG}_{ab}$, $\bar{\vartheta}$ and $\delta\vartheta$ can be written as $g^{(0,0)}$, $g^{(0,2)}$, $g^{(1,0)}$, $g^{(1,2)}$, $\vartheta^{(0,1)}$ and $\vartheta^{(1,1)}$, respectively. For conventional reasons and ease of reading, however, we will continue to decompose the metric and the scalar field as in Eqs. 2.10 and 2.11. Henceforth, we work to leading order in ϵ and ξ'.

We consider a background metric $\bar{g}_{ab} + \xi' g^M_{ab}$ that is a vacuum solution to the modified field equations to leading order in ξ'. A trivial example of such a solution is the Minkowski spacetime (in this case, the ξ' perturbation vanishes), while more complicated ones are the BH spacetimes found in [85] and [86]. In this paper, we will work with a generic background metric $\bar{g}_{ab} + \xi' g^M_{ab}$ and only later specialize to these

BH solutions. The solutions have been shown to actually represent slowly-rotating BHs and not naked singularities in [85, 116].

We seek plane-wave solutions to the perturbed metric and scalar field of the form

$$h_{ab} = A_{ab}(t, x^j) e^{i\phi(t,x^k)/\epsilon_\phi} , \tag{2.13}$$

$$\delta\vartheta = B(t, x^j) e^{i\phi(t,x^k)/\epsilon_\phi} . \tag{2.14}$$

We further impose the geometric optics approximation, where we require that the phase ϕ varies much faster than the amplitudes (A_{ab}, B). This is enforced by requiring that the geometric optics, order-counting parameter ϵ_ϕ be much smaller than unity. With the above ansatz, we are also restricting this analysis to steady-state solutions, hence the scalar field and metric perturbation have the same phase.

The modified field equations and equation of motion for the scalar field can now be expanded trivariately in $\epsilon << 1$, $\xi' << 1$, and $\epsilon_\phi << 1$. The dominant term in the expansion will be $\mathcal{O}(\epsilon, \xi', \epsilon_\phi^{-2})$. We will discard all higher order terms, and thus, our analysis will not be valid in the non-linear regime $\xi' \sim 1$ by construction.

2.3.1 Perturbed Scalar Field Equations

The only non-vanishing contribution to the expansion of the left-hand side of the scalar field evolution equation [Eq. 2.9] to $\mathcal{O}(\epsilon, \xi')$ is

$$\begin{aligned}(\Box\vartheta)^{(1,1)} =& \bar{\Box}\delta\vartheta - h^{ab}_{\rm GR}\bar{\nabla}_a\bar{\nabla}_b\bar{\vartheta} - \frac{1}{2}\bar{g}^{ab}[\bar{g}^{cd}(\partial_a h^{\rm GR}_{bd} + \partial_b h^{\rm GR}_{da} - \partial_d h^{\rm GR}_{ab}) \\ & - h^{cd}_{\rm GR}(\partial_a \bar{g}_{bd} + \partial_b \bar{g}_{da} - \partial_d \bar{g}_{ab})]\partial_c\bar{\vartheta} \\ =& \bar{\Box}\delta\vartheta + \mathcal{O}(\epsilon_\phi^{-1}).\end{aligned} \tag{2.15}$$

$\bar{\nabla}_a$ and $\bar{\Box}$ denote the covariant derivative and D'Almbertian operator associated with $\bar{g}_{ab}$, respectively. We are only keeping leading-order terms in ϵ_ϕ and so only terms proportional to second derivatives of a perturbation are kept in the last equality.

The right-hand side of Eq. 2.9 depends on the Riemann tensor which, when expanded about a given background, is given by [117]

$$R_{abc}{}^{d} = \bar{R}_{abc}{}^{d} - 2\bar{\nabla}_{[a|}C^{d}{}_{b]c} + 2C^{e}{}_{c[a|}C^{d}{}_{b]e}. \tag{2.16}$$

$\bar{R}_{abc}{}^{d}$ is the Riemann tensor associated with $\bar{g}_{ab}$. A similar definition applies to $\bar{R}_{ab}$ and $\bar{R}$. The tensor field $C^{c}{}_{ab}$ is defined as

$$C^{c}{}_{ab} = \frac{1}{2}g^{cd}(\bar{\nabla}_a g_{bd} + \bar{\nabla}_b g_{ad} - \bar{\nabla}_d g_{ab}). \tag{2.17}$$

Using Eq. 2.16, the only non-vanishing contribution to the expansion of the right-hand side of Eq. 2.9 to $\mathcal{O}(\epsilon, \xi'^0)$ depends on

$$(R_{abcd}R^{abcd})^{(1,0)} = 4\bar{R}^{abcd}\bar{\nabla}_a\bar{\nabla}_c h^{\rm GR}_{bd} + \mathcal{O}(\epsilon_\phi^{-1}), \tag{2.18}$$

$$(R_{abcd}{}^{*}R^{abcd})^{(1,0)} = 2\bar{R}_{abcd}\bar{\epsilon}^{cdef}\bar{\nabla}^a\bar{\nabla}_e h^{b}_{f,\rm GR} + \mathcal{O}(\epsilon_\phi^{-1}), \tag{2.19}$$

$$(R_{ab}R^{ab})^{(1,0)} = 0, \tag{2.20}$$

$$(R^2)^{(1,0)} = 0\,. \tag{2.21}$$

We are only considering vacuum solutions, so the background Ricci tensor $\bar{R}_{ab}$ and scalar $\bar{R}$ both vanish. Thus, there is no perturbation to the Ricci tensor and scalar squared to the order considered.

Using Eqs. 2.15, 2.18, 2.19, 2.20, and 2.21 in Eq. 2.9, we find the perturbed scalar field equations to leading order in the geometric optics approximation

$$\beta\bar{\Box}\delta\vartheta = -2\bar{R}_{abcd}\left(2\alpha_3\bar{\nabla}^a\bar{\nabla}^c h^{bd}_{\rm GR} + \alpha_4\bar{\epsilon}^{cdef}\bar{\nabla}^a\bar{\nabla}_e h^b_{f,{\rm GR}}\right). \tag{2.22}$$

Let us now separate the even and odd-sectors of QG theories. That is, we now specialize to the even-parity subclass of theories with $(\alpha_3, \alpha_4) = (\alpha_3, 0)$ and the odd-parity subclass of theories with $(\alpha_3, \alpha_4) = (0, \alpha_4)$. Defining the four-dimensional wave-vector $k_a = (\partial_a\phi)/\epsilon_\phi$, and noting that $\partial_d h^{\rm GR}_{ab} = h^{\rm GR}_{ab}k_d$ to leading order in ϵ_ϕ, the perturbed scalar field equations are then

$$(\delta\vartheta_3)k_a k^a = -4\bar{R}^{abcd}h^{\rm GR}_{bd}k_a k_c, \tag{2.23}$$

$$(\delta\vartheta_4)k_a k^a = -2\bar{R}_{abcd}\bar{\epsilon}^{cdef}h^b_{f,{\rm GR}}k^a k_e, \tag{2.24}$$

where we have rescaled the background scalar field and its perturbation via

$$\bar{\vartheta}_A = \frac{\alpha_A}{\beta}\bar{\vartheta}_A, \tag{2.25}$$

$$\delta\vartheta_A = \frac{\alpha_A}{\beta}\delta\vartheta_A\,, \tag{2.26}$$

with $A = 3$ or 4. Equation 2.24 matches the perturbed scalar field equation for dCS modified gravity found in [82], while Eq. 2.23 is new. The main difference between these two equations is in the appearance of the Levi-Civita tensor associated with

the background GR metric in the right-hand side (source) of Eq. 2.24. This shows clearly that dCS gravity excites modifications to the spectrum of perturbations only for parity-odd backgrounds.

2.3.2 Perturbed Gravitational Field Equations

Let us first analyze the right-hand side of Eq. 2.3. Recall we are only considering vacuum solutions and so $T^{\rm mat}_{ab}$ vanishes. The scalar field stress-energy tensor $T^{(\vartheta)}_{ab}$ only depends on first derivatives of the scalar field. Thus, $T^{(\vartheta)}_{ab}$ goes as ϵ_ϕ^{-1} to lowest order in ϵ_ϕ. The left-hand side of Eq. 2.3 has terms that depend on the second derivatives of the scalar field, which go as ϵ_ϕ^{-2}. Only keeping lowest-order terms in ϵ_ϕ, the right-hand side of Eq. 2.3 is then zero.

Before analyzing the left-hand side of Eq. 2.3, let us first make some simplifications. As before, the background Ricci scalar and tensor vanish, since we are only considering vacuum solutions. The $\mathcal{O}(1,0)$ Ricci scalar and tensor also vanish, because they are proportional to $\bar{\Box} h^{\rm GR}_{ab}$, which vanishes because $h^{\rm GR}_{ab}$ must satisfied the $\mathcal{O}(1,0)$ perturbed (Einstein) field equations without a source.

With these simplifications, the perturbed field equations are

$$\begin{aligned}\frac{\kappa}{4}\left(\bar{g}^{cd}\tilde{R}_{acbd} + g^{cd}_{M}\tilde{R}_{acbd}\right) =& -\alpha_3\left[\tilde{R}_{acbd}\bar{\nabla}^c\bar{\nabla}^d\bar{\vartheta} + \bar{R}_{acbd}\bar{\nabla}^c\bar{\nabla}^d\left(\delta\vartheta\right)\right] \\ & -\alpha_4\left[{}^*\tilde{R}_{(a|c|b)d}\bar{\nabla}^d\bar{\nabla}^c\bar{\vartheta} + {}^*\bar{R}_{(a\ \ b)}^{\ c\ \ d}\bar{\nabla}_d\bar{\nabla}_c\left(\delta\vartheta\right)\right], \qquad (2.27)\end{aligned}$$

where $\tilde{R}_{abcd} = R^{(1,0)}_{abcd} + \xi' R^{(1,2)}_{abcd}$. The perturbed Riemann and its dual, as well as the contraction of the GR background metric with the perturbed Riemann, are

$$\tilde{R}_{acbd} = \left(\tilde{h}_{[c|d}k_{|a]}k_b - \tilde{h}_{[c|b}k_{|a]}k_d\right), \tag{2.28}$$

$$^*\tilde{R}_{(a|c|b)d} = \frac{1}{2}\bar{\varepsilon}_{(a|d}{}^{ef}\left(\tilde{h}_{ce}k_{|b)}k_f - \tilde{h}_{|b)e}k_c k_f\right), \tag{2.29}$$

$$\bar{g}^{cd}\tilde{R}_{acbd} = \frac{1}{2}\tilde{h}_{ab}k_c k^c. \tag{2.30}$$

As with the perturbed Riemann, $\tilde{h}_{ab} = h^{(1,0)}_{ab} + \xi' h^{(1,2)}_{ab}$.

Let us now specialize the analysis by again separating the even-parity and odd-parity sectors of QG. We thus use the expansions for the scalar field in Eqs. 2.25 and 2.26 and the following rescaling the modified and perturbed metric:

$$g^{M_A}_{ab} = \xi_A g^{M_A}_{ab}\,, \tag{2.31}$$

$$\tilde{h}^A_{ab} = h^{A(1,0)}_{ab} + \xi'_A h^{A(1,2)}_{ab}\,, \tag{2.32}$$

where $A = 3$ or 4. The even- and odd-parity perturbed field equations, those proportional to only α_3 and α_4, are then

$$\tilde{h}^3_{ab}k_c k^c = -8\xi_3\bar{R}_{acbd}\left(\delta\vartheta_3\right)k^c k^d - 8\xi_3\tilde{R}^3_{acbd}\bar{\nabla}^c\bar{\nabla}^d\bar{\vartheta}_3 - 2\xi_3 g^{cd}_{M_3}\tilde{R}^3_{acbd}, \tag{2.33}$$

$$\tilde{h}^4_{ab}k_c k^c = -8\xi_4{}^*\bar{R}_{(a|c|b)d}\left(\delta\vartheta_4\right)k^c k^d - 8\xi_4{}^*\tilde{R}^4_{(a|c|b)d}\bar{\nabla}^c\bar{\nabla}^d\bar{\vartheta}_4 - 2\xi_4 g^{cd}_{M_4}\tilde{R}^4_{acbd}\,, \tag{2.34}$$

where $\tilde{R}^A_{acbd}$ denotes the perturbed Riemann proportional to $\tilde{h}^A_{cd}$, with $A = 3$ or 4.

2.4 Dispersion Relations

We now combine the perturbed scalar and gravitational field equations to obtain dispersion relations in both the even- (EdGB) and odd-parity (dCS) sectors of QG. To achieve this goal, one needs to first replace $h^{\rm GR}_{ab}$ in Eqs. 2.23 and 2.24 with $\tilde{h}_{ab}$. This is justified because the difference between $h^{\rm GR}_{ab}$ and $\tilde{h}_{ab}$ is of $\mathcal{O}(\xi')$, and thus, it does not affect the final result to the working order. Using the perturbed field equations, together with Eqs. 2.33 and 2.34, we find the dispersion relations

$$\begin{aligned}(k_a k^a)^2 =& 32\xi_3 \bar{R}^{abcd}\bar{R}_{bedf}k_a k_c k^e k^f + \frac{32\xi_3}{(\delta\vartheta_3)}\bar{R}^{abcd}\tilde{R}^3_{bedf}k_a k_c \bar{\nabla}^e\bar{\nabla}^f\bar{\vartheta}_3 \\ &+ \frac{8\xi_3}{(\delta\vartheta_3)}\bar{R}^{abcd}\tilde{R}^3_{bedf}k_a k_c g^{ef}_{M_3},\end{aligned} \tag{2.35}$$

in the even-parity sector and

$$\begin{aligned}(k_a k^a)^2 =& 16\xi_4 \bar{\epsilon}^{cdef}\bar{R}_a{}^b{}_{cd}{}^*\bar{R}_{(b|g|f)h}k^a k_e k^g k^h + \frac{16\xi_4}{(\delta\vartheta_4)}\bar{\epsilon}^{cdef}\bar{R}_a{}^b{}_{cd}{}^*\tilde{R}^4_{(b|g|f)h}k^a k_e \bar{\nabla}^g\bar{\nabla}^h\bar{\vartheta}_4 \\ &+ \frac{4\xi_4}{(\delta\vartheta_4)}\bar{\epsilon}^{cdef}\bar{R}_a{}^b{}_{cd}\tilde{R}^4_{bgfh}k^a k_e g^{gh}_{M_4}.\end{aligned} \tag{2.36}$$

in the odd-parity sector. We immediately notice that these relations are not quite dispersion relations because the right-hand side depend on the perturbations. In a slight abuse of nomenclature, however, we will continue to refer to them as dispersion relations [118].

We can simplify these relations by rewriting the GR background Riemann tensor in terms of the GR background Weyl tensor $\bar{C}_{abcd}$, since the GR background considered is vacuum. Let us then define the tensors $\bar{W}_{ab}$ and $\bar{S}_{ab}$ in analogy with the electric

and magnetic parts of the background Weyl tensor

$$\bar{W}_{ac} = \bar{C}_{abcd} k^b k^d, \tag{2.37}$$

$$\bar{S}_{ac} = {}^*\bar{C}_{abcd} k^b k^d = \frac{1}{2}\varepsilon_{cd}{}^{ef}\bar{C}_{abef} k^b k^d. \tag{2.38}$$

Note that a further contraction of $\bar{S}_{ac}$ or $\bar{W}_{ac}$ with k_a or k_c vanishes due to symmetry. The dispersion relations in terms of these tensors become

$$\begin{aligned}(k_a k^a)^2 =& 32\xi_3(\bar{W}^{ab})(\bar{W}_{ab}) + 32\xi_3\frac{(\bar{W}^{ab})}{(\delta\vartheta_3)}\tilde{R}^3_{acbd}\bar{\nabla}^c\bar{\nabla}^d\bar{\vartheta}_3 \\ &+ 8\xi_3\frac{(\bar{W}^{ab})}{(\delta\vartheta_3)}g^{cd}_{M_3}\tilde{R}^3_{acbd},\end{aligned} \tag{2.39}$$

in the even-parity sector and

$$\begin{aligned}(k_a k^a)^2 =& 32\xi_4(\bar{S}^{ab})(\bar{S}_{ab}) + 32\xi_4\frac{(\bar{S}^{ab})}{(\delta\vartheta_4)}{}^*\tilde{R}^4_{acbd}\bar{\nabla}^c\bar{\nabla}^d\bar{\vartheta}_4 \\ &+ 8\xi_4\frac{(\bar{S}^{ab})}{(\delta\vartheta_4)}g^{cd}_{M_4}\tilde{R}^4_{acbd},\end{aligned} \tag{2.40}$$

in the odd-parity sector. Note that when ξ_3 and ξ_4 vanish, the dispersion relations are both null, returning the GR result as expected.

The dispersion relations in Eqs. 2.39 and 2.40 depend on the amplitude of the incident scalar and gravitational wave. Therefore, in order to make analytic progress, we will define two different perturbative regimes: one in which the magnitude of the scalar perturbation dominates over the magnitude of the metric perturbation (the scalar regime), and another one in which the opposite is true (the GW regime). To achieve this, let us treat the perturbation to the metric as a GW, and decompose it

into + and × polarizations:

$$A_{ab} \equiv A_+ e^+_{ab} + A_\times e^\times_{ab} \equiv A_{+,\times} e^{+,\times}_{ab}. \tag{2.41}$$

which clearly only affects the magnitude of the perturbation. In what follows, we define and study each of these perturbative regimes in more detail.

Physically, whether a perturbed black hole will be in scalar or GW regime depends on the particular type of perturbation considered. For example, consider the case where the perturbations are generated from the quasi-circular inspiral of two black holes into each other (that are far away from the background black hole that is being perturbed). In this case, [79] computed the far-zone perturbations both in the even and odd parity sectors of quadratic gravity. They found that $B_{\rm even} \sim (M/D_L)v_{12}$, while $B_{\rm odd} \sim (M/D)v_{12}^4\chi$, where M is the total mass of the binary, D_L is the luminosity distance from the binary's center of mass to the field point (in this case, the location of the background black hole), v_{12} is the magnitude of the orbital velocity of the binary and χ is the dimensionless magnitude of the spin angular momenta of either black hole binary component.

To determine which regime dominates, these scalar amplitudes are to be compared with the amplitude of the GR gravitational wave metric perturbation, which is simply $A_{+,\times} \sim (M/D)v_{12}^2$. We then see that, in this example, $B_{\rm even} \gg A_{+,\times}$ (scalar regime) but $B_{\rm odd} \ll A_{+,\times}$ (GW regime), because during the inspiral $v_{12} \ll 1$. Of course, this is just an example, since in general, the magnitude of $A_{+,\times}$ and B will depend on the particular system considered (e.g. during a supernovae, B and $A_{+,\times}$ will have a different scaling). Thus, to determine whether one is in one regime or the other, the particular scenario that is producing the perturbation must be carefully analyzed.

2.4.1 Scalar Regime

Let us define the scalar regime as that in which the amplitude of the scalar field perturbation is much larger than the amplitude of the metric perturbation, i.e.

$$B \gg A_{+,\times} \,. \tag{2.42}$$

In this limit the second and third terms in each dispersion relation is dominated by the first term giving the following dispersion relation:

$$(k_a k^a)^2 = 32\xi_A(\bar{S}^{ab})(\bar{S}_{ab}) \,, \tag{2.43}$$

where $A = 3$ or 4. This relation has been obtained using the identity $S_{ab}S^{ab} = W_{ab}W^{ab}$, which is only valid to leading order in ξ' (see Appendix A for a full discussion). Notice that this relation is the same for both parity-sectors (with the obvious change of coupling constant). Notice also that, in the scalar-regime, the perturbations disappear from the right-hand side, and thus, Eq. 2.43 is actually a true dispersion relation.

In the dCS case, the general dispersion relation of Eq. 2.40 reduces to that of Eq. 2.43 with $A = 4$ when the GR background is spherically symmetric. This is because in that case the background scalar field vanishes $\bar{\vartheta}_4 = 0$, since the source to the scalar evolution equation also vanishes. This then implies that the dCS correction to the GR background metric also vanishes $g^{M_4}_{cd} = 0$, since there is no scalar field to source a modification. One then sees that the second and third lines of Eq. 2.40 vanish identically, reducing to Eq. 2.40. This agrees with the findings of [82].

Already at this stage, we can make some interesting observations about the modified dispersion relations in the scalar regime. For any Petrov type D spacetime [119],

$$\bar{S}_{ac} = {}^*\bar{C}_{abcd}k^b k^d = \lambda k_a k_c \,, \tag{2.44}$$

for some constant λ, assuming k^a is a principal null direction of the Weyl tensor. It follows then that $\bar{S}_{ab}\bar{S}^{ab} = \lambda^2(k_a k^a)^2 = \mathcal{O}(\xi'^2)$ for such spacetimes, because $k_a k^a = \mathcal{O}(\xi')$, since $h^{\rm GR}_{ab}$ satisfies the linearized Einstein equations. Thus, the modified dispersion relation in Eq. 2.43 reduces to the GR expression. In particular, background GR spacetimes that represent BHs, such as the Schwarzschild and Kerr metrics, are Petrov type D with principal null directions in the radial direction. Therefore, it follows that for radial modes propagating in such BH backgrounds, QG leads to the same dispersion relation as GR [118].

A trivial generalization of the above result is that the modified dispersion relations reduce to the GR one for any Petrov type N spacetime with waves propagating along the null directions of the Weyl tensor. This follows from the fact that for such spacetimes, $\bar{C}_{abcd}k^c = 0$ [119].

2.4.2 GW Regime

Let us define the GW regime as that in which the amplitude of the metric perturbation is much larger than the amplitude of the scalar field perturbation, i.e.

$$B \ll A_{+,\times} \tag{2.45}$$

In this limit the second and third terms in the dispersion relations dominate, and one finds

$$(k_a k^a)^2 = 16\xi_3 \frac{A^3_{+,\times}}{B_3} \bar{W}^{ab} e^{+,\times}_{ab} k_c k_d \bar{\nabla}^c \bar{\nabla}^d \bar{\vartheta}_3 + 4\xi_3 \frac{A^3_{+,\times}}{B_3} \bar{W}^{ab} e^{+,\times}_{ab} k_c k_d g^{cd}_{M_3}, \tag{2.46}$$

in the even-parity sector and

$$(k_a k^a)^2 = 16\xi_4 \frac{A^4_{+,\times}}{B_4} \bar{S}^{ab} \bar{\varepsilon}_{ad}{}^{ef} e^{+,\times}_{be} k_c k_f \bar{\nabla}^c \bar{\nabla}^d \bar{\vartheta}_4 + 4\xi_4 \frac{A^4_{+,\times}}{B_4} \bar{S}^{ab} e^{+,\times}_{ab} k_c k_d g^{cd}_{M_4}, \tag{2.47}$$

in the odd-parity sector. The 3 and 4 indices on $A_{+,\times}$ and B denote that they are the amplitude or wave tensor associated with h_3 and ϑ_3, or h_4 and ϑ_4, respectively.

2.5 Propagation Speed in BH Backgrounds

The dispersion relations we found in the previous section can be solved to find the speed of propagating modes in a specific background that is a solution to QG. To do so we parameterize the four wave-vector as

$$k^a \equiv [\Omega, k_1, k_2, k_3] \tag{2.48}$$

and solve Eq. 2.43 or Eqs. 2.46 and 2.47 for Ω.

2.5.1 Scalar Regime

The dispersion relations in the scalar regime only depend on the GR background so the Schwarzschild and Kerr metrics can be used for non-spinning and spinning BHs, respectively. Moreover, recall that the dispersion relations are the same for the even- (EdGB) and odd-parity (dCS) sectors of QG, with the obvious change of coupling constant.

2.5.1.1 Non-spinning BH background Let us first concentrate on a Schwarzschild background in Schwarzschild coordinates (t, r, θ, ϕ). Keeping only the lowest-order in ξ' correction, one finds

$$\Omega_{\mathrm{QG},\chi^0} = \Omega_{\mathrm{Schw}} \left[1 \pm \frac{12M^3}{r^3} \zeta_A^{1/2} \left(1 - \frac{k_1^2}{\Omega_{\mathrm{Schw}}{}^2 f^2} \right) \right]. \tag{2.49}$$

Here $\zeta_A = \xi_A/M^4$, M is the physical BH mass defined in terms of the "bare" mass M_0 as $M = M_0\,[1 + (49/80)\,\zeta_A]$, $f = 1 - 2M/r$, and the GR dispersion result is

$$\Omega_{\mathrm{Schw}} = \pm \frac{1}{f} \sqrt{k_1^2 + f r^2 k_2^2 + f r^2 \sin^2(\theta) k_3^2}. \tag{2.50}$$

Notice that there are four independent solutions because the dispersion relations in Eqs. 2.39 and 2.40 are quartic polynomials in Ω. This matches the result found in [82] for dCS gravity, as expected. Interestingly, we find the same exact GW speed for the EdGB case, modulo the coupling constant. This stems from the identity in Appendix A.

Note when dealing with an ingoing or outgoing spherical wavefront ($k_{2,3} = 0$), there is no QG correction. This is because the QG modification to the propagation speed is proportional to the difference $(\Omega_{\mathrm{Schw}}^2 - k_1^2)$, which identically vanishes when $k_{2,3} = 0$. Therefore, in the far zone limit (a distance much farther than the GW wavelength), where any GW observations would be made and all waves approach a spherical wavefront, the four distinct solution of Eq. 2.49 degenerate into the GR prediction exactly. Thus, distinguishing a GR BH from a QG BH based on wave speed would be impossible.

2.5.1.2 Spinning BH Let us now concentrate on a Kerr background, expanded to $\mathcal{O}(\chi^2)$ with $\chi \equiv a/m$, where a is the Kerr spin parameter and m is the physical

BH mass. Keeping only the lowest-order in ξ' correction, one finds

$$\Omega = \Omega_{\mathrm{QG},\chi^0} + \chi\ \Omega_{\mathrm{QG},\chi^1} + \chi^2\ \Omega_{\mathrm{QG},\chi^2}, \tag{2.51}$$

where $\Omega_{\mathrm{QG},\chi^0}$ is the solution in the non-spinning case, already given in Eq. 2.49. $\Omega_{\mathrm{QG},\chi^1}$ and $\Omega_{\mathrm{QG},\chi^2}$ are $\mathcal{O}(\chi)$ and $\mathcal{O}(\chi^2)$ corrections, respectively, which are given by

$$\Omega_{\mathrm{QG},\chi^1} = \Omega_{\mathrm{Kerr},\chi^1}\left[1 - \frac{12M^2}{r^2}\zeta_A^{1/2}\right], \tag{2.52}$$

$$\Omega_{\mathrm{QG},\chi^2} = \Omega_{\mathrm{Kerr},\chi^2} + \zeta_A^{1/2}\Omega_{\Delta,\,\chi^2}, \tag{2.53}$$

where

$$\Omega_{\mathrm{Kerr},\chi^1} = \pm\,\frac{2M^2 k_3 \sin^2(\theta)}{rf}, \tag{2.54}$$

$$\Omega_{\mathrm{Kerr},\chi^2} = \pm\,\frac{M^2}{2r^2 f^2\left(\Omega_{\mathrm{Schw}} f\right)}\left[{\Omega_{\mathrm{Schw}}}^2 f^2\cos^2(\theta)\left(1 - \frac{4M}{r}\right) - k_1^2 + k_3^2 r^2 f\sin^4(\theta)\right], \tag{2.55}$$

$$\begin{aligned}\Omega_{\Delta,\,\chi^2} = \pm\,\frac{6M^5}{r^5 f^2\left(\Omega_{\mathrm{Schw}} f\right)}\Bigg[&\left(1 - \frac{k_1^2}{{\Omega_{\mathrm{Schw}}}^2 f^2}\right) \\ &\times\left(k_1^2 - k_3^2 r^2 f\sin^4(\theta) - 2D_{\mp}{\Omega_{\mathrm{Schw}}}^2 f^2\cos^2(\theta)\right) \\ &+E\left(2{\Omega_{\mathrm{Schw}}}^2 f^2\sin^2(\theta) + 4k_3^2 r^2 f\sin^2(\theta)\right)\Bigg],\end{aligned} \tag{2.56, 2.57}$$

$D_- = \frac{M}{r}$, $D_+ = (1 - \frac{M}{r})$, $E = -1$ for the D_- case and $E = +1$ for the D_+ case. Here (t, r, θ, ϕ) are standard Boyer-Lindquist coordinates. The result in GR is

$$\Omega_{\mathrm{GR}} = \Omega_{\mathrm{Schw}} + \chi\ \Omega_{\mathrm{Kerr},\chi^1} + \chi^2\ \Omega_{\mathrm{Kerr},\chi^2}. \tag{2.58}$$

We can once again analyze this solution in the far field limit, where waves are essentially radial ($k_{2,3} = 0$). As in the non-spinning BH background case, the QG correction that is χ-independent identically vanishes, as also does the linear-in-χ correction. However, at $\mathcal{O}(\chi^2)$ the QG modification does not vanish. The correction is

$$\Omega_{\Delta,\,\chi^2}(k_{2,3}=0) = \mp 12\left(\frac{M}{r}\right)^5 k_1 \sin^2(\theta) + \mathcal{O}\left(\frac{M^6}{r^6}\right), \tag{2.59}$$

and

$$\Omega_{\rm Kerr,\chi^2}(k_{2,3}=0) = \mp\frac{1}{2}\left(\frac{M}{r}\right)^2 k_1 \sin^2(\theta) + \mathcal{O}\left(\frac{M^3}{r^3}\right). \tag{2.60}$$

Notice again that the four independent solutions of Eq. 2.51 degenerate into two independent solution in the far-field limit. Notice also that the QG correction decays much faster with distance from the BH, and, in turn, will be a much weaker effect in the far zone compared to the GR term. Thus, even in the spinning BH case, the effect produced by QG on the wave speed would be essentially impossible to distinguish from the GR prediction.

2.5.2 GW Regime

For simplicity we only analyze radial waves ($k_{2,3} = 0$) in the far-zone regime. In this regime, the polarization tensor is simple [120]. The background scalar field and QG modification to the metric are given in [85] and [86] for the non-spinning and spinning cases, respectively. In this case, however, recall that the dispersion relations are different for the even- and odd-parity sectors of QG.

2.5.2.1 Non-spinning BH

Let us first consider the odd-parity (dCS) case. For non-spinning backgrounds, the background scalar field is zero, and thus, the background QG modification also vanishes. As before, then, the QG modification to the dispersion relation vanishes in the far-zone and we have $\Omega = \Omega_{\rm GR} = \pm k_1$.

In the even-parity (EdGB) case, however, the background scalar-field does not vanish. However, expanding the solution in the far-zone we still find that it reduces to the GR solution $\Omega = \Omega_{\rm GR} = \pm k_1$. This is because the source term to the modifications of the dispersion relation scale with a high power of $1/r$, even higher than in the scalar regime. Thus, just as in the latter, radial waves propagating in the far-zone are indistinguishable from the GR prediction.

2.5.2.2 Spinning BH For spinning BH backgrounds, both the odd-parity dCS and the even-parity EdGB background scalar fields are non-vanishing, thus sourcing a QG correction to the background metric. However, when expanding the solution in the far-zone, the speed of the propagating modes reduces exactly to the GR prediction $\Omega = \Omega_{\rm GR} = \pm k_1$, to leading order in M/r and irrespective of whether one considers a plus or a cross-polarized wave.

We can see this phenomenon clearly in the $\mathcal{O}(\chi^2)$ term of the solution to the dispersion relation. Such a correction enters first at $\mathcal{O}(M^2/r^2)$, and thus, to leading order in M/r it must be discarded. Notice that this is true regardless of whether one considers the even- or odd-parity dispersion relations. We thus conclude that the speed of propagating modes in QG is the same when considering spinning and non-spinning BH backgrounds, and in both cases identical to the GR prediction in the far-field.

2.6 Conclusion

In this paper, we have studied the linear stability to high-frequency perturbations of certain background solutions in the far-zone. We focused on perturbations of non-spinning [85] and spinning [86] BHs, expanding on previous work by including spinning BH backgrounds. We started by considering generic QG theories, but soon

after specialized to even-parity and odd-parity subclasses of QG theories. We derived dispersion relations in these two subclasses and solved them in two special regimes: the scalar-dominated and GW-dominated regimes, defined by whether the amplitude of the scalar to the GW perturbations is much larger or smaller than unity. In all cases, we find that the speed of propagating modes is not equal to that of light, but rather faster or slower, depending on the direction of incidence. These GR corrections, however, are too weak to be measurable by Earth-bound detectors due to its rapid radial fall off.

Our work extends all previous work on metric and scalar perturbations in dCS gravity. In addition to the work in [82], Motohashi and Suyama [83] have performed a perturbation analysis of this theory assuming a spherically symmetric background spacetime and using a spherical harmonic decomposition. They found that all modes propagate at the speed of light if the background scalar field vanishes. If one takes the high-frequency limit of their analysis, their wave ansatz corresponds to a spherical wavefront, and our result automatically reduce to theirs (and also those of [82]). It would be interesting to extend the analysis of [83] to see if any ghost mode exists in QG assuming a spherically symmetric background.

We have omitted a full analysis of the dispersion relations in the GW regime, Eqs. 2.46 and 2.47, on the backgrounds that we studied. The dispersion relations are directly dependent on the amplitudes of the metric and scalar field perturbations. Due to this dependence, it is not obvious whether the scalar and GWs will be generically stable. The analysis we carried out in the far field, however, suggests there are no imaginary terms in the solution and so the waves should be stable, but it is possible that taking this limit suppresses imaginary terms.

Our stability analysis was performed only to linear order in ϵ and ϵ_ϕ. Instabilities, if they exist, commonly are found at higher than linear order in the perturbation.

Another possible extension would be to perform a stability analysis to second or even higher order in ϵ and ϵ_ϕ. However, going to higher order in ξ' would not be possible, without including terms of higher order in the curvature in the quadratic action.

2.7 Acknowledgements

The authors thank Frans Pretorius and David Garfinkle for very useful suggestions and comments. Some calculations used the computer algebra systems MAPLE, in combination with the GRTensor II package [121]. NY acknowledges support from NSF grant PHY-1114374, as well as support provided from the National Aeronautics and Space Administration from grant NNX11AI49G, under sub-award 00001944.

SLOWLY ROTATING BLACK HOLES IN EINSTEIN-DILATON-GAUSS-BONNET GRAVITY: QUADRATIC ORDER IN SPIN SOLUTIONS

Contribution of Authors and Co-Authors

Manuscript in Chapter 3

Author: Dimitry Ayzenberg

Contributions: Implemented the study design. Wrote first draft of the manuscript.

Co-Author: Dr. Nicolás Yunes

Contributions: Conceived the study design. Provided feedback of analysis and comments on drafts of the manuscript.

Manuscript Information Page

Dimitry Ayzenberg, Nicolás Yunes

Physical Review D

Status of Manuscript:

___Prepared for submission to a peer-reviewed journal

___Officially submitted to a peer-reviewed journal

___Accepted by a peer-reviewed journal

_x_Published in a peer-reviewed journal

Published by the American Physical Society

Published August, 2014, Phys. Rev. D 90, 044066

Erratum published March, 2015, Phys. Rev. D 91, 069905

Abstract

We derive a stationary and axisymmetric black hole solution in Einstein-Dilaton-Gauss-Bonnet gravity to quadratic order in the ratio of the spin angular momentum to the black hole mass squared. This solution introduces new corrections to previously found nonspinning and linear-in-spin solutions. The location of the event horizon and the ergosphere are modified, as well as the quadrupole moment. The new solution is of Petrov type I, although lower order in spin solutions are of Petrov type D. There are no closed timelike curves or spacetime regions that violate causality outside of the event horizon in the new solution. We calculate the modifications to the binding energy, Kepler's third law, and properties of the innermost stable circular orbit. These modifications are important for determining how the electromagnetic properties of accretion disks around supermassive black holes are changed from those expected in general relativity.

3.1 Introduction

The mass of Sagittarius A* (Sgr A*), the supermassive black hole in the center of the Milky Way galaxy, is known to about 10% uncertainty [122, 123]. Due to past technological limitations, mass was the only property that could be inferred from the observation of the orbital motion of nearby stars. The next generation of upgrades to telescopes used in very long baseline interferometers will allow for the determination of other important properties, such as the location of the event horizon and the innermost stable circular orbit (ISCO) from observations of the black hole (BH) shadow and accretion disk, respectively [124–135]. One other property that we wish to infer is whether Sgr A* satisfies the so-called *Kerr hypothesis*, i.e. that the massive compact objects at the center of galaxies are Kerr BHs. The Kerr metric is the external spacetime of a vacuum, stationary, and axisymmetric BH in general relativity (GR) [136–141]. Modified theories of gravity that may or may not satisfy the Kerr hypothesis, and thus, observations of Sgr A* allow us to test them.

A modified gravity theory that does not satisfy the Kerr hypothesis is Einstein-dilaton-Gauss-Bonnet (EdGB) gravity. EdGB modifies the Einstein-Hilbert action through a dynamical scalar field coupled to the Gauss-Bonnet invariant. BHs in EdGB are not described by the Schwarzschild or Kerr metric, and thus, this theory violates the Kerr hypothesis. Instead, BHs acquire corrections that modify important properties, such as the location of the event horizon and the ISCO, relative to the Kerr expectation. EdGB is a well-motivated theory, for example arising from a four-dimensional compactification and low-energy expansion of heterotic string theory, wherein the scalar field is the dilaton [48,142]. In this context, EdGB should be viewed as an *effective field theory* valid up to a cutoff energy scale above which higher order operators cannot be neglected. If the theory is not treated as effective, instabilities can be nonlinearly generated [59], which would render the theory ill posed.

Numerical solutions for rapidly rotating BHs in EdGB gravity have been found in [143–146], but did not treat EdGB as an effective field theory. Early analytic BH solutions in theories motivated by string theory were found and studied in [147–150]. More recently, analytic BH solutions in EdGB gravity were found in [85, 86]. Our work focuses on purely analytic solutions. Reference [85] found an exact, stationary and spherically symmetric solution that represents nonspinning BHs. Reference [86] found an approximate, stationary and axisymmetric solution that represents a slowly rotating BH to leading order in the ratio of the spin angular momentum to the BH mass squared. In both cases, the EdGB metrics differed from the Kerr one by modifying certain key properties of BH spacetimes, such as the location of the event horizon and ergosphere. Nonetheless, both solutions were found to be of Petrov type D, just as the Kerr metric.

In this paper, we find an approximate, slowly rotating BH solution in EdGB gravity to quadratic order in the ratio of the spin angular momentum to the BH

mass squared. To derive this solution, we use a new BH perturbation theory method [151, 152], first employed in [57] in the context of modified gravity theories. We treat the second-order-in-spin correction to the EdGB metric as a perturbation away from the leading-order-in-spin one of [86]. The perturbation then satisfies a system of differential equations that we decouple through a tensor spherical harmonic decomposition. We finally verify the solution by reinserting it into the field equation and using symbolic manipulation software. Both here and in [85, 86], we work in a *small-coupling approximation*, i.e. we assume the EdGB modifications to GR are small and controlled by a dimensionless coupling constant. Such an approximation is consistent with the fact that EdGB is an effective theory, derived from a leading order truncation in the couplings of a more fundamental theory. Thus, its action and associated field equations are only valid to leading order in the coupling.

We then use this solution to study properties of the spacetime. First, we establish that the new solution truly represents a black hole, i.e. that it contains a singularity that is hidden inside an event horizon, and we compute the shift in the location of the event horizon and the ergosphere. Such a study was not possible with the linear-in-spin solution of [86], since it requires quadratic-in-spin corrections to the metric. Second, we show that no closed timelike curves exist and that the signature of the metric does not flip outside of the event horizon. This helps justify the perturbative construction of the solution, as small GR deformations should not lead to large modifications in the causal structure of spacetime. Third, we find that the quadratic-order-in-spin corrections force the new solution to be of Petrov type I. This is in contrast to black hole solutions in GR and the nonspinning and linear-in-spin black hole solutions in [85] and [86], all of which are of Petrov type D. Knowledge of the Petrov type may aid in the construction of analytic black hole solutions that are rapidly spinning. Finally, we study the behavior of test particles in

orbit around the new EdGB black hole, by obtaining corrections to the orbital binding energy, the angular momentum, the orbital frequency, and the ISCO frequency, and we compute the deformation to the quadrupole moment of the spacetime. All of this could aid in constraining EdGB observationally in the future with electromagnetic [42] or gravitational wave observations [48].

The remainder of this paper presents the details pertaining to these results. Section 3.2 gives a brief summary of EDGB gravity. Section 3.3 first describes the approximation scheme used to find BH solutions and then describes the solutions found in [85] and [86] and the new solution found in this paper. Section 3.4 studies the basic properties of the new solution, such as the location of the event horizon and ergosphere. Section 3.5 discusses the properties associated with particles in orbit around the BH, such as the ISCO and curves of zero velocity. Section 3.6 concludes by summarizing the results, discussing the observational implications, and proposing possible future research.

Throughout we use the following conventions: the metric signature $(-,+,+,+)$; latin letters in index lists stand for spacetime indices; parentheses and brackets in index lists for symmetrization and antisymmetrization, respectively, i.e. $A_{(ab)} = (A_{ab} - A_{ba})/2$ and $A_{[ab]} = (A_{ab} - A_{ba})/2$; geometric units with $G = c = 1$.

3.2 EDGB Gravity

This theory is defined by the action

$$S \equiv \int d^4x\sqrt{-g}\left\{\kappa R + \alpha e^{\vartheta}\left[R^2 - 4R_{ab}R^{ab} + R_{abcd}R^{abcd}\right]\right.$$
$$\left. -\frac{\beta}{2}\left[\nabla_a\vartheta\nabla^a\vartheta + 2V(\vartheta)\right] + \mathcal{L}_{\rm mat}\right\}. \tag{3.1}$$

Here, g stands for the determinant of the metric g_{ab}. R, R_{ab}, and R_{abcd} are the Ricci scalar, Ricci tensor, and the Riemann tensor. $\mathcal{L}_{\rm mat}$ is the external matter Lagrangian. ϑ is a field and $V(\vartheta)$ is an additional potential. (α, β) are coupling constants, and $\kappa = 1/(16\pi)$. For convenience, we define a dimensionless parameter

$$\zeta = \frac{\alpha^2}{\kappa\beta M^4}, \tag{3.2}$$

where M is the typical mass of the system.

We assume ϑ is small, otherwise e^{ϑ} becomes large which effectively rescales the coupling constant α to large values and the theory will no longer be effective. Moreover, a large value of e^{ϑ} would lead to a large modification to GR, which has been ruled out by weak-field tests. Assuming small ϑ, we Taylor expand $e^{\vartheta} = 1+\vartheta+\mathcal{O}(\vartheta^2)$ and note the ϑ-independent terms are irrelevant, ie. they lead to a theory identical to GR because the Gauss-Bonnet invariant is a topological invariant. The field equations are then

$$G_{ab} + \frac{\alpha}{\kappa}\mathcal{D}^{(\vartheta)}_{ab} = \frac{1}{2\kappa}\left(T^{\rm mat}_{ab} + T^{(\vartheta)}_{ab}\right), \tag{3.3}$$

where

$$T^{(\vartheta)}_{ab} = \beta\left[\nabla_a\vartheta\nabla_b\vartheta - \frac{1}{2}g_{ab}\left(\nabla_c\vartheta\nabla^c\vartheta - 2V(\vartheta)\right)\right] \tag{3.4}$$

is the scalar field stress-energy tensor and

$$\begin{aligned}\mathcal{D}^{(\vartheta)}_{ab} \equiv& -2R\nabla_a\nabla_b\vartheta + 2\left(g_{ab}R - 2R_{ab}\right)\nabla^c\nabla_c\vartheta \\ &+ 8R_{c(a}\nabla^c\nabla_{b)}\vartheta - 4g_{ab}R^{cd}\nabla_c\nabla_d\vartheta \\ &+ 4R_{acbd}\nabla^c\nabla^d\vartheta.\end{aligned} \tag{3.5}$$

Notice that the field equations remain of second-order. Variation of the action with respect to ϑ yields the scalar field equation

$$\beta\Box\vartheta - \beta\frac{dV}{d\vartheta} = -\alpha\left(R^2 - 4R_{ab}R^{ab} + R_{abcd}R^{abcd}\right). \tag{3.6}$$

Before proceeding, we must make a choice for the potential $V(\vartheta)$. If we chose a nonzero potential, usually a mass for the scalar field would be generated, rendering the field short ranged. But EDGB has a shift symmetry ($\vartheta \to \vartheta$+const) and theories with such a symmetry do not allow mass terms, rendering the field long ranged. Henceforth, we choose $V(\vartheta) = 0$.

3.3 Rotating Black Hole Solutions

We use two approximation schemes as set out in [57] to obtain a slowly rotating BH solution in EdGB gravity at quadratic order in spin. To find the second-order-in-spin solution we use the non-spinning and linear in spin solutions found by [85] and [86], respectively.

3.3.1 Approximation schemes

Following [107], we consider stationary and axisymmetric BH solutions in EdGB gravity with small coupling ($\zeta \ll 1$) and slow rotation ($\chi \ll 1$). Throughout M is the mass of the BH, $a \equiv J/M$ where J is the magnitude of the spin angular momentum of the BH, so that $\chi \equiv a/M$ is dimensionless. The small-coupling approximation treats EdGB modifications as small perturbations to the GR solution.

In the small-coupling approximation, we can expand the full metric as

$$g_{ab} = g^{(0)}_{ab} + \alpha'^2 g^{(2)}_{ab} + \mathcal{O}(\alpha'^4), \tag{3.7}$$

where α' is a bookkeeping parameter that labels the order of the small-coupling approximation, with $g^{(n)}_{ab} \propto \alpha^n$. In the above equation, $g^{(0)}_{ab}$ is the full Kerr metric, while $g^{(2)}_{ab}$ is a deformation of the GR metric to leading order in α'. Notice, therefore, that in the GR limit ($\alpha \to 0$ or $\zeta \to 0$), the full metric reduces exactly to the Kerr metric.

We will here work in Boyer-Lindquist-like coordinates (t, r, θ, ϕ), so that we can work with the Kerr metric in the form

$$\begin{aligned} ds^2_{\rm K} =& -\left(1-\frac{2Mr}{\Sigma}\right)dt^2 - \frac{4Mar\sin^2\theta}{\Sigma}dtd\phi + \frac{\Sigma}{\Delta}dr^2 \\ &+ \Sigma d\theta^2 + \left(r^2+a^2+\frac{2Ma^2r\sin^2\theta}{\Sigma}\right)\sin^2\theta d\phi^2, \end{aligned} \tag{3.8}$$

with $\Delta \equiv r^2 - 2Mr + a^2$ and $\Sigma \equiv r^2 + a^2\cos^2\theta$.

In the slow-rotation approximation, one can reexpand the ζ-expanded metric of Eq. 3.7. The Kerr metric, for example, can be expanded in the familiar form

$$g^{(0)}_{ab} = g^{(0,0)}_{ab} + \chi' g^{(1,0)}_{ab} + \chi'^2 g^{(2,0)}_{ab} + \mathcal{O}(\chi'^3), \tag{3.9}$$

where χ' is another bookkeeping parameter that labels the order of the slow-rotation approximation. The quantity $g^{(0,0)}_{ab}$ is here the Schwarzschild metric, while $g^{(1,0)}_{ab}$ and $g^{(2,0)}_{ab}$ are χ' perturbations. In this paper, we will expand the GR deformation $g^{(2)}_{ab}$ in the slow-rotation approximation as follows

$$\alpha'^2 g^{(2)}_{ab} = \alpha'^2 g^{(0,2)}_{ab} + \chi'\alpha'^2 g^{(1,2)}_{ab} + \chi'^2\alpha'^2 g^{(2,2)}_{ab} + \mathcal{O}(\alpha'^2\chi'^3), \tag{3.10}$$

where note that $g^{(i,j)}_{ab} \propto \chi^i \alpha^j$. Such an expansion is justified from the previous work in [85,86]. Even though we find the GR deformation $g^{(2)}_{ab}$ in a slow-rotation expansion,

the Kerr metric part of the full metric can be kept in full χ'-unexpanded form when working on astrophysical applications.

We will also expand the scalar field as follows

$$\vartheta = \alpha' \left[\vartheta^{(0,1)} + \chi' \vartheta^{(1,1)} + \chi'^2 \vartheta^{(2,1)}\right] + \mathcal{O}(\alpha' \chi'^3). \tag{3.11}$$

Note that the leading-order term is proportional to α, as must be the case from Eq. 2.9. There is no $\mathcal{O}(\alpha'^2)$ term and we have neglected terms of $\mathcal{O}(\alpha'^3)$ as they do not affect the metric perturbation at $\mathcal{O}(\alpha'^2)$.

3.3.2 BH solutions to $\mathcal{O}(\alpha'^2\chi^0)$ and $\mathcal{O}(\alpha'^2\chi')$

Yunes and Stein found that to $\mathcal{O}(\alpha'^2\chi'^0)$ [85]

$$\vartheta^{(0,1)} = \frac{\alpha}{\beta}\frac{2}{Mr}\left(1 + \frac{M}{r} + \frac{4}{3}\frac{M^2}{r^2}\right) \tag{3.12}$$

and the only nonvanishing terms in $g_{ab}^{(0,2)}$ is

$$g_{tt}^{(0,2)} = -\frac{\zeta}{3}\frac{M^3}{r^3}\left[1 + \frac{26M}{r} + \frac{66}{5}\frac{M^2}{r^2} + \frac{96}{5}\frac{M^3}{r^3} - \frac{80M^4}{r^4}\right], \tag{3.13}$$

$$g_{rr}^{(0,2)} = -\frac{\zeta}{f^2}\frac{M^2}{r^2}\left[1 + \frac{M}{r} + \frac{52}{3}\frac{M^2}{r^2} + \frac{2M^3}{r^3} + \frac{16}{5}\frac{M^4}{r^4} - \frac{368}{3}\frac{M^5}{r^5}\right], \tag{3.14}$$

where $f = 1 - \frac{2M}{r}$ and $\zeta = \frac{\alpha^2}{\beta\kappa M^4}$, with M the BH mass. This mass is the *physical mass*, ie. that which an observer at infinity would measure for example by observing the motion of stars in orbit around this BH.

Pani et al. found that at $\mathcal{O}(\alpha'^2\chi')$ the scalar field has no correction [86]. The only nonvanishing term in $g_{ab}^{(1,2)}$ is

$$g_{t\phi}^{(1,2)} = \frac{3}{5}\zeta M\chi\frac{M^3\sin^2\theta}{r^3}\left[1+\frac{140}{9}\frac{M}{r}+\frac{10M^2}{r^2}+\frac{16M^3}{r^3}-\frac{400}{9}\frac{M^4}{r^4}\right]. \tag{3.15}$$

3.3.3 BH solutions at $\mathcal{O}(\alpha'^2\chi'^2)$

3.3.3.1 Scalar field

The right-hand side of Eq. 2.9 is proportional to α and thus, the Gauss-Bonnet invariant need only be expanded to $\mathcal{O}(\alpha'^0)$. Thus, we can substitute the Kerr solution and expand in powers of χ', noting the first two terms, R^2 and $R_{ab}R^{ab}$, vanish and we are left with the Kretchmann scalar

$$R_{abcd}R^{abcd} = \frac{48M^2}{r^6}-\frac{1008\chi^2M^4\cos^2\theta}{r^8}+\mathcal{O}(\chi'^4). \tag{3.16}$$

The Gauss-Bonnet invariant is a parity even quantity, and as such, it can only depend on even powers of χ'. Thus, $\vartheta^{(n,1)}=0$ for all odd n.

Expanding $\Box\vartheta$ to $\mathcal{O}(\alpha'\chi'^2)$ and solving Eq. 2.9 we find

$$\vartheta^{(2,1)} = -\frac{\alpha\chi^2}{2\beta Mr}\left[1+\frac{M}{r}+\frac{4}{5}\frac{M^2}{r^2}+\frac{2}{5}\frac{M^3}{r^3}+\frac{28}{5}\frac{M^2\cos^2\theta}{r^2}\left(1+\frac{3M}{r}+\frac{48}{7}\frac{M^2}{r^2}\right)\right]. \tag{3.17}$$

Our result matches that found in [86].

3.3.3.2 Metric tensor

We can rewrite the expansion of the metric in Eq. 3.10 as $g_{ab}=g_{ab}^{(0,0)}+h_{ab}$ where h_{ab} is a metric perturbation away from the Schwarzschild solution. Let us further expand h_{ab} as

$$h_{ab} = \chi' g_{ab}^{(1,0)}+\chi'^2 g_{ab}^{(2,0)}+\alpha'^2 g_{ab}^{(0,2)}+\chi'\alpha'^2 g_{ab}^{(1,2)}+\chi'^2\alpha'^2 g_{ab}^{(2,2)}. \tag{3.18}$$

The Einstein tensor can then be expanded as

$$G_{ab} = G^{[0]}_{ab} + G^{[1]}_{ab} + G^{[2]}_{ab} + G^{[3]}_{ab} + \mathcal{O}(h^4), \tag{3.19}$$

where the superscript in square brackets counts the power of h_{ab} that appears in each expression. The Schwarzschild metric satisfies the vacuum Einstein equations, and so the first term $G^{[0]}_{ab}$ vanishes.

We can split the $\mathcal{O}(\alpha'^2\chi'^2)$ part of the Einstein tensor into two terms

$$G^{(2,2)}_{ab} = G^{[1]}_{ab}\left(g^{(2,2)}_{ab}\right) + G^{[2]}_{ab}\left(g^{(1,0)}_{ab}, g^{(2,0)}_{ab}, g^{(0,2)}_{ab}, g^{(1,2)}_{ab}\right) + G^{[3]}_{ab}\left(g^{(1,0)}_{ab}, g^{(0,2)}_{ab}\right), \tag{3.20}$$

where the first term depends on the unknown $g^{(2,2)}_{ab}$ and the second term depends on the known $g^{(1,0)}_{ab}$ and $g^{(1,2)}_{ab}$ only. At $\mathcal{O}(\alpha'^2\chi'^2)$ the field equations can then be rewritten as

$$G^{[1]}_{ab}\left(g^{(2,2)}_{ab}\right) = S^{(2,2)}_{ab}, \tag{3.21}$$

where the source term is simply

$$\begin{aligned} S^{(2,2)}_{ab} \equiv &- G^{[2]}_{ab}\left(g^{(1,0)}_{ab}, g^{(2,0)}_{ab}, g^{(0,2)}_{ab}, g^{(1,2)}_{ab}\right) - G^{[3]}_{ab}\left(g^{(1,0)}_{ab}, g^{(0,2)}_{ab}\right) \\ &- 4\left[\frac{\alpha}{\kappa} R_{acbd}\nabla^c\nabla^d\vartheta\right]^{(2,2)} + \frac{1}{2\kappa} T^{(\vartheta)\ (2,2)}_{ab}\,. \end{aligned} \tag{3.22}$$

In this form, the field equations resemble the equations of BH perturbation theory [151, 152]. We can interpret $G^{[1]}_{ab}\left(g^{(2,2)}_{ab}\right)$ as the linear part of the Einstein tensor built from an unknown perturbation $g^{(2,2)}_{ab}$ in a Schwarzschild background $g^{(0,0)}_{ab}$. Since the source term $S^{(2,2)}_{ab}$ can be computed exactly, we can use Schwarzschild BH perturbation theory tools to solve for $g^{(2,2)}_{ab}$.

As outlined in [151, 152], we decompose the metric perturbation $g^{(2,2)}_{ab}$ and the source term $S^{(2,2)}_{ab}$ in tensor spherical harmonics. We need only consider the even-parity sector of the metric perturbation, as terms of $\mathcal{O}(\alpha'^2\chi'^2)$ are obviously parity even. The even-parity sector only contains seven independent metric components. We only consider stationary and axisymmetric solutions, which further reduces the independent components to five as well as allowing us to focus only on the $m = 0$ mode in the decomposition. We are left with two gauge degrees of freedom, which we fix by using the Zerilli gauge [153]. These conditions leave three independent degrees of freedom, which are used to parametrize the metric perturbation as

$$g^{(2,2)}_{ab} = \sum_{\ell} \left[f(r) H_{0\ell 0}(r) a^{\ell 0(0)}_{ab} + \frac{1}{f(r)} H_{2\ell 0}(r) a^{\ell 0}_{ab} + \sqrt{2} K_{\ell 0}(r) g^{\ell 0}_{ab} \right]. \tag{3.23}$$

and the source term

$$S^{(2,2)}_{ab} = \sum_{\ell} \left[A^{(0)}_{\ell 0}(r) a^{\ell 0(0)}_{ab} + A_{\ell 0}(r) a^{\ell 0}_{ab} + B_{\ell 0}(r) b^{\ell 0}_{ab} + G^{(2)}_{\ell 0}(r) g^{\ell 0}_{ab} + F_{\ell 0}(r) f^{\ell 0}_{ab} \right], \tag{3.24}$$

where $f(r) = 1 - 2M/r$ is the Schwarzschild factor and $[a^{\ell 0(0)}_{ab}, a^{\ell 0}_{ab}, b^{\ell 0}_{ab}, g^{\ell 0}_{ab}, g^{\ell 0}_{ab}]$ are tensor spherical harmonics defined in Appendix B. The radial functions $A^{(0)}_{\ell 0}(r)$, $A_{\ell 0}(r)$, $B_{\ell 0}(r)$, $G^{(s)}_{\ell 0}(r)$, and $F_{\ell 0}(r)$ can be obtained by decomposing the source $S^{(2,2)}_{ab}$ in tensor spherical harmonics, and they are presented explicitly in Appendix B, being non-vanishing only for $\ell = 0$ and $\ell = 2$.

The metric, radial functions $[H_{0\ell 0}, H_{2\ell 0}, K_{\ell 0}]$ are to be determined by solving the expanded modified field equations [Eq. 3.21]. The decomposition turns these equations into a system of coupled ordinary differential equations [151, 152]:

$$-A^{(0)}_{\ell 0} = f^2 \frac{d^2 K_{\ell 0}}{dr^2} + \frac{1}{r} f \left(3 - \frac{5M}{r} \right) \frac{dK_{\ell 0}}{dr} - \frac{1}{r} f^2 \frac{dH^{\ell 0}_2}{dr}$$

$$- \frac{1}{r^2} f \left(H_2^{\ell 0} - K_{\ell 0} \right) - \frac{\ell(\ell+1)}{2r^2} f \left(H_2^{\ell 0} + K_{\ell 0} \right), \tag{3.25}$$

$$\begin{aligned} -A_{\ell 0} =& - \frac{r-M}{r^2 f} \frac{dK_{\ell 0}}{dr} + \frac{1}{r} \frac{dH_0^{\ell 0}}{dr} + \frac{1}{r^2 f} \left(H_2^{\ell 0} - K_{\ell 0} \right) \\ & + \frac{\ell(\ell+1)}{2r^2 f} \left(K_{\ell 0} - H_0^{\ell 0} \right), \end{aligned} \tag{3.26}$$

$$\frac{rf}{\sqrt{\ell(\ell+1)/2}} B_{\ell 0} = f \frac{d}{dr} \left(H_0^{\ell 0} - K_{\ell 0} \right) + \frac{2M}{r^2} H_0^{\ell 0} + \frac{1}{r} \left(1 - \frac{M}{r} \right) \left(H_2^{\ell 0} - H_0^{\ell 0} \right), \tag{3.27}$$

$$\begin{aligned} \sqrt{2} G_{\ell 0}^{(s)} =& f \frac{d^2 K_{\ell 0}}{dr^2} + \frac{2}{r} \left(1 - \frac{M}{r} \right) \frac{dK_{\ell 0}}{dr} - f \frac{d^2 H_0^{\ell 0}}{dr^2} - \frac{1}{r} \left(1 - \frac{M}{r} \right) \frac{dH_2^{\ell 0}}{dr} \\ & - \frac{r+M}{r^2} \frac{dH_{0\ell 0}}{dr} + \frac{\ell(\ell+1)}{2r^2} \left(H_0^{\ell 0} - H_2^{\ell 0} \right), \end{aligned} \tag{3.28}$$

$$\frac{H_0^{\ell 0} - H_2^{\ell 0}}{2} = \frac{r^2 F_{\ell 0}}{\sqrt{\ell(\ell+1)(\ell-1)(\ell+2)/2}}. \tag{3.29}$$

In Eqs. 3.25, 3.26, and 3.28, ℓ can take the values 0 or 2, but in Eqs. 3.27 and 3.29 ℓ can only equal 2.

There is one remaining gauge freedom in the $\ell = 0$ mode, which we will use to further simplify Eqs. 3.25-3.29. After imposing stationarity and axisymmetry, there are three independent variables associated with the $\ell = 0$ mode. One of these leads to a redefinition of the spherical areal radius. We set $K_{00} = 0$ to eliminate this variable.

To solve the system of differential equations in Eqs. 3.25-3.29 we start by solving Eq. 3.25 for H_{200}. Equations 3.26 and 3.28 can then be solved for H_{000}. With H_{000} and H_{200}, the $\ell = 2$ functions can be found, $H_{0\ell 0}$, $H_{2\ell 0}$, and $K_{\ell 0}$. The full solution is presented in Appendix B. Each function is a sum of a homogeneous and inhomogeneous piece, with the former containing integration constants. We choose

these constants by requiring (1) that the metric be asymptotically flat at spatial infinity, and (2) that the mass and (magnitude of the) spin angular momentum associated with the new solution is given by M and Ma, as measured by an observer at spatial infinity.

The metric at $\mathcal{O}(\alpha'^2\chi'^2)$ is then

$$\begin{aligned} g_{tt}^{(2,2)} =& -\frac{4463}{2625}\zeta\chi^2\frac{M^3}{r^3}\left[\left(1+\frac{M}{r}+\frac{27479}{31241}\frac{M^2}{r^2}-\frac{2275145}{187446}\frac{M^3}{r^3}-\frac{2030855}{93723}\frac{M^4}{r^4}\right.\right. \\ &\left.-\frac{99975}{4463}\frac{M^5}{r^5}+\frac{1128850}{13389}\frac{M^6}{r^6}+\frac{194600}{4463}\frac{M^7}{r^7}-\frac{210000}{4463}\frac{M^8}{r^8}\right)\left(3\cos^2\theta-1\right) \\ &-\frac{875}{8926}\left(1+\frac{14M}{r}+\frac{52}{5}\frac{M^2}{r^2}+\frac{1214}{15}\frac{M^3}{r^3}+\frac{68M^4}{r^4}+\frac{724}{5}\frac{M^5}{r^5}\right. \\ &\left.\left.-\frac{11264}{15}\frac{M^6}{r^6}+\frac{160}{3}\frac{M^7}{r^7}\right)\right], \end{aligned} \tag{3.30}$$

$$\begin{aligned} g_{rr}^{(2,2)} =& -\zeta\frac{\chi^2}{f^3}\frac{M^3}{r^3}\left[\frac{4463}{2625}\left(1-\frac{5338}{4463}\frac{M}{r}-\frac{59503}{31241}\frac{M^2}{r^2}-\frac{7433843}{187446}\frac{M^3}{r^3}+\frac{13462040}{93723}\frac{M^4}{r^4}\right.\right. \\ &-\frac{7072405}{31241}\frac{M^5}{r^5}+\frac{9896300}{13389}\frac{M^6}{r^6}-\frac{28857700}{13389}\frac{M^7}{r^7}+\frac{13188000}{4463}\frac{M^8}{r^8} \\ &\left.-\frac{7140000}{4463}\frac{M^9}{r^9}\right)\left(3\cos^2\theta-1\right)-\frac{r}{2M}\left(1-\frac{M}{r}+\frac{10M^2}{r^2}-\frac{12M^3}{r^3}+\frac{218}{3}\frac{M^4}{r^4}\right. \\ &\left.\left.+\frac{128}{3}\frac{M^5}{r^5}-\frac{724}{15}\frac{M^6}{r^6}-\frac{22664}{15}\frac{M^7}{r^7}+\frac{25312}{15}\frac{M^8}{r^8}+\frac{1600}{3}\frac{M^9}{r^9}\right)\right], \end{aligned} \tag{3.31}$$

$$\begin{aligned} g_{\theta\theta}^{(2,2)} =& -\frac{4463}{2625}\zeta\chi^2\frac{M^3}{r^3}\left(1+\frac{10370}{4463}\frac{M}{r}+\frac{266911}{62482}\frac{M^2}{r^2}+\frac{63365}{13389}\frac{M^3}{r^3}-\frac{309275}{31241}\frac{M^4}{r^4}\right. \\ &\left.-\frac{81350}{4463}\frac{M^5}{r^5}-\frac{443800}{13389}\frac{M^6}{r^6}+\frac{210000}{4463}\frac{M^7}{r^7}\right)r^2\left(3\cos^2\theta-1\right), \end{aligned} \tag{3.32}$$

$$g_{\phi\phi}^{(2,2)} = g_{\theta\theta}^{(2,2)}\sin^2\theta. \tag{3.33}$$

where all other metric components are zero. We have checked explicitly that this solution satisfies the field equations (Eq. 2.3) to $\mathcal{O}(\alpha'^2\chi'^2)$ using symbolic manipulation software.

3.3.3.3 Accuracy of the approximate solution The approximate solution we derived in the previous subsections is valid only when $\zeta \ll 1$, where recall that ζ is proportional to the coupling constants of EdGB theory. For this reason, it should be clear that as $\zeta \to 0$, then EdGB theory reduces to GR, and the approximate black hole solution derived in the paper reduces identically to the Kerr metric. To be precise, when $\zeta \to 0$, then the $\mathcal{O}(\chi^0)$ GR deformations in Eqs. 3.13 and 3.14 vanish, the $\mathcal{O}(\chi)$ deformation in Eq. 3.15 vanishes and the new, $\mathcal{O}(\chi^2)$ deformations in Eqs. 3.30-3.33 vanish, reducing the metric in Eq. 3.7 to the Kerr metric. Recall also that an expansion in $\zeta \ll 1$ is valid because EdGB theory must be treated as an effective theory, as explained in the Introduction.

The approximate solution here derived is also clearly only valid when $\chi \ll 1$, but how large a value of χ can the solution tolerate without incurring an error larger than some tolerance τ? The only precise way to find this maximum value would be to compare the $\mathcal{O}(\chi^2)$-accurate metric to a numerical, exact solution, like those of [143–146]. Lacking those numerical solutions, all we can do is estimate the error from the next terms expected in the $\chi \ll 1$ series. From the structure of the solution, we have here neglected terms of $\mathcal{O}(\chi^3)$ in the (t, ϕ) component of the metric and $\mathcal{O}(\chi^4)$ in the diagonal components of the metric. More precisely, the terms neglected in the approximate solution should be of the form $\chi^3 f(r)S(\theta)$ and $\chi^4 g(r)T(\theta)$. From the study of black holes in dynamical Chern-Simons gravity [111], we expect $f(r)T(\theta)$ and $g(r)S(\theta)$ to be of order unity on the horizon and at the equator, where they will acquire their largest numerical values. Given this, requiring that the neglected terms

be smaller than some threshold τ, one expects the approximate solution to be valid up to roughly

$$\chi \lesssim \tau^{1/3}\,, \qquad \text{and} \qquad \chi \lesssim \tau^{1/4} \tag{3.34}$$

for the (t,ϕ) and diagonal components of the metric, respectively. For concreteness, if one picks $\tau = 10\%$, then $a/M \lesssim 0.46$ and $a/M \lesssim 0.56$ respectively.

We can carry out such an accuracy analysis explicitly in the case of the scalar field. This is because one can systematically solve Eq. 2.9 order by order in χ, to find higher-order-in-χ corrections, which we present in Appendix C. The error in ϑ due to not including terms of $\mathcal{O}(\chi^4)$ and higher is then largest at the event horizon, where it reduces to

$$\vartheta^{(4,1)} + \vartheta^{(6,1)} + \vartheta^{(8,1)} = -\frac{\alpha}{\beta}\left(\frac{9}{40}\chi^4 + \frac{91}{384}\chi^6 + \frac{25}{112}\chi^8\right)\,. \tag{3.35}$$

As expected, notice that the leading-order error in χ is of the form predicted above, i.e. a term of order unity (9/40 in this case) times χ^4. We can evaluate Eq. 3.35 as a function of χ to find the value of the spin at which the error equals some tolerance τ. Doing so, and setting $\beta = \alpha$ for this estimate, we find

$$\chi \lesssim \frac{2^{3/4}5^{1/4}}{3^{1/2}}\tau^{1/4}\left[1 - \frac{455}{1296}\frac{5^{1/2}}{2^{1/2}}\tau^{1/2} + \mathcal{O}(\tau)\right]\,, \tag{3.36}$$

where we expanded in the small tolerance parameter $\tau \ll 1$. If we set $\tau = 10\%$, we then find $\chi \lesssim 0.67$, which is consistent with the estimate presented above.

3.4 Properties of the Solution

3.4.1 Singularity, horizon, and ergosphere

The spacetime solution we have found has a true singularity at $r = 0$. We determined this by calculating the Kretchmann invariant $R_{abcd}R^{abcd}$:

$$\begin{aligned} R_{abcd}R^{abcd} =& 48\frac{M^2}{r^6}\left(1-\frac{21a^2\cos^2\theta}{r^2}\right) - 32\zeta\frac{M^3}{r^7}\left(1+\frac{1}{2}\frac{M}{r}+\frac{72M^2}{r^2}+\frac{7M^3}{r^3}+\frac{64}{5}\frac{M^4}{r^4}\right. \\ &\left.-\frac{840M^5}{r^5}\right) - \frac{428448}{875}\zeta\frac{M^4}{r^8}\chi^2\left(1+\frac{104315}{80334}\frac{M}{r}+\frac{593165}{281169}\frac{M^2}{r^2}-\frac{6239885}{160668}\frac{M^3}{r^3}\right. \\ &\left.-\frac{3108445}{80334}\frac{M^4}{r^4}-\frac{5959775}{80334}\frac{M^5}{r^5}+\frac{22532275}{40167}\frac{M^6}{r^6}+\frac{97300}{4463}\frac{M^7}{r^7}-\frac{105000}{4463}\frac{M^8}{r^8}\right) \\ &\times\left(3\cos^2\theta-1\right)+16\zeta\frac{M^3}{r^7}\chi^2\left(1+\frac{1}{2}\frac{M}{r}+\frac{122}{3}\frac{M^2}{r^2}+\frac{19}{3}\frac{M^3}{r^3}+\frac{2453}{3}\frac{M^4}{r^4}\right. \\ &\left.+\frac{272}{3}\frac{M^5}{r^5}+\frac{3338}{15}\frac{M^6}{r^6}-\frac{255056}{15}\frac{M^7}{r^7}+\frac{80M^8}{r^8}\right). \end{aligned} \tag{3.37}$$

Note that this quantity clearly diverges *only* at $r = 0$ in these coordinates.

This metric also possesses an event horizon, i.e. a null surface generated by null geodesic generators. Since the normal to the surface n^μ must itself be null, event horizons must satisfy the horizon equation [116]

$$g^{\mu\nu}\partial_\mu F\partial_\nu F = 0\,, \tag{3.38}$$

where $F(x^\alpha)$ is a level surface function such that $n_\mu = \partial_\mu F$. Using that the spacetime is stationary, axisymmetric, and reflection symmetric about the poles and the equator, the level surfaces can only depend on radius. Without loss of generality, we then let $F(x^\alpha) = r - r_{\rm H}$, where $F = 0$ defines the horizon location. This then forces Eq. 3.38 into $g^{rr} = 0$, which is nothing but $g_{tt}g_{\phi\phi} - g_{t\phi}^2 = 0$ [154]. Solving this equation, we

find

$$r_{\rm H} = r_{\rm H,K} - \frac{49}{40}\zeta M - \frac{277}{960}\zeta M\chi^2\,, \tag{3.39}$$

with $r_{\rm H,K} = M + (M^2 - a^2)^{1/2}$ the Kerr result. Our results agree to $\mathcal{O}(\chi^0)$ with those of Yunes and Stein [85]. Notice that the $\mathcal{O}(\chi^2)$ corrections act to further shrink the event horizon relative to its Kerr analogue.

The location of the ergosphere can be found by solving $g_{tt} = 0$ for r. We find

$$r_{\rm ergo} = r_{\rm ergo,K} - \frac{49}{40}\zeta M - \frac{277}{960}\zeta M\chi^2\left(1 - \frac{850}{277}\sin^2\theta\right), \tag{3.40}$$

with the ergosphere in Kerr given by $r_{\rm ergo,K} = M + (M^2 + a^2\cos^2\theta)^{1/2}$. Notice that this time the $\mathcal{O}(\chi^2)$ term does not have a definite sign, but can either act to shrink or enlarge the ergosphere, depending on the latitude angle θ.

Note that our choice of homogeneous integration constants in computing the metric depends on how we choose to define the mass M and the reduced spin angular momentum a. We choose to define these quantities as measured by an observer at infinity, which leads to the metric presented in Sec. 3.3.3.2. The angular velocity and area of the event horizon become modified with these definitions

$$\Omega_{\rm H} \equiv -\frac{g_{tt}}{g_{t\phi}}\Big|_{r=r_{\rm H}} = \Omega_{\rm H,K}\left(1 + \frac{21}{20}\zeta\right), \tag{3.41}$$

$$A_{\rm H} \equiv 2\pi\int_0^\pi \sqrt{g_{\theta\theta}g_{\phi\phi}}|_{r=r_H}\,d\theta = A_{\rm H,K}\left[1 - \frac{49}{40}\zeta\left(1 + \frac{19}{98}\chi^2\right)\right], \tag{3.42}$$

where $\Omega_{\rm H,K} = a/\left(r_{\rm H,K}^2 + a^2\right)$ and $A_{\rm H,K} = 4\pi(r_{\rm H,K}^2 + a^2)$ are the horizon's angular velocity and area for the Kerr metric.

3.4.2 Lorentz signature

If the Lorentzian signature of the metric is not preserved outside the horizon, our perturbative construction is not well justified. We show here that the signature is preserved for a small coupling constant. We denote the determinant of the new metric as g and the determinant of the Kerr metric as $g_{\rm K} \equiv -r^2 \sin^2\theta\,(r^2 + a^2\cos^2\theta) + \mathcal{O}(\chi'^3)$. The determinant of the metric is then given by

$$\begin{aligned}\frac{g}{g_{\rm K}} =& 1 + \frac{M^2}{r^2}\chi^2\cos^2\theta - \zeta\frac{M^2}{r^2}\left(1 + \frac{8}{3}\frac{M}{r} + \frac{14M^2}{r^2} + \frac{128}{5}\frac{M^3}{r^3} + \frac{48M^4}{r^4}\right) \\ &+ \frac{1}{2}\zeta\frac{M^2}{r^2}\chi^2\left(1 + \frac{8284}{875}\frac{M}{r} + \frac{13546}{525}\frac{M^2}{r^2} + \frac{874372}{18375}\frac{M^3}{r^3} - \frac{1422}{175}\frac{M^4}{r^4} + \frac{26234}{147}\frac{M^5}{r^5}\right. \\ &\left. - \frac{1120M^8}{r^8}\right) - \frac{8926}{875}\zeta\frac{M^3}{r^3}\chi^2\left(1 + \frac{19865}{8926}\frac{M}{r} + \frac{323804}{93723}\frac{M^2}{r^2} - \frac{106915}{8926}\frac{M^3}{r^3}\right. \\ &\left. - \frac{103475}{31241}\frac{M^4}{r^4} - \frac{205425}{4463}\frac{M^5}{r^5} + \frac{618800}{4463}\frac{M^6}{r^6} - \frac{735000}{4463}\frac{M^7}{r^7}\right)\cos^2\theta. \end{aligned} \tag{3.43}$$

The correction terms fall off rapidly as $r \to \infty$, so it is important to look at the signature of $g/g_{\rm K}$ at the horizon $r_{\rm H}$

$$\frac{g}{g_{\rm K}} = 1 + \frac{1}{4}\chi^2\cos^2\theta - \frac{361}{120}\zeta\left[1 - \frac{731411}{7075600}\chi^2\left(1 - \frac{1420033}{731411}\cos^2\theta\right)\right]. \tag{3.44}$$

Notice that the term in square brackets is always positive, so the ζ correction is always negative, which could be a problem for a sufficiently large value of the coupling constant. The correction is at a maximum when $\chi = 0$, which means the signature flip does not take place as long as $\zeta \lesssim 0.33$. The strongest current constraints on EdGB come from low-mass x-ray binary observations, $\sqrt{|\alpha|} < 1.9 \times 10^5$cm [111]. Setting $\beta = 1$ and using a very low-mass BH with $M = 5M_\odot$, this constraint implies $\zeta \lesssim 0.2$. We then see that current constraints already exclude the region of parameter space in which a Lorentz signature flip could occur. Of course, if the BH mass is small

enough, then ζ will become larger, as it scales with m^{-4}, but then the small-coupling approximation would break down.

3.4.3 Closed timelike curves

Closed timelike curves, if they exist, can be found by solving for the region where $g_{\phi\phi} < 0$. The explicit form of $g_{\phi\phi}$ was already presented in Eq. 3.33, where we see that the corrections fall off rapidly as r^{-3} relative to the Kerr value of this metric component. Thus, the corrections are largest at the horizon $r_{\rm H}$, where

$$g_{\phi\phi} = 4M^2 \sin^2\theta \left\{ 1 - \frac{1}{4}\chi^2 \cos^2\theta - \frac{49}{40}\zeta \left[1 - \frac{102673}{180075}\chi^2 \left(1 - \frac{2041527}{821384} \cos^2\theta \right) \right] \right\}. \tag{3.45}$$

The sign of the correction terms depend on the spin, but for small spin the χ^0 term dominates and the correction is always negative. In this case, we see that $\zeta > 0.8$ for $g_{\phi\phi}$ to vanish. As already argued, such values of ζ are excluded by current constraint for realistic BH masses, and thus, closed timelike curves do not occur.

3.4.4 Multipolar structure

Following Thorne [155], the multipole moment can be read off by transforming the metric to asymptotically Cartesian and mass-centered (ACMC) coordinates. In these coordinates the multipole moments are defined in a spacetime region asymptotically far from the source. To find the quadrupole moment, the coordinate transformation to ACMC must be done such that g_{tt} and g_{ij} at $\mathcal{O}(r^{-2})$ do not contain any angular dependence. In these coordinates, g_{tt} for a stationary and axisymmetric spacetime can be written as

$$g_{tt} = -1 + \frac{2M}{r} + \frac{\sqrt{3}}{2}\frac{1}{r^3}\left[Q_{20} Y^{20} + (\ell = 0 \text{ pole}) \right] + \mathcal{O}(\frac{1}{r^4}). \tag{3.46}$$

Y^{20} is the $(\ell, m) = (2, 0)$ spherical harmonic and Q_{20} is the $(m = 0)$ quadrupole moment.

The correction in the new metric is at $\mathcal{O}(\alpha'^2\chi'^2)$, so it is not affected by the coordinate transformation. The quadrupole moment in the new solution is then

$$Q_{20} = Q_{20,\text{K}} \left(1 + \frac{4463}{2625}\zeta\right) , \tag{3.47}$$

where $Q_{20,\text{K}}$ is the Kerr quadrupole moment.

3.4.5 Petrov type

Generic spacetimes can be classified into Petrov types by finding the number of distinct principal null directions (PNDs) k^a of the Weyl tensor C_{abcd} [119, 156], where k^a must satisfy

$$k^b k^c k_{[e} C_{a]bc[d} k_{f]} = 0. \tag{3.48}$$

This is the same as finding the number of distinct PNDs l^a that make one of the Weyl scalars $\Psi_0 = 0$, which simplifies to finding the number of distinct roots for b in [119]

$$\Psi_0 + 4b\Psi_1 + 6b^2\Psi_2 + 4b^3\Psi_3 + b^4\Psi_4 = 0. \tag{3.49}$$

The Ψ's are five complex Weyl scalars in an arbitrary tetrad with the restriction that $\Psi_4 \neq 0$.

The spacetime is said to be *algebraically special* if Eq. 3.49 has at least one degenerate root, and the following relation holds:

$$I^3 = 27J^2. \tag{3.50}$$

The quadratic and cubic Weyl quantities I and J are defined by [119]

$$I \equiv \frac{1}{2}\tilde{C}_{abcd}\tilde{C}^{abcd} = 3\Psi_2^2 - 4\Psi_1\Psi_3 + \Psi_4\Psi_0, \tag{3.51}$$

$$J \equiv -\frac{1}{6}\tilde{C}_{abcd}\tilde{C}^{cd}{}_{ef}\tilde{C}^{efab} = -\Psi_2^3 + 2\Psi_1\Psi_3\Psi_2 + \Psi_0\Psi_4\Psi_2 - \Psi_4\Psi_1^2 - \Psi_0\Psi_3^2, \tag{3.52}$$

where

$$\tilde{C}_{abcd} \equiv \frac{1}{4}\left(C_{abcd} + \frac{i}{2}\epsilon_{abef}C^{ef}{}_{cd}\right). \tag{3.53}$$

The spacetime is of Petrov type I if Eq. 3.50 does not hold. The Kerr BH is known to be of Petrov type D. For a spacetime to be type D Eq. 3.50 must hold along with the following conditions:

$$K = 0, \tag{3.54}$$

$$N - 9L^2 = 0, \tag{3.55}$$

where K, L, and N are

$$K \equiv \Psi_1\Psi_4^2 - 3\Psi_4\Psi_3\Psi_2 + 2\Psi_3^3, \tag{3.56}$$

$$L \equiv \Psi_2\Psi_4 - \Psi_3^2, \tag{3.57}$$

$$N \equiv \Psi_4^2 I - 3L^2 = \Psi_4^3\Psi_0 - 4\Psi_4^2\Psi_1\Psi_3 + 6\Psi_4\Psi_2\Psi_3^2 - 3\Psi_3^4. \tag{3.58}$$

One can find a null tetrad for the no-rotating BH solution in EdGB such that Ψ_2 is the only nonvanishing Newman-Penrose scalar. Equations 3.50, 3.54, and 3.55 are then trivially satisfied. Thus, the nonspinning solution found in [85] is of Petrov Type D.

For the slowly rotating BH solution in EdGB gravity to linear order in spin [86], we first find a principal null tetrad that is a deformation away from the Kerr principal null tetrad. We then find that Eqs. 3.51, 3.54, and 3.55 are all satisfied to $\mathcal{O}(\alpha'^4\chi'^2)$. Thus, we find the slowly rotating solution to $\mathcal{O}(\alpha'^2\chi')$ is also of Petrov Type D. [1]

For the new BH solution at $\mathcal{O}(\alpha'^2\chi'^2)$ the story is different. We first find a principal null tetrad by adding $\mathcal{O}(\alpha'^2\chi'^2)$ deformations to the null tetrad found in the $\mathcal{O}(\alpha'^2\chi')$ case. We then find that Eq. 3.51 is *not* satisfied to $\mathcal{O}(\alpha'^4\chi'^4)$. Thus, the new metric found in this paper is of Petrov Type I, and breaks symmetries that the $\mathcal{O}(\alpha'^2\chi')$ metric had. This suggests that the exact BH solution should be of Petrov type I.

3.5 Properties of Test-Particle Orbits

3.5.1 Conserved quantities

The metric found here is stationary and axisymmetric, and thus, it possess a timelike and an azimuthal Killing vector, which imply the existence of two conserved quantities: the energy and the (z component of the) angular momentum. The definitions of E and L_z lead to

$$\dot{t} = \frac{E g_{\phi\phi} + L_z g_{t\phi}}{g_{t\phi}^2 - g_{tt} g_{\phi\phi}}, \tag{3.59}$$

[1] For a discussion of the order in the perturbation used to compute the Petrov Type see [57].

$$\dot{\phi} = -\frac{E g_{t\phi} + L_z g_{tt}}{g_{t\phi}^2 - g_{tt} g_{\phi\phi}}, \tag{3.60}$$

where the overhead dot represents a derivative with respect to the affine parameter. Substituting the above equations into $u^a u_a = -1$, where u^a is the particle's four-velocity, we find

$$g_{rr}\dot{r}^2 + g_{\theta\theta}\dot{\theta}^2 = V_{\text{eff}}(r, \theta; E, L_z), \tag{3.61}$$

where the effective potential is

$$V_{\text{eff}} \equiv \frac{E^2 g_{\phi\phi} + 2EL_z g_{t\phi} + L_z^2 g_{tt}}{g_{t\phi}^2 - g_{tt} g_{\phi\phi}} - 1. \tag{3.62}$$

For simplicity, we restrict our attention to equatorial, circular orbits. E and L_z can then be obtained from $V_{\text{eff}} = 0$ and $\partial V_{\text{eff}}/\partial r = 0$ in the form

$$E = E_{\text{K}} + \delta E, \tag{3.63}$$

$$L_z = L_{z,\text{K}} + \delta L_z. \tag{3.64}$$

E_{K} and $L_{z,\text{K}}$ are the energy and z component of the orbital angular momentum for the Kerr spacetime given by [157]

$$E_{\text{K}} \equiv \frac{r^{3/2} - 2Mr^{1/2} + aM^{1/2}}{r^{3/4}\left(r^{3/2} - 3Mr^{1/2} + 2aM^{1/2}\right)^{1/2}}, \tag{3.65}$$

$$L_{z,\text{K}} \equiv \frac{M^{1/2}\left(r^2 - 2aM^{1/2}r^{1/2} + a^2\right)}{r^{3/4}\left(r^{3/2} - 3Mr^{1/2} + 2aM^{1/2}\right)^{1/2}}, \tag{3.66}$$

where ϕ is defined to be positive in the direction of prograde orbits. This implies negative a corresponds to retrograde orbits. The corrections from EdGB are

$$\begin{aligned}\delta E \equiv &-\frac{1}{12}\zeta\frac{M^3}{r^{3/2}\left(r-3M\right)^{3/2}}\left(1+\frac{54M}{r}+\frac{198}{5}\frac{M^2}{r^2}+\frac{252}{5}\frac{M^3}{r^3}-\frac{2384}{5}\frac{M^4}{r^4}+\frac{480M^5}{r^5}\right)\\&+\frac{23}{20}\zeta\chi\frac{M^{9/2}}{r^2\left(r-3M\right)^{5/2}}\left(1+\frac{492}{23}\frac{M}{r}-\frac{458}{23}\frac{M^2}{r^2}-\frac{8}{23}\frac{M^3}{r^3}-\frac{4272}{23}\frac{M^4}{r^4}+\frac{5760}{23}\frac{M^5}{r^5}\right)\\&+\frac{205821}{441000}\zeta\chi^2\frac{r^{1/2}M^3}{\left(r-3M\right)^{7/2}}\left(1+\frac{29926}{9801}\frac{M}{r}-\frac{2584229}{68607}\frac{M^2}{r^2}-\frac{317782}{68607}\frac{M^3}{r^3}\right.\\&+\frac{14792212}{205821}\frac{M^4}{r^4}+\frac{207551}{6237}\frac{M^5}{r^5}+\frac{5757700}{9801}\frac{M^6}{r^6}-\frac{257772890}{205821}\frac{M^7}{r^7}+\frac{4064600}{9801}\frac{M^8}{r^8}\\&\left.-\frac{6499000}{3267}\frac{M^9}{r^9}+\frac{4715200}{1089}\frac{M^{10}}{r^{10}}-\frac{280000}{121}\frac{M^{11}}{r^{11}}\right),\end{aligned}\tag{3.67}$$

$$\begin{aligned}\delta L_z \equiv &-\frac{1}{4}\zeta\frac{M^{5/2}}{\left(r-3M\right)^{3/2}}\left(1+\frac{100}{3}\frac{M}{r}-\frac{30M^2}{r^2}+\frac{16}{5}\frac{M^3}{r^3}-\frac{752}{3}\frac{M^4}{r^4}+\frac{320M^5}{r^5}\right)\\&+\frac{30}{20}\zeta\chi\frac{M^4}{r^{1/2}\left(r-3M\right)^{5/2}}\left(1+\frac{31}{2}\frac{M}{r}-\frac{47}{3}\frac{M^2}{r^2}+\frac{M^3}{r^3}-\frac{126M^4}{r^4}+\frac{1976}{15}\frac{M^5}{r^5}\right.\\&\left.+\frac{80M^6}{r^6}\right)+\frac{617463}{441000}\zeta\chi^2\frac{r^2M^{5/2}}{\left(r-3M\right)^{7/2}}\left(1-\frac{86288}{29403}\frac{M}{r}-\frac{2144627}{205821}\frac{M^2}{r^2}+\frac{924068}{68607}\frac{M^3}{r^3}\right.\\&+\frac{27006916}{617463}\frac{M^4}{r^4}-\frac{18616907}{205821}\frac{M^5}{r^5}+\frac{49732516}{205821}\frac{M^6}{r^6}-\frac{427757690}{617463}\frac{M^7}{r^7}\\&\left.+\frac{197940200}{205821}\frac{M^8}{r^8}-\frac{12547000}{9801}\frac{M^9}{r^9}+\frac{4715200}{3267}\frac{M^{10}}{r^{10}}-\frac{280000}{363}\frac{M^{11}}{r^{11}}\right).\end{aligned}\tag{3.68}$$

Expanding E and L_z in powers of M/r, the leading-order corrections to the binding energy $E_b \equiv E-1$ and L_z are

$$E_b = E_{b,\mathrm{K}}\left[1+\frac{1}{6}\zeta\frac{M^2}{r^2}\left(1-\frac{9801}{1750}\chi^2\right)\right],\tag{3.69}$$

$$L_z = L_{z,\mathrm{K}}\left[1-\frac{1}{4}\zeta\frac{M^2}{r^2}\left(1-\frac{9801}{1750}\chi^2\right)\right].\tag{3.70}$$

Note that the corrections are of 2PN order [proportional to $(M/r)^2$] relative to the leading-order Kerr terms for the energy and angular momentum respectively. These results agree with those of [85] to leading order in χ.

3.5.2 Kepler's third law

The correction to Kepler's third law for a circular orbit can be found by calculating the orbital angular frequency of a test-particle $\omega \equiv L_z/r^2$,

$$\omega^2 = \omega_{\rm K}^2 \left[1 - \frac{1}{2}\zeta \frac{M^2}{r^2}\left(1 - \frac{9801}{1750}\chi^2\right)\right], \tag{3.71}$$

where $\omega_{\rm K}^2 \equiv M\left(r^{3/2} + aM^{1/2}\right)^{-2}$ [157].

The expressions above for E, L_z, and ω are not gauge invariant. We can obtain gauge invariant relations between E and ω by expanding Eqs. 3.69 and 3.71 to 2PN order and eliminating M/r. The result is

$$\begin{aligned}\omega(E) =& \frac{2\sqrt{2}}{M}|E_b|^{3/2}\left\{1 + \frac{9}{4}|E_b| + 8\sqrt{2}\chi|E_b|^{3/2}\right. \\ &\left. + \frac{891}{32}\left[1 + \frac{64}{297}\chi^2 - \frac{32}{891}\zeta\left(1 - \frac{9801}{1750}\chi^2\right)\right]|E_b|^2\right\} + \mathcal{O}\left[|E_b|^4\right],\end{aligned} \tag{3.72}$$

and its inverse

$$\begin{aligned}E(\omega) =& 1 - \frac{1}{2}(M\omega)^{2/3} + \frac{3}{8}(M\omega)^{4/3} - \frac{4}{3}\chi(M\omega)^{5/3} \\ &+ \frac{27}{16}\left[1 + \frac{8}{27}\chi^2 - \frac{4}{81}\zeta\left(1 - \frac{9801}{1750}\chi^2\right)\right](M\omega)^2 + \mathcal{O}\left[(M\omega)^{7/3}\right].\end{aligned} \tag{3.73}$$

This agrees with the standard PN E-ω relation to $\mathcal{O}(\alpha'^0\chi'^0)$ [158].

3.5.3 ISCO

Let us now derive the location of the ISCO in this new spacetime. We do so by substituting Eqs. 3.63 and 3.64 into Eq. 3.62, and then solving $\partial^2 V_{\rm eff}/\partial r^2 = 0$ for r. The result is

$$r_{\rm ISCO} = r_{\rm ISCO,K} - \frac{16297}{9720}\zeta M\left(1 + \frac{205982\sqrt{6}}{440019}\chi - \frac{1167369773}{9702418950}\chi^2\right), \tag{3.74}$$

where the Kerr ISCO radius is given by [157]

$$r_{\rm ISCO,K} \equiv M\left\{3 + Z_2 - \left[(3 - Z_1)\left(3 + Z_1 + 2Z_2\right)\right]^{1/2}\right\} \tag{3.75}$$

with

$$Z_1 \equiv 1 + \left(1 - \chi^2\right)^{1/3}\left[(1+\chi)^{1/3} + (1-\chi)^{1/3}\right], \tag{3.76}$$

$$Z_2 \equiv \left(3\chi^2 + Z_1^2\right)^{1/2}. \tag{3.77}$$

The EdGB correction at $\mathcal{O}(\chi'^0)$ agrees with that found in [85]. Note that the radial location of the ISCO is not gauge invariant. For a gauge invariant quantity, we compute the angular orbital frequency at ISCO, $\omega_{\rm ISCO}$:

$$\omega_{\rm ISCO} = \omega_{\rm ISCO,K} - \frac{13571\sqrt{3}}{3149280}\zeta\frac{1}{M}\left(1 + \frac{129655\sqrt{6}}{122139}\chi + \frac{2740701487}{897721650}\chi^2\right), \tag{3.78}$$

where $\omega_{\rm ISCO,K} = M^{1/2}\left(r_{\rm ISCO,K}^{3/2} + \chi M^{3/2}\right)^{-1}$.

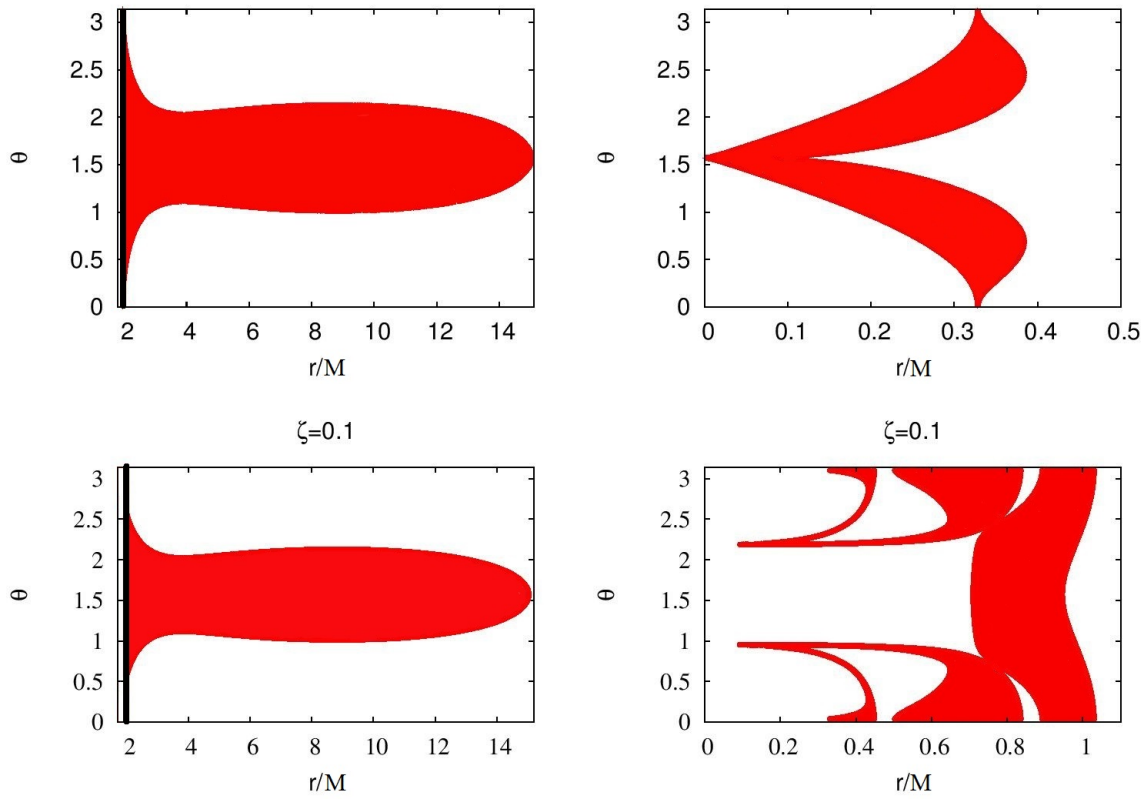

Figure 3.1: Curves of zero velocity ($V_{\rm eff} = 0$) for the Kerr (top) and EdGB (bottom) metric with $\zeta = 0.1$. The red shaded regions show the allowed bound-orbit regions ($V_{\rm eff} \geq 0$) with $E = 0.95$, $L_z = 3M$, and $\chi = 0.3$. The left panels corresponds to the region outside the horizon, while the right ones show the region inside the horizon. The thick black lines at $r/M = 1.955$ (top) and $r/M = 1.832$ (bottom) correspond to the location of the horizon for this example.

3.5.4 Curves of zero velocity

Last, we will consider curves of zero velocity (CZVs) [159, 160] in the r-θ plane. These curves are where $V_{\rm eff} = 0$ and since the left-hand side of Eq. 3.62 is always positive, bound orbits are allowed only if $V_{\rm eff} \geq 0$. Figure 3.1 shows the CZVs for the Kerr and the new solution. Red shaded regions are where $V_{\rm eff} \geq 0$ and the thick black lines correspond to the location of the event horizon for the particular case considered

in the figures. To draw these figures, we expand the metric g_{ab} in the spin parameter a and then calculate $V_{\rm eff}$.

For both the GR and EdGB case there is one allowed bound-orbit region clearly visible in the region outside of the event horizon. For the region inside the horizon, there is one allowed orbit region in GR, but there are five in the EdGB case. While the regions outside the horizon look similar in GR and EdGB, there are differences not easily visible due to the scale of the figures.The orbits in this outer region are, in principle, distinguishable with gravitational wave observations, as shown in [161] and [162]. The inner regions are drastically different, which is expected as the field is strongest within the horizon and the EdGB corrections modify the strong field regime. However, since these inner regions are within the horizon they cannot be probed with any observations.

3.6 Conclusion

We found a stationary, axisymmetric BH solution in EdGB gravity in the small-coupling and slow-rotation approximations at linear order in the coupling constant and quadratic order in the spin. The technique used, based on BH perturbation theory, involved decomposing the metric perturbation and source terms in tensor spherical harmonics, which reduced the field equations to a set of coupled, ordinary differential equations. We found new corrections to the metric at quadratic order in spin. We then studied a plethora of properties of this metric, proving that (i) it possesses a curvature singularity inside an event horizon, (ii) the location of the event horizon, ergosphere, horizon area and horizon's angular velocity are all modified relative to the Kerr analogue and (iii) that test-particle orbits in this spacetime are different than those in Kerr due to corrections in the orbital binding energy, angular momentum and effective potential.

As the method used is not specialized to quadratic order in spin and linear order in the coupling constant, an obvious extension of this work is to find solutions to higher order in spin and/or higher order in the coupling constant. In the case of EdGB, however, as it is a linear-order truncation in the coupling constant of a more fundamental theory, any solution is only valid to linear order in the coupling constant.

An interesting and nontrivial property of the new solution is that it is of Petrov type I. This is especially interesting because to zeroth and linear order in spin the solution remains of Petrov type D, and because the Kerr metric is of Petrov type D to all orders in spin. This suggests that the full, exact solution must also be of Petrov type I. Petrov type I spacetimes do not possess a second-order Killing tensor or a Carter-like constant. This implies that geodesic motion may by chaotic once corrections of $\mathcal{O}(\alpha'^2\chi'^2)$ are included. Future work could study whether geodesics in this new metric are chaotic, specifically if there exist chaotic orbits outside of the event horizon.

The new metric solution as well as its properties are important in determining the properties of electromagnetic radiation from accretion disks around a BH. Observations of the electromagnetic radiation near observable BHs, such as Sgr A*, can be a powerful way to test GR [42]. An avenue of study would be to determine how observables, such as BH shadows [163] and strong lensing [164], are modified if the BH is described by the new solution found in this paper. Of course, the metric derived here would be appropriate for such tests if and only if the black hole observed has a sufficiently small spin, roughly $J^2/M^4 \lesssim 0.5$. For other, more rapidly rotating black holes, either numerical solutions would have to be used or a higher-order-in-spin approximate solution would have to be derived.

3.7 Acknowledgements

We thank Kent Yagi for useful discussions. N.Y. acknowledges support from NSF Grant PHY-1114374 and the NSF CAREER Grant No. PHY-1250636, as well as support provided by the National Aeronautics and Space Administration from Grant No. NNX11AI49G, under sub-award 00001944. This research was supported in part by the National Science Foundation under Grant No. NSF PHY11-25915. Some calculations used the computer algebra systems MAPLE, in combination with the GRTensor II package [121].

CAN THE SLOW-ROTATION APPROXIMATION BE USED IN ELECTROMAGNETIC OBSERVATIONS OF BLACK HOLES?

Contribution of Authors and Co-Authors

Manuscript in Chapter 4

Author: Dimitry Ayzenberg

Contributions: Conceived and implemented the study design. Wrote first draft of the manuscript.

Co-Author: Dr. Kent Yagi

Contributions: Helped conceive the study design. Provided feedback of analysis and comments on drafts of the manuscript.

Co-Author: Dr. Nicolás Yunes

Contributions: Helped conceive the study design. Provided feedback of analysis and comments on drafts of the manuscript.

Manuscript Information Page

Dimitry Ayzenberg, Kent Yagi, Nicolás Yunes

Classical and Quantum Gravity

Status of Manuscript:

___Prepared for submission to a peer-reviewed journal

___Officially submitted to a peer-reviewed journal

___Accepted by a peer-reviewed journal

_x_Published in a peer-reviewed journal

Published by the Institute of Physics

Published April, 2016, Class. Quant. Grav. 33, 105006

Abstract

Future electromagnetic observations of black holes may allow us to test General Relativity in the strong-field regime. Such tests, however, require knowledge of rotating black hole solutions in modified gravity theories, a class of which does not admit the Kerr metric as a solution. Several rotating black hole solutions in modified theories have only been found in the slow-rotation approximation (i.e. assuming the spin angular momentum is much smaller than the mass squared). We here investigate whether the systematic error due to the approximate nature of these black hole metrics is small enough relative to the observational error to allow their use in electromagnetic observations to constrain deviations from General Relativity. We address this by considering whether electromagnetic observables constructed from a slow-rotation approximation to the Kerr metric can fit observables constructed from the full Kerr metric with systematic errors smaller than current observational errors. We focus on black hole shadow and continuum spectrum observations, as these are the least influenced by accretion disk physics, with current observational errors of about 10%. We find that the fractional systematic error introduced by using a second-order, slowly rotating Kerr metric is at most 2% for shadows created by black holes with dimensionless spins $\chi \leq 0.6$. We also find that the systematic error introduced by using the slowly rotating Kerr metric as an exact metric when constructing continuum spectrum observables is negligible for black holes with dimensionless spins of $\chi \lesssim 0.9$. Our results suggest that the modified gravity solutions found in the slow-rotation approximation may be used to constrain realistic deviations from General Relativity with continuum spectrum and black hole shadow observations.

4.1 Introduction

In the next five to ten years, current and new, ground and space-based telescopes will provide unprecedented electromagnetic observations of black holes (BHs). The Event Horizon Telescope (EHT) is already taking images of the BH shadow of Sagittarius A* and the supermassive BH at the center of M87, placing some bounds on each BH's angular momentum, as well as providing evidence of their event horizons [131–135, 165–169]. As more telescopes are added to the EHT, the quality of images of the shadows will only improve. Past telescopes, such as the Rossi X-ray Timing Explorer (RXTE), and current telescopes, such as the Chandra X-ray

Observatory, XMM-Newton, and NuSTAR, have observed continuum spectra and Kα iron line emissions from the accretion disk of stellar mass and supermassive BHs, allowing for estimates of the angular momenta of a few dozen BHs [8]. ASTRO-H, launching this year, will provide significantly more accurate estimates of BH angular momenta, possibly doubling the current number of estimates and improving on past estimates over the next decade [170].

Electromagnetic observations of BHs are of paramount importance to learning about BH and accretion disk physics, but also, they can be excellent tools in experimental relativity. These observations can tell us about the mass and spin angular momenta of BHs, as well as about accretion disk properties, such as the temperature, accretion rate, short and long term evolution of the disk, and the presence and strength of magnetic fields [11,171]. These electromagnetic observations, however, can also be used, at least in principle, to test General Relativity (GR) in the *strong-field* regime [16,37,42], i.e. where the gravitational interaction is non-linear and the spacetime curvature is large.

The astrophysical information in these electromagnetic observations is teased from the noise through modeling of the expected signal and its fitting to the data. In the BH shadow case, one observes the shadow cast by the BH on its accretion disk. This shadow can be modeled through null-ray tracing on the BH spacetime. In the continuum spectrum case, one observes X-ray radiation emitted by the disk around the BH. This spectrum can be modeled as a black body with the disk described by the Novikov-Thorne [12] approach for geometrically-thin and optically-thick disks. With models for the observables at hand, one then fits the parameters of the model to the data, exploring the likelihood surface, for example, through Markov-Chain Monte-Carlo techniques.

Such electromagnetic observations depend on the properties of the BH spacetime. BH shadows are sensitive to the location of the photon sphere, the surface inside which photon orbits are unstable [172]. In principle, the image is contaminated by accretion flow, but this can be removed without a model through image processing methods, such as gradient detection [77]. Continuum spectra in thin disks are sensitive to emission near the inner edge of the disk, which can be well approximated by the innermost stable circular orbit (ISCO) [16]. In principle, there is radiation also originating inside the ISCO, but this has been shown to be subdominant [21–26].

Electromagnetic observations of BHs could then allow us, at least in principle, to determine whether BH spacetimes are truly described by the Kerr metric. The *Kerr hypothesis* states that all isolated, stationary and axisymmetric astrophysical (uncharged) BHs are described by the Kerr metric, and therefore are completely determined by two parameters, their mass M and (the magnitude of) their spin angular momentum $|\vec{J}|$ [136–141]. The Kerr metric is the external spacetime of a Ricci-flat, stationary, and axisymmetric (uncharged) BH, which is a solution to the Einstein equations in vacuum, but it can also be a solution in certain modified gravity theories [173]. Some modified theories of gravity, however, do not satisfy the Kerr hypothesis, and thus, electromagnetic observations of BHs could allow us to place constraints on these.

Rotating BH solutions in modified gravity theories, unfortunately, are not easy to find. Although some numerical solutions valid for arbitrary rotation are known [143, 174, 175], most BH solutions are obtained in the slow-rotation approximation [57, 86, 107, 109, 176–183] (e.g. in dynamical Chern-Simons (dCS) gravity [57, 84, 107–109, 184–187]). This approximation assumes the BH spin angular momentum J is much smaller than its mass squared M^2, and thus, one expands the field equations in the ratio $|\vec{J}|/M^2$. Lacking an exact solution in these theories that is valid for all spin

magnitudes, the regime of validity of these metrics is not clear. Thus, it is not clear either whether the approximate nature of these spacetimes has a significant impact on electromagnetic observables. Some observations may be less sensitive to the slow-rotation approximation than others, and whether this sensitivity matters ultimately depends on the accuracy of the observations.

The goal of this paper is to determine whether such approximate, slowly rotating BH solutions in modified gravity theories can be used to construct electromagnetic observables with which to test these theories. As a first step toward answering this question we investigate how well electromagnetic observables constructed from the slow-rotation approximation to the Kerr metric can fit observables constructed with the full Kerr solution. We specifically study BH shadow and continuum spectrum observations of BHs because they are strongly dependent on the background metric and weakly dependent on the properties of the accretion disk.

Whether the slow-rotation approximation can be used in tests of GR will depend on whether the errors introduced by this approximation are larger than other statistical, instrumental, environmental and systematic errors inherent in electromagnetic observations. Statistical error arises due to the finite accuracy and length of observation of telescopes, as well as due to covariances in the model parameters [16]. Instrumental error is rooted, for example, in inaccuracies in the calibration of the telescopes, while environmental error is sourced, for example, by atmospheric events. The combination of statistical, instrumental and environmental error will be referred to here as *observational error*, and it affects the accuracy to which BH properties can be estimated by roughly 10% [8, 77]. Astrophysical systematic error is sourced by our imperfect knowledge of the astrophysical model for the electromagnetic observable. Since accretion disks can be quite complicated and there are a number of models for them, there is still great uncertainty over which

model(s) best describes observations [11, 171]. The impact of this uncertainty on the estimated model parameters is not quantitively known, and thus, we will not take it into account when comparing the slow-rotation systematic error to the observational error[1].

We show that the slowly rotating approximation of the Kerr metric, when appropriately resummed, is a very accurate representation of the full Kerr metric for continuum spectrum and BH shadow observations. The continuum spectrum of the slowly rotating Kerr metric agrees with the spectrum of the full Kerr metric to within our numerical accuracy with reduced $\chi^2 < 10^{-6}$ for BHs with $\vec{J}/M^2 \lesssim 0.9$. The BH shadows agree to within 2%, with reduced $\chi^2 \lesssim 10^{-3}$ for BHs with $\vec{J}/M^2 \lesssim 0.6$. In both cases, the systematic error introduced by the approximate nature of the slowly rotating metric is much smaller than the observational error.

We also show that the maximum spin values mentioned above are not determined by the systematic error exceeding the observational error, but rather by the slowly rotating spacetime ceasing from being a physically valid metric. In the continuum spectrum case, curvature singularities appear outside of the BH event horizon when $|\vec{J}|/M^2 \gtrsim 0.9$. In the BH shadow case, the photon sphere falls inside of the event horizon when $\vec{J}/M^2 \gtrsim 0.6$. These values of spin angular momenta, thus, provide natural cutoffs above which the approximate slowly rotating metric should no longer be used.

The remainder of this paper presents the details pertaining to these results. Section 4.2 presents the Kerr and slowly rotating solutions, as well as the relevant properties of each. Section 4.3 details how the continuum spectrum is calculated, the

[1]Astrophysical systematic error should, in principle, be added to observational error, when comparing to the systematic error introduced by the slow-rotation approximation. Neglecting astrophysical systematics, thus, yields a conservative bound of the $|\vec{J}|/m^2$ range for which the slow-rotation approximation is valid.

methodology of our analysis, and the results. Section 4.4 presents the same for the BH shadow. Section 4.5 concludes by summarizing our results and discussing the implications. Throughout, we use the following conventions: the metric signature $(-,+,+,+)$; Latin letters in index lists stand for spacetime indices; geometric units with $G = c = 1$ (e.g. $1M_\odot$ becomes 1.477 km by multiplying by G/c^2 or 4.93×10^{-6} s by multiplying by G/c^3), except where otherwise noted.

4.2 Rotating BH Solutions

The Kerr metric in Boyer-Lindquist coordinates (t, r, θ, ϕ) is given by

$$\begin{aligned} ds^2_{\rm K} = &- \left(1 - \frac{2Mr}{\Sigma_{\rm K}}\right) dt^2 - \frac{4Mar\sin^2\theta}{\Sigma_{\rm K}} dt d\phi + \frac{\Sigma_{\rm K}}{\Delta_{\rm K}} dr^2 \\ &+ \Sigma_{\rm K} d\theta^2 + \left(r^2 + a^2 + \frac{2Ma^2 r \sin^2\theta}{\Sigma_{\rm K}}\right) \sin^2\theta d\phi^2, \end{aligned} \tag{4.1}$$

with $\Delta_{\rm K} \equiv r^2 - 2Mr + a^2$ and $\Sigma_{\rm K} \equiv r^2 + a^2\cos^2\theta$. Here M is the mass of the BH and $a \equiv J/M$ is the Kerr spin parameter, where $J := |\vec{J}|$ is the magnitude of the BH spin angular momentum.

The slowly rotating approximation to the Kerr metric is found by expanding the Kerr metric to a given order in the dimensionless spin parameter $\chi \equiv a/M$. To quadratic order, one finds

$$\begin{aligned} ds^2_{\rm SR} = &- \left(f_{\rm S} + \frac{2Ma^2\cos^2\theta}{r^3}\right) dt^2 - \frac{4Ma\sin^2\theta}{r} dt d\phi \\ &+ \left[\frac{1}{f_{\rm S}} - \frac{a^2}{r^2 f_{\rm S}^2}\left(1 - f_{\rm S}\cos^2\theta\right)\right] dr^2 + \left(r^2 + a^2\cos^2\theta\right) d\theta^2 \\ &+ \left[r^2 + a^2\left(1 + \frac{2M}{r}\sin^2\theta\right)\right] \sin^2\theta d\phi^2 \,, \end{aligned} \tag{4.2}$$

where $f_{\rm S} = 1 - 2M/r$ is the Schwarzschild factor. Note that the controlling factor in this approximation, i.e. the background metric, is nothing but the Schwarzschild metric in Schwarzschild coordinates. Note also that both the background and its perturbation diverge at $f_{\rm S} = 0$, i.e. at the Schwarzschild event horizon due to a coordinate singularity. Note finally that in the equatorial plane ($\theta = \pi/2$) the Kerr metric and the slowly rotating metric only differ in the g_{rr} component[2].

This paper is concerned with studying whether the approximate slowly rotating BH solutions of certain modified gravity theories suffice to carry out tests of GR with electromagnetic observations. This is important because exact BH solutions valid for any spin are currently not available in many modified theories. To address this problem we will treat the Kerr metric of Eq. 4.1 as the correct solution of Nature for rotating BHs and study whether the slowly rotating metric of Eq. 4.2 is sufficiently accurate to model the true electromagnetic observables. That is, we will use the Kerr metric to create simulated data for electromagnetic observables and then attempt to extract these observables with a model based on the approximate, slowly rotating metric. The whole point of this analysis is to determine the range of spins for which the systematic error we will incur in the extraction of parameters from this approximate model is smaller than the statistical errors due to observational uncertainties.

One can enhance the accuracy of the model for electromagnetic observables constructed with the slowly rotating metric by *resumming* the latter in spin. An example of what we mean by resummation in this paper is the replacement $r \to \Sigma_{\rm K}^{1/2}$. Of course, if one does not know the functional form of the exact solution valid for all spins (i.e. the Kerr metric in this case), one does not know how to resum the

[2]Certain rotating BH solutions valid for arbitrary spin in modified theories of gravity, such as rotating dilaton BHs [188], share the same property.

approximate solution. Indeed, there are an infinite number of possible resummations of the slowly rotating metric that generate an infinite number of different resummed metrics, all of which agree in the far-field regime but potentially disagree close to the event horizon. Perhaps, the most straightforward resummation one can think of is to simply treat the slowly rotating metric as *exact* (i.e. not expanding in χ when computing observables) and study the consequences of making such a choice. Of course, the electromagnetic model one will obtain from this resummed treatment of the slowly rotating metric will still be different from the simulated data constructed from the Kerr metric, which will thus still introduce a systematic error in the extraction of parameters.

Resumming the slowly rotating metric is not only done to enhance the accuracy of the model, but also to simplify the calculation of electromagnetic observables. A consistent treatment in slow-rotation, where one expands all calculations to second order in χ, is not straightforward when computing electromagnetic observables through *numerical* ray-tracing algorithms. This is simply because once the slowly rotating metric has been numerically sampled discretely, the null geodesic equations can no longer be expanded in χ. Henceforth, we treat the slowly rotating metric as exact when computing the electromagnetic model that we fit to the simulated Kerr data.

4.2.1 Properties of the BH Metrics

4.2.1.1 Event Horizon

The event horizon is defined as a null surface created by null geodesic generators. The normal to the surface n^a must itself be null, thus event horizons must satisfy the horizon equation

$$g^{ab}\partial_a F \partial_b F = 0, \tag{4.3}$$

where $F(x^a)$ is a level surface function that defines the location of the horizon, where $n_a = \partial_a F$. Since the spacetime is stationary, axisymmetric, and reflection symmetric about the poles and the equator, the level surfaces can only depend on radius. Without loss of generality, we let $F(x^a) = r - r_{\rm H}$, where $F = 0$ yields the radial horizon location. Equation 4.3 then becomes $g^{rr} = 0$, and this metric element in the Kerr and resummed slowly rotating BH spacetimes is given by

$$g^{rr}_{\rm K} = \frac{\Delta_{\rm K}}{\Sigma_{\rm K}} = \frac{r^2 - 2Mr + a^2}{r^2 + a^2\cos^2\theta}, \tag{4.4}$$

$$g^{rr}_{\rm SR} = \frac{r^3\left(1 - \frac{2M}{r}\right)^2}{r^3 - 2Mr^2 - a^2 r\sin^2\theta - 2Ma^2\cos^2\theta}. \tag{4.5}$$

Notice that we do not re-expand $g^{rr}_{\rm SR}$ in slow-rotation, since we are treating the slowly rotating metric as exact. This is the first example we encounter in this paper that exemplifies the resummation described earlier.

We find the horizon location by solving $g^{rr} = 0$ with the Kerr and the resummed slowly rotating metric for the horizon radius, which yields

$$r_{\rm H,K} = M + (M^2 - a^2)^{1/2}, \tag{4.6}$$

$$r_{\rm H,SR} = 2M. \tag{4.7}$$

Notice that the horizon location of the resummed slowly rotating Kerr metric agrees with that of the Schwarzschild metric, yet it is different from expanding $r_{\rm H,K}$ to quadratic order in spin.

4.2.1.2 Conserved Quantities Both the Kerr metric and slowly rotating metric are stationary and axisymmetric, and thus, each possesses a timelike and an azimuthal Killing vector, implying the existence of two conserved quantities: the specific energy E and the z-component of the specific angular momentum L_z. The corresponding components of the four-momentum are $p_t = -E$ and $p_\phi = L_z$. From this we find two of the geodesic equations:

$$\dot{t} = \frac{E g_{\phi\phi} + L_z g_{t\phi}}{g_{t\phi}^2 - g_{tt} g_{\phi\phi}}, \tag{4.8}$$

$$\dot{\phi} = -\frac{E g_{t\phi} + L_z g_{tt}}{g_{t\phi}^2 - g_{tt} g_{\phi\phi}}, \tag{4.9}$$

where the overhead dot represents a derivative with respect to the affine parameter (proper time for a massive particle).

With these constants of the motion, we can write the motion of test particles on these backgrounds in first-order form. Substituting Eqs. 4.8 and 4.9 into the normalization condition $u^a u_a = -1$, where $u^a = (\dot{t}, \dot{r}, \dot{\theta}, \dot{\phi})$ is the particle's four-velocity, we find

$$g_{rr}\dot{r}^2 + g_{\theta\theta}\dot{\theta}^2 = V_{\rm eff}(r, \theta; E, L_z), \tag{4.10}$$

where the effective potential is

$$V_{\rm eff} \equiv \frac{E^2 g_{\phi\phi} + 2E L_z g_{t\phi} + L_z^2 g_{tt}}{g_{t\phi}^2 - g_{tt} g_{\phi\phi}} - 1. \tag{4.11}$$

We restrict attention to equatorial, circular orbits of test particles in these backgrounds. We can then solve $V_{\text{eff}} = 0$ and $\partial V_{\text{eff}}/\partial r = 0$ for E and L_z to find

$$E = -\frac{g_{tt} + g_{t\phi}\Omega}{\sqrt{-\left(g_{tt} + 2g_{t\phi}\Omega + g_{\phi\phi}\Omega^2\right)}}, \tag{4.12}$$

$$L_z = \frac{g_{t\phi} + g_{\phi\phi}\Omega}{\sqrt{-\left(g_{tt} + 2g_{t\phi}\Omega + g_{\phi\phi}\Omega^2\right)}}, \tag{4.13}$$

where

$$\Omega = \frac{d\phi}{dt} = \frac{-g_{t\phi,r} + \sqrt{\left(g_{t\phi,r}\right)^2 - g_{tt,r}g_{\phi\phi,r}}}{g_{\phi\phi,r}}, \tag{4.14}$$

represents the angular velocity of equatorial circular geodesics, i.e. the angular velocity of zero angular-momentum observers. Since the Kerr metric and the slowly rotating metric in the equatorial plane are the same except for the g_{rr} component, the energy and angular momentum are also the same in both spacetimes as neither depends on g_{rr}.

4.2.1.3 ISCO The ISCO plays a very important role in the calculation of the continuum spectrum of an accretion disk model. This is because any test particle inside the ISCO plunges, rapidly crossing the event horizon. Many accretion disk models assume the inner radius of the disk is at the ISCO, an assumption well-motivated by physical arguments, simulations, and observational evidence [21–25]. We make this same assumption throughout this work.

The ISCO radius can be found by substituting Eqs. (4.12) and (4.13) into Eq. (4.11), and then solving $\partial^2 V_{\text{eff}}/\partial r^2 = 0$ for r. Note this will be the same in both Kerr and the slowly rotating spacetime on the equatorial plane because Eqs. (4.11)–

(4.13) do not depend on g_{rr}. The ISCO radius for equatorial geodesics is then

$$r_{\rm ISCO} = M\left\{3 + Z_2 \mp \left[(3 - Z_1)\,(3 + Z_1 + 2Z_2)\right]^{1/2}\right\}, \tag{4.15}$$

where

$$Z_1 = 1 + \left(1 - \chi^2\right)^{1/3}\left[(1+\chi)^{1/3} + (1-\chi)^{1/3}\right], \tag{4.16}$$

$$Z_2 = \left(3\chi^2 + Z_1^2\right)^{1/2}, \tag{4.17}$$

and $\mp$ denotes whether the accretion disk's angular momentum is in the same $(-)$ or opposite $(+)$ direction as the BH's angular momentum.

The ISCO of the resummed slowly rotating Kerr metric can be inside of its event horizon, since the former can shrink all the way down to M for maximal spins ($\chi = 1$), while the latter stays at $2M$. This is, of course, a problem if one is concerned with observables that depend sensitively on the location of the ISCO, as is the case for continuum spectrum observations. However, as we will discuss in the following section, there is an upper spin limit above which the resummed slowly rotating metric is no longer valid (essentially due to the metric determinant vanishing); this upper limit excludes values of spin for which the location of the ISCO is smaller than $2M$. Thus, the fact that the ISCO can un-physically enter the horizon for the resummed slowly rotating Kerr metric will not be a concern in this paper.

4.2.1.4 Metric Determinant The metric determinant is necessary to calculate observables in continuum spectrum observations, as we will discuss in Sec. 4.3. The

metric determinants of the Kerr and the resummed slowly rotating metrics are

$$\mathbf{g}_{\mathrm{K}} = -r^2, \tag{4.18}$$

$$\mathbf{g}_{\mathrm{SR}} = -r^2 \frac{\left(1 - \frac{2M}{r} + \frac{a^2}{r^2}\right)\left(1 - \frac{2M}{r} - \frac{a^2}{r^2}\right)}{\left(1 - \frac{2M}{r}\right)^2}, \tag{4.19}$$

respectively. Notice that if we were to consistently expand $\mathbf{g}_{\mathrm{SR}}$ to $\mathcal{O}(\chi^2)$, we would find that it equals $\mathbf{g}_{\mathrm{K}}$ plus uncontrolled remainders of $\mathcal{O}(\chi^4)$, but again, we do not do so since we treat the slowly rotating metric as exact.

The metric determinant can be used to define a region of validity for the resummed slowly rotating metric in the context of the continuum spectrum. This is because the energy flux goes as $1/\sqrt{-\mathbf{g}}$, as we will discuss in Sec. 4.3, and thus it diverges when the determinant vanishes. Physically, this is because the determinant of the metric is tied to the Lorentz signature of spacetime. Requiring that the determinant be strictly negative everywhere outside the ISCO requires that $\chi \lesssim 0.8967$. Figure 4.1 shows the radial profile of the ratio between the metric determinants of the slowly rotating and Kerr spacetimes.

With this cutoff there are still values of χ for which the slowly rotating metric determinant changes sign outside the horizon radius but inside the ISCO. The Lorentz signature not being preserved outside the horizon suggests the slowly rotating solution is not well-justified for those values of spin. As we will discuss, though, the continuum spectrum calculation we use ignores any behavior below the ISCO radius; this is supported by simulations that take into account emission inside the ISCO radius and find that the contribution of that emission is below typical observational errors [26]. Thus, continuum spectrum observables in this model should not be affected by the

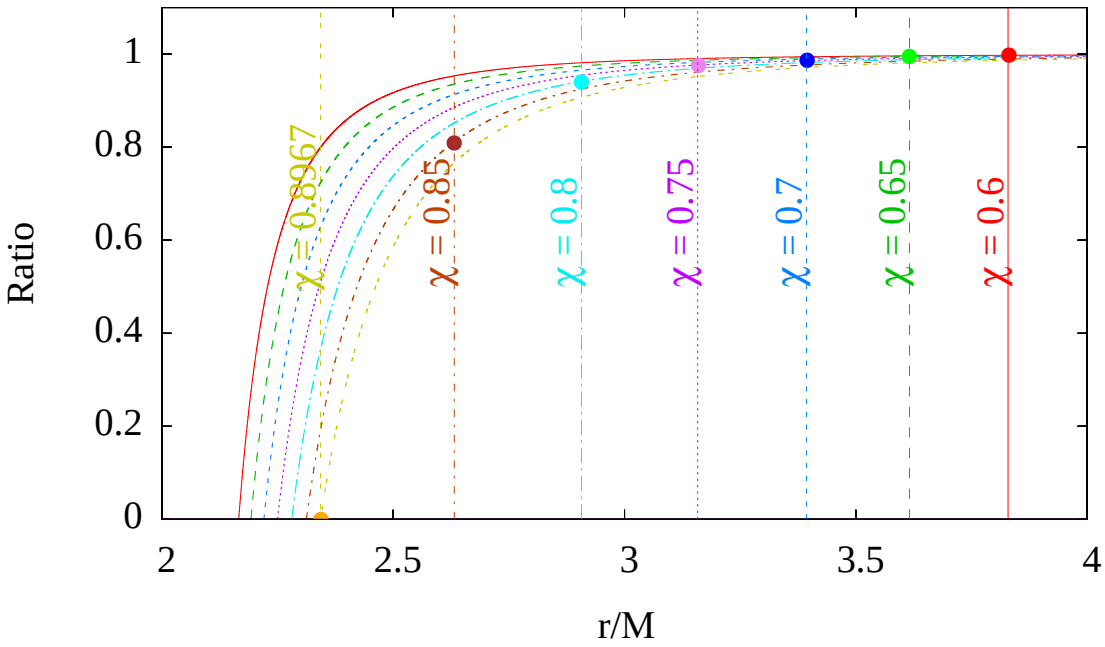

Figure 4.1: Ratio between the metric determinant of the slowly rotating spacetime and the metric determinant of the Kerr spacetime. Vertical lines represent the ISCO radius. Each line style and color represents a different value of spin as labeled. Note the ratio deviates significantly from 1 for large spin and very near the ISCO radius. The points indicate the metric determinant at the ISCO.

Lorentz signature changing sign outside the horizon, as long as it does not do so outside the ISCO.

4.2.1.5 Redshift Photons emitted in the strong-field region of a BH are greatly redshifted when they climb out of the extreme gravitational potential. The redshift factor is defined by

$$g \equiv \frac{E_o}{E_e} = \frac{(p_a u^a)_o}{(p_a u^a)_e}, \tag{4.20}$$

where p_a is the four momentum of a photon traveling from the emitter to the observer, and u^a_o and u^a_e are the four velocities of the observer and the emitter, respectively. Both the Kerr and the resummed slowly rotating metrics are independent of the t and ϕ coordinates, so the corresponding components of the photon's four momentum are conserved

$$p_a = (p_t, p_r, p_\theta, p_\phi) = (-E, p_r, p_\theta, L_z)\,. \tag{4.21}$$

Treating the observer as static, $u^a_0 = (1, 0, 0, 0)$, the numerator of Eq. (4.20) is trivially $(p_a u^a)_o = -E$. To calculate the denominator we need to know the four velocity of the emitter, that is, the orbiting emitting material. For material in a circular orbit on the equatorial plane, this is given by

$$u^a_e = u^t_e\,(1, 0, 0, \Omega)\,, \tag{4.22}$$

where

$$u^t_e = \frac{1}{\sqrt{-\left(g_{tt} + 2g_{t\phi}\Omega + g_{\phi\phi}\Omega^2\right)}}, \tag{4.23}$$

to enforce the timelike normalization condition. The denominator of Eq. (4.20) is now given by $(p_a u^a)_e = -E u_e^t + u_e^t \Omega L_z$, and the redshift factor is thus

$$g = \frac{\sqrt{-\left(g_{tt} + 2g_{t\phi}\Omega + g_{\phi\phi}\Omega^2\right)}}{1 - \Omega\,\xi}, \tag{4.24}$$

where $\xi := L_z/E$.

Let us now make some standard assumptions about the observer to simplify the redshift expression. We first assume the observer is at spatial infinity ($r = +\infty$) at an inclination angle ι relative to the BH, i.e. ι is the angle between the rotation axis of the BH and the observer's line of sight. The celestial coordinates (α, β) of the observer are defined as the apparent angular distances of the object on the celestial sphere, measured along the directions perpendicular and parallel to the rotation axis of the BH when projected onto this sphere, respectively. The celestial coordinates in terms of the photon momentum can then be written as

$$\alpha = \lim_{r\to\infty} \frac{-r p^{(\phi)}}{p^{(t)}}, \tag{4.25}$$

$$\beta = \lim_{r\to\infty} \frac{r p^{(\theta)}}{p^{(t)}}, \tag{4.26}$$

where $p^{(a)}$ denotes the components of the photon's four momentum with respect to a locally non-rotating reference frame [157]. $p^{(a)}$ and p^a are related through a coordinate transformation (e.g. $p^\phi = p^{(\phi)}/\sin\iota$). Using the fact that the BH metrics we work with are asymptotically flat, $\alpha = -\xi/\sin\iota$. For simplicity, we will neglect light-bending in the continuum spectrum, and thus α can be related to the coordinates of the emitting point in the disk via $\alpha = r\cos\phi$, where $\phi = 0$ corresponds to the line of nodes at which the observer's plane overlaps with the disk. Solving for ξ, one then

finds $\xi = -r\cos\phi\sin\iota$, and substituting ξ into Eq. (4.24), one finally obtains [189]

$$g = \frac{\sqrt{-\left(g_{tt} + 2g_{t\phi}\Omega + g_{\phi\phi}\Omega^2\right)}}{\left(1 + r\Omega\cos\phi\sin\iota\right)}. \tag{4.27}$$

4.3 Continuum Spectrum

We model the accretion disk with the Novikov-Thorne approach [12], the standard general relativistic model for geometrically-thin and optically-thick accretion disks. This model assumes the disk is in the equatorial plane and the disk particles move on nearly geodesic circular orbits, i.e. geodesics except for a small radial momentum. There are three equations that describe the time-averaged radial structure of the disk, two of which are used for calculating the continuum spectrum,

$$\dot{M} = -2\pi\sqrt{-\mathbf{g}}\Sigma(r)u^r = \text{constant}, \tag{4.28}$$

$$\mathcal{F}(r) = \frac{\dot{M}}{4\pi\sqrt{-\mathbf{g}}}f(r), \tag{4.29}$$

where $\dot{M}$ and $\mathcal{F}$ are the time-averaged mass accretion rate and radially-dependent energy flux, respectively. $\Sigma(r)$ is the surface density, u^r is the radial four-velocity of the disk particles, $\mathbf{g}$ is the determinant of the near equatorial-plane metric in cylindrical coordinates, and the function $f(r)$ is defined by

$$f(r) = \frac{-\partial_r\Omega}{\left(E - \Omega L_z\right)^2}\int_{r_{\rm in}}^{r}\left(E - \Omega L_z\right)\left(\partial_{r'}L_z\right)dr'. \tag{4.30}$$

Here $r_{\rm in}$ is the inner radius of the accretion disk which we choose to be the location of the ISCO. Note that the energy flux computed with the Kerr metric and the

resummed slowly rotating metric only differ through the $\mathbf{g}$ factor, since E, L_z and Ω do not differ in these two metrics on the equatorial plane.

One could use $\dot{M}$ as a parameter in the continuum spectrum model, but another commonly used parameter is the Eddington ratio, $\ell = L_{\rm bol}/L_{\rm Edd}$, i.e. the ratio between the bolometric and Eddington luminosities, where $L_{\rm Edd} = 1.2572\times10^{38}\,(M/M_\odot)\,{\rm erg/s}$. We here use this ratio to write $\dot{M}$ in terms of the observable ℓ, which can be re-expressed as $\dot{M}/\dot{M}_{\rm Edd}$. The accretion rate $\dot{M}$ can then be written as

$$\dot{M} = \ell \dot{M}_{\rm Edd}. \tag{4.31}$$

We define the radiative efficiency $\eta \equiv L_{\rm Edd}/\dot{M}_{\rm Edd}$, the efficiency of conversion between rest-mass and electromagnetic energy. The energy radiated by a particle falling into a BH is approximately equal to the binding energy of the ISCO [190], so the radiative efficiency can also be written as $\eta = 1 - E(r_{\rm ISCO})$. The accretion rate $\dot{M}$ is then

$$\dot{M} = \frac{\ell L_{\rm Edd}}{1 - E(r_{\rm ISCO})}. \tag{4.32}$$

We model the radiation emitted by the disk as a black-body, a good assumption provided the disk is in thermal equilibrium. Using the Stefan-Boltzmann law, we can relate the radial energy flux to the radial effective temperature of the disk:

$$T(r) = \left(\frac{\mathcal{F}(r)}{\sigma}\right)^{1/4}, \tag{4.33}$$

where σ is the Stefan-Boltzmann constant and where, after putting the results presented above together, the radial energy flux of Eq. 4.29 can be rewritten as

$$\mathcal{F}(r) = \frac{\ell L_{\rm Edd}}{4\pi\sqrt{-\mathbf{g}}\,[1 - E(r_{\rm ISCO})]} \frac{-\partial_r \Omega}{(E - \Omega L_z)^2} \int_{r_{\rm in}}^{r} (E - \Omega L_z)\,(\partial_{r'} L_z)\,dr'. \tag{4.34}$$

The luminosity is then given by [191][3]

$$L(\nu) = \frac{8\pi h}{c^2}\cos\iota \int_{r_{\rm in}}^{r_{\rm out}} \int_0^{2\pi} \frac{\nu^3\sqrt{-\mathbf{g}}}{e^{[h\nu/gk_{\rm B}T(r)]}-1} dr d\phi, \tag{4.35}$$

where g is the redshift as found in Eq 4.27, h is the Planck constant, $k_{\rm B}$ is the Boltzmann constant, ν is the observed frequency, $r_{\rm out}$ is the outer radius of the disk, and we have restored the speed of light c. As long as the latter satisfies $r_{\rm out} \gg M$, the choice of $r_{\rm out}$ does not significantly impact our ability to compare spectra in different spacetimes [191].

4.3.1 Method

Let us treat the Kerr metric as the correct, but unknown, description of a BH and its associated spectrum as our observation, which we shall refer to as the *injected synthetic signal* or *injection* for short. Let us further use the spectrum calculated with the resummed slowly rotating metric as our *model* and fit it to the injection. In both cases, the spectrum is computed from Eq. 4.35, with the integrals numerically evaluated through Simpson's rule with step sizes chosen to ensure numerical error is small. For the energy flux integration, we choose a radial step size of $\delta r = 0.1M$, with a much smaller step size of $\delta r = 10^{-4}M$ for $r \leq r_{\rm ISCO} + 2.5M$, as the energy flux is very steep near the ISCO radius. For the luminosity integration, we choose step sizes of $\delta r = M$ and $\delta\phi = 0.1$. These choices were made after a lengthy numerical investigation to guarantee that numerical error is under control.

The parameters of the spectrum model used in this paper are $\vec{\lambda} = (M, \chi, \iota, \ell)$, namely the BH mass, its dimensionless spin, the inclination angle, and the Eddington

[3]Strictly speaking, the inclination ι in this equation is the angle between the observer's line of sight and the direction perpendicular to the disk. However, if one assumes that the rotation axis of the BH is normal to the disk, ι is equivalent to the angle between the observer's line of sight and the BH spin direction, as introduced in Sec. 4.2.1.5.

ratio ℓ respectively. The BHs for which spins have been found using continuum spectrum observations have fairly well-known masses and inclination angles from other observations (e.g. modeling of orbits using variability in electromagnetic emission [24, 192–197]). We thus assume *a priori* that these parameters are known, and for simplicity we choose the representative values $M = 10M_\odot$ and $\iota = \pi/4$; the BHs for which spins have been measured using continuum spectrum observations have masses and inclination angles in the range $6.3M_\odot \leq M \leq 15.65M_\odot$ and $0.36 \leq \iota \leq 1.30$, respectively. Moreover, since the Eddington ratio ℓ is weakly correlated with the spin χ in the spectrum model, we also assume that it is known *a priori* and set it to $\ell = 0.1$. This is a somewhat arbitrary choice that should have little to no impact on our analysis, but about half of the BHs with estimated spins from continuum spectrum observations have an estimated $\ell \approx 0.1$. This then leaves the spin χ as the only parameter of the spectrum model, for which we choose a flat prior with range $-0.899 \leq \chi \leq 0.896$. The upper bound on this range is to avoid the divergence of the metric determinant at $\chi = 0.8967$ in the resummed slowly rotating spacetime. The lower bound is to avoid a super-maximally spinning BH, i.e. $\chi - \delta\chi = -0.999$ when $\chi = -0.899$ and $\delta\chi = 0.1$, where $\delta\chi$ is the average observational error to which spins have been measured.

We fit the model to the injection by minimizing their relative χ^2 over all model parameters. The reduced χ^2 is defined as

$$\chi^2_{\rm red} = \frac{\chi^2}{N} = \frac{1}{N}\sum_{i=1}^{N}\left[\frac{L_{\rm SR}(\nu_i,\chi) - L_{\rm K}(\nu_i,\chi^*)}{\sigma\left(\nu_i\right)}\right]^2, \tag{4.36}$$

where the summation is over N sampling frequencies $\nu_i \in (10^{15}, 10^{18})$ Hz with 10 samples per decade equally spaced logarithmically. This sampling choice corresponds to that made in the observed spectra of BHs with estimated spins [24, 192–197]. The

function $L_{\rm SR}(\nu,\chi)$ is the spectrum model, which depends only on the frequency ν and on the model parameter χ, while the function $L_{\rm K}(\nu,\chi^*)$ is the injection, which depends only on the frequency and the injected parameters χ^*. The value of the model parameter that minimizes the reduced χ^2 is the best-fit model parameter. A more realistic analysis would include all parameters in the vector $\vec{\lambda}$ in a Markov-Chain Monte-Carlo exploration of the likelihood surface, but we leave this for future work.

The standard deviation of the distribution, σ, in Eq. 4.36 is modeled via

$$\sigma\left(\nu_i\right) = \frac{\left|L_{\rm K}\left(\nu_i,\chi^*+\delta\chi\right) - L_{\rm K}\left(\nu_i,\chi^*-\delta\chi\right)\right|}{2}, \tag{4.37}$$

where χ^* is the injected spin of the Kerr spectrum. $\delta\chi$ serves as a means to represent the observational error in the continuum spectrum, and thus, we choose $\delta\chi = 0.1$, which is comparable to or better than the error in all current BH spin measurements using continuum spectrum observations [8].

4.3.2 Results

We find that the injected spin and best fit spin agree exactly for all the values of injected spin we explored. In other words, the resummed slowly rotating spectrum and the Kerr spectrum agree with each other best when $\chi = \chi^*$. The left panel of Fig. 4.2 shows the Kerr and slowly rotating spectra for several values of spin. Observe that there is no obviously noticeable difference between the spectra in the Kerr and in the slowly rotating spacetimes. The right panel of Fig. 4.2 shows the minimized $\chi^2_{\rm red}$ as a function of the injected spin. Observe that $\chi^2_{\rm red} \ll 1$ for all injected spins, which shows that the resummed slowly rotating model is a very good fit of the Kerr injection. The spectra at $\chi = 0$ are exactly the same, and as the spin is increased the fits get worse. The scatter in the $\chi^2_{\rm red}$ values is primarily due to the frequency sampling, with

its range decreasing by about an order of magnitude if the discretization is made smaller by a factor of 10.

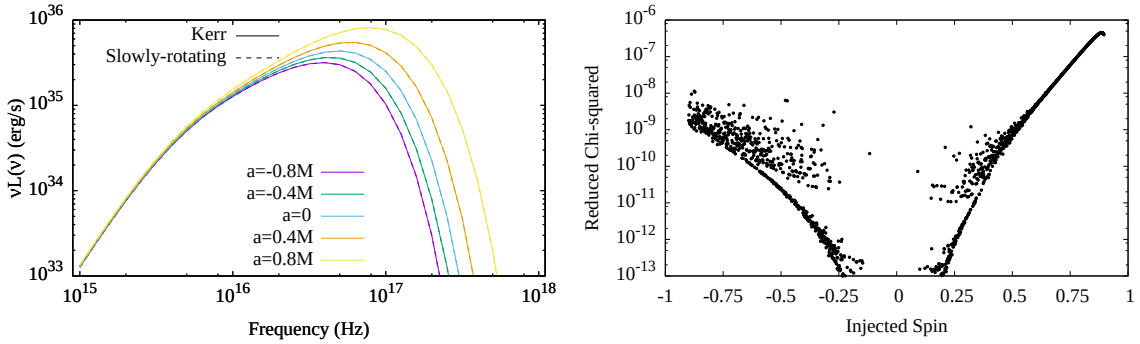

Figure 4.2: Left: Continuum spectra for the Kerr and slowly rotating spacetimes for several values of spin. The Kerr spectra are shown with solid lines, while the slowly rotating spectra are shown with dashed lines. There is no obviously noticeable difference between the Kerr and slowly rotating spectra. Right: Reduced χ^2 as a function of injected spin as defined in Eq. 4.36. The fits are very good for all values of spin, but do become worse for larger values of spin, particularly for positive spins.

The slowly rotating spectrum can fit the Kerr spectrum very well because the two spacetimes are identical in the $\theta = \pi/2$ plane except for the (r, r) component of the metrics. As mentioned previously, this component of the metric only impacts the metric determinant in the continuum spectrum calculation. As shown in Fig. 4.1, the resummed slowly rotating metric determinant only shows deviations from Kerr that can be seen by eye when $r \lesssim 3M$ and $\chi \gtrsim 0.8$. Therefore, the fact that the model is an excellent fit to the injection is simply because the two only differ greatly when spins are very large and for trajectories very near the ISCO radius. While the accretion disk near the ISCO radius has the largest impact on the spectrum, the region where the determinants differ significantly only reaches out to about $r = r_{\rm ISCO} + M$ at most; this is not a large enough region to contribute significantly to the continuum spectrum observables, relative to the contributions from the rest of the accretion disk.

4.4 BH Shadow

Let us define the BH shadow as follows. Suppose light rays are emitted at $r = \infty$ and propagate toward the BH. If a light ray reaches an observer at $r = \infty$ after scattering, the direction of the light ray as seen by the observer is not dark. If a light ray crosses the event horizon of the BH it can never reach the observer. The light rays that do not reach the observer create a dark region, which we call the BH shadow. This is, of course, an idealization of a BH shadow; in reality, the photons that reach the observer originate from an accretion disk around the BH, which makes the shadow dependent on the properties of the accretion disk, although weakly. The shape of the boundary of the BH shadow is thus strongly dependent on the evolution of unstable spherical photon orbits near the BH, and thus, it contains information about the BH spacetime.

The shadow boundary can be found analytically if the Hamilton-Jacobi equation is separable for the metric describing the BH, as we show explicitly in D. Separability is not only a property of the spacetime, but also of the coordinates chosen to describe this spacetime. For example, the Kerr metric is separable in Boyer-Lindquist coordinates, but the resummed slowly rotating metric is not. Therefore, the BH shadow boundary in the resummed slowly rotating spacetime case must be constructed numerically by solving the null geodesic equations.

The BH shadow boundary cannot be constructed for all values of the spin of the resummed slowly rotating metric. This is simply because there is a range of spins for which the shadow boundary is inside the resummed slowly rotating horizon, i.e. the horizon is at $r_{\rm H,SR} = 2M$, while the boundary of the shadow can be inside $2M$ for some range of spins [see Sec. 4.2.1.1]. To find these values of χ, we study the spins for which the Kerr metric has spherical photon orbits at $r = 2M$, following the discussion

in D. We find that provided $\chi < 1/\sqrt{2} \approx 0.707$ equatorial photon orbits exist outside of $r = 2M$ for the Kerr metric. The divergence at $r = 2M$ in the slowly rotating equations of motion prevents us from doing a similar analysis for the slowly rotating metric. We thus conservatively choose to investigate resummed slowly rotating BH shadow models with $\chi \leq 0.6$.

We parameterize the boundary of the BH shadow in terms of the horizontal displacement from the center of the image D, the average radius of the sphere $\langle R \rangle$, and the asymmetry parameter A. D, $\langle R \rangle$, and A are the three BH shadow boundary observables we analyze. There are many ways to model the shape of the shadow (see e.g. [198, 199]) and the conclusions of this work will be similar regardless of the chosen parameterization. The horizontal displacement D is the shift of the center of the boundary of the shadow from the center of the BH and it is defined by

$$D \equiv \frac{|\alpha_{\rm min} - \alpha_{\rm max}|}{2}, \tag{4.38}$$

where $\alpha_{\rm min}$ and $\alpha_{\rm max}$ are the minimum and maximum horizontal coordinates of the image on the observer's viewing plane, respectively. The Kerr and the resummed slowly rotating spacetimes are axially symmetric so there is no vertical displacement of the image. The average radius $\langle R \rangle$ is the average distance of the shadow boundary from its center and it is defined by

$$\langle R \rangle \equiv \frac{1}{2\pi} \int_0^{2\pi} R(\vartheta)\, d\vartheta, \tag{4.39}$$

where $R(\vartheta) \equiv \left[(\alpha - D)^2 + \beta(\alpha)^2\right]^{1/2}$ and $\vartheta \equiv \tan^{-1}\left[\beta(\alpha)/\alpha\right]$. The asymmetry parameter is the distortion of the shadow boundary from a circle and it is defined by

$$A \equiv 2\left[\frac{1}{2\pi}\int_0^{2\pi}\left(R - \langle R\rangle\right)^2 d\vartheta\right]^{1/2}. \tag{4.40}$$

4.4.1 Method

As with the continuum spectrum, let us treat the Kerr metric as the correct, but unknown, description of a BH and its associated BH shadow as our observation, which we shall refer to as the *injected synthetic signal* or *injection* for short. Let us further use the BH shadow boundary calculated with the resummed slowly rotating metric as our *model* and fit it to the injection. In both cases, the BH shadow boundary is computed by first numerically evolving null geodesics with GRay [200], a general relativistic ray-tracing code, and then parameterizing the boundary of the shadow as an off-centered deformed sphere [165]. We use GRay because the resummed slowly rotating metric is not separable, so the Hamilton-Jacobi equation must be solved numerically.

The parameters of the BH shadow boundary model are $\vec{\lambda} = (M, \iota, \chi)$, namely the BH mass, the inclination angle and the dimensionless spin parameter respectively. We assume that the BH mass is known *a priori* from other measurements (e.g. the mass of Sagittarius A* is known to about 10% uncertainty from observations of stellar orbits [122,123]); for our analysis, we set $M = 1$ without loss of generalization, because the BH mass only modifies the overall size of the shadow boundary without changing its shape. We further assume that the inclination is also known *a priori* for simplicity, and we choose its value in a conservative fashion, as we explain below in Sec. 4.4.2. These priors, thus, reduce the parameter vector to just $\vec{\lambda} = (\chi)$. The prior range on χ will be chosen to be $0 \leq \chi \leq 0.6$, since negative values of χ would only reflect the

shadow across the α axis. The upper bound on the prior range is due to the photon sphere falling inside of the horizon of the resummed slowly rotating metric.

As in the spectrum case, we fit the model to the injection by minimizing their relative χ^2 over all model parameters. The reduced χ^2 in this case is defined as

$$\chi^2_{\rm red} = \frac{\chi^2}{3} = \frac{1}{3}\sum_{i=1}^{3}\left(\frac{\alpha^i_{\rm SR}(\chi) - \alpha^i_{\rm K}(\chi^*)}{\sigma_i}\right)^2, \tag{4.41}$$

where the three BH shadow boundary observables are $\alpha^i = [D, \langle R\rangle, A]$, $\alpha^i_{\rm K}$ is the injection, which depends only on the injected spin χ^*, and $\alpha^i_{\rm SR}$ is the model, which depends only on the model parameter χ. The value of the spin χ that minimizes the reduced χ^2 shall be referred to as the best-fit parameter of the model. A more realistic analysis would remove the priors on the other parameters and include all parameters in a Markov-Chain Monte-Carlo exploration of the likelihood surface, but we leave this for future work.

The standard deviations, σ_i, in Eq. 4.41 are modeled through

$$\sigma_i = \frac{\alpha^i_{\rm K}(\chi^* + \delta\chi) - \alpha^i_{\rm K}(\chi^* - \delta\chi)}{2}, \tag{4.42}$$

where χ^* is the injected spin of the Kerr shadow boundary and $\delta\chi$ represents the observational error to which this injected spin can be measured in BH shadow observations. The best BH shadow observations have only placed lower or upper bounds on spin [132, 201], but future observations should be able to do much better [202]. For simplicity, and to compare with continuum spectrum observations, we assume $\delta\chi = 0.1$ below.

4.4.2 Results

There are two physical parameters that determine the BH shadow boundary in the Kerr and the resummed slowly rotating spacetimes, the spin χ and the inclination angle ι. We here wish to determine a *conservative* bound, i.e. a bound on how much the resummed slowly rotating shadow boundary could deviate from the Kerr shadow boundary *at most*. To address this, we first fix the spin χ and find the inclination angle at which the resummed slowly rotating shadow boundary deviates the most from the Kerr shadow boundary. We then fix the inclination angle to that value and fit the slowly rotating BH shadow boundary model to the injection as a function of the model spin. This provides an upper bound on the systematic error associated with using the slowly rotating metric instead of the Kerr metric when fitting to a BH shadow observation.

Let us then begin by calculating the Kerr and resummed slowly rotating BH shadow boundaries at a fixed $\chi = 0.6$, but as a function of inclination angle $\iota \in (0, \pi/2)$. We parameterize the shape of each shadow boundary using the displacement, the average radius, and the asymmetry parameter, as shown in the left panel of Fig. 4.3. Observe that the difference in the average radius computed with the Kerr metric and the resummed slowly rotating is approximately constant, while the difference in the displacement and asymmetry parameters varies with inclination angle. Observe also that the maximum difference in the latter two is at $\iota \approx \pi/4$.

We confirm that the largest deviation between the shadow boundaries is near $\iota = \pi/4$ by calculating the reduced χ^2 between the Kerr shadow boundary and the resummed slowly rotating shadow boundary with $\chi = 0.6$ as a function of the inclination angle. We choose the standard deviations to be an order of magnitude smaller than the injected values ($\sigma_D = 0.1, \sigma_{\langle R \rangle} = 0.01, \sigma_A = 0.01$). The right panel of

Fig. 4.3 shows that χ^2 is largest at approximately $\iota = \pi/4$. Therefore, we henceforth choose $\iota = \pi/4$ for analyzing the shadow boundaries as a function of spin.

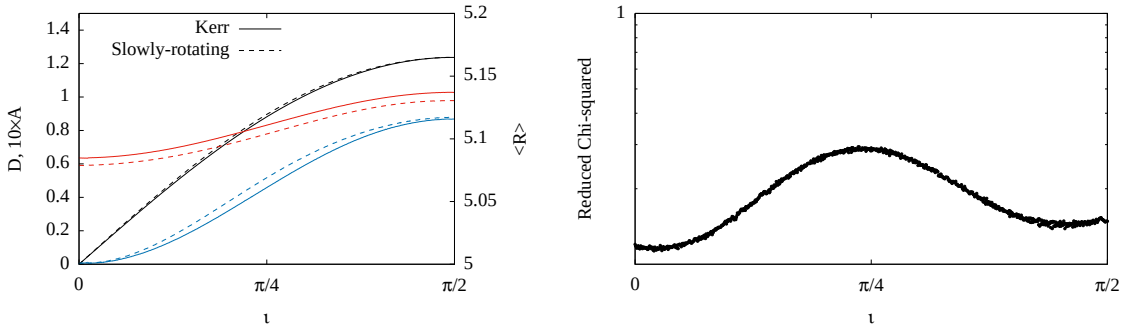

Figure 4.3: Left: Displacement (black), average radius (red), and asymmetry parameter (blue) for Kerr (solid) and slowly rotating (dashed) shadows as a function of inclination angle at a spin of $\chi = 0.6$. Right: $\chi^2_{\rm red}$ as a function of inclination angle for comparing the Kerr and slowly rotating shadow boundaries. Only shadow boundaries with equal inclination angles are compared. The spin is set at $\chi = 0.6$. The errors chosen for each parameter are $(\sigma_D = 0.1, \sigma_{\langle R\rangle} = 0.01, \sigma_A = 0.01)$.

Let us now fit a BH shadow model constructed with the resummed slowly rotating metric to the Kerr BH shadow injection as a function of model parameter χ with ι fixed at $\pi/4$. As in the continuum spectrum case, we find that the injected and best fit spins agree exactly for all the values of injected spin we explored, i.e. the resummed slowly rotating BH shadow and the Kerr shadow agree with each other best when $\chi = \chi^*$. Figure 4.4 shows the BH shape observables computed with the resummed slowly rotating metric and the Kerr metric using $\iota = \pi/4$ and the same values of spin. Once again, observe that the resummed slowly rotating shadow with $\chi = \chi^*$ matches the full Kerr shadow shadow quite well; the difference between the shadow boundaries increases, becoming noticeable by eye only at very high spin.

The left panel of Fig. 4.5 shows the absolute difference between the injected spin and the best fit spin as a function of injected spin. Observe that the absolute

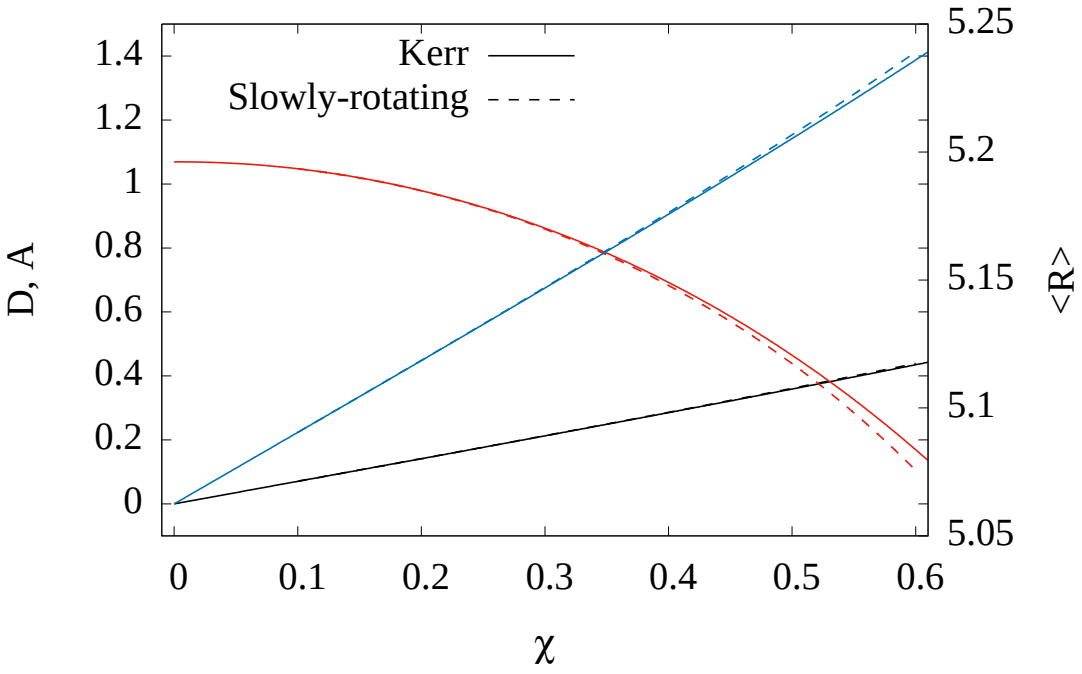

Figure 4.4: Displacement (black), average radius (red), and asymmetry parameter (blue) for Kerr (solid) and slowly rotating (dashed) shadow boundaries as a function of spin at an inclination angle of $\iota = \pi/4$.

difference is at most 0.012 at an injected spin of 0.6, or equivalently the fractional systematic error on the estimated spin is at most 2%. The right panel of Fig. 4.5 shows $\chi^2_{\rm red}$ as a function of injected spin. Observe that the goodness-of-fit deteriorates with increasing injected spin, with $\chi^2_{\rm red}$ reaching at most about 0.003 at the edge of the prior range. The $\chi^2_{\rm red}$ at low spins is dominated by numerical errors and thus exhibits some scattering. In conclusion, the best fit spin value deviates more and more from the injected spin as the latter increases, while the fit deteriorates; however, the fractional systematic error in the estimated spin is smaller than reasonable estimates of the observational error expected in BH shadow observations [77].

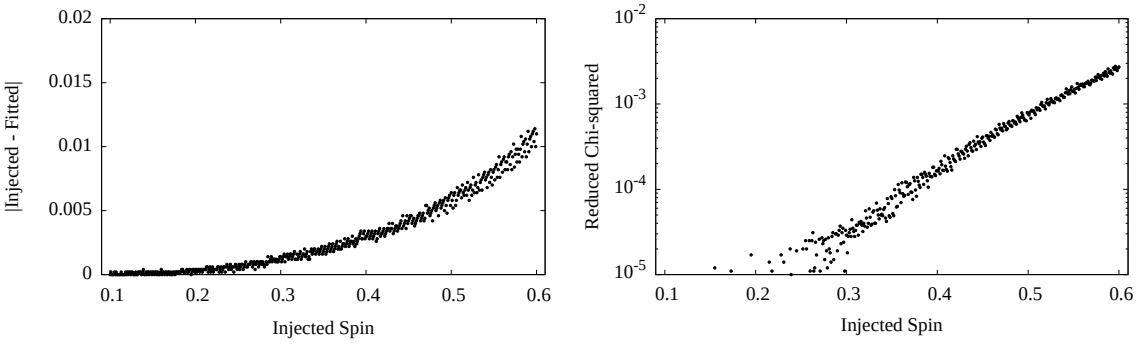

Figure 4.5: Left: Absolute difference between the injected spin of the Kerr shadow boundary and the spin of the best fit slowly rotating shadow boundary as a function of injected spin. Right: $\chi^2_{\rm red}$ as defined in Eq. 4.41. Inclination angle is set at $\iota = \pi/4$.

4.5 Discussion

We have studied whether the slow-rotation approximation when constructing BH spacetimes is appropriate for modeling two electromagnetic observables associated with BH accretion disks: the continuum spectrum and BH shadows. We have found that this approximation does not introduce a significant systematic error when fitting resummed slowly rotating models to an exact Kerr injection. In the

continuum spectrum case, the slowly rotating model can capture the Kerr spectrum to within our numerical accuracy. In the BH shadow case, the slowly rotating model incurs a fractional systematic error in the estimation of the spin parameter of 2% at worst. These systematic errors are smaller than the observational errors (statistical, astrophysical and instrumental) associated with continuum spectrum and BH shadow observations [8, 77] for all spins considered for which the slowly rotating metric is physically valid.

We have also found that the slow-rotation approximation cannot be used to model BHs with too high a spin. In particular, one should not construct slowly rotating continuum spectra and BH shadows to model BHs with dimensionless spin larger than approximately 0.9 and 0.6 respectively. This is because above these values of spin the approximate spectrum and the shadow are unphysical due to the volume element vanishing and the photon sphere falling inside of the event horizon of the slowly rotating metric respectively.

Our results suggest that the continuum spectrum and BH shadow observations can be analyzed with approximate slowly rotating BH solutions, since this approximation introduces less systematic error than the observational error of current and future telescopes. This opens the door to carrying out tests of GR with approximate, slowly rotating BH solutions in modified gravity theories using electromagnetic observations; this is important because there is a wide class of modified gravity theories, such as dCS gravity [57,107,109], for which an exact BH solution valid for all spins is currently not known.

The conclusions derived here, however, are only valid provided the difference between slowly rotating BHs and exact BHs in modified theories can be captured by the difference between the slowly rotating Kerr metric and the Kerr metric. This assumption could be verified by carrying out a similar study in modified gravity

theories for which exact rotating BH solutions are known. Analytic and exact rotating BH solutions have not been found in many modified gravity theories (e.g. dCS gravity [57, 107, 109]), but there are some for which analytic, exact rotating BH solutions exist (e.g. massive gravity [203]).

Yet another possible extension is to improve on the accretion disk model used in the continuum spectrum calculation. The Novikov-Thorne model (and models that are adapted from it) is the most commonly used framework when fitting for continuum spectrum observations. However, there are other models that incorporate different assumptions or different physics [11], such as the advection-dominated accretion flow (ADAF) model, which could potentially produce a significantly different continuum spectrum [204]. It is possible that the agreement in the continuum spectrum between the slowly rotating metric and the Kerr metric disappears in other accretion disk models and this is worth investigating in the future.

A final extension of our work could be to relax other assumptions we made in this paper to further verify the conclusions we arrived at. The resummation used for the slowly rotating metric is the simplest choice possible, but is certainly not the only one. The effect of light-bending was neglected for the continuum spectrum calculation and could be incorporated with a ray-tracing algorithm. Values of mass, inclination angle, Eddington ratio, and outer disk radius were assumed known *a priori* for the continuum spectrum and BH shadow. A full multi-dimensional Bayesian analysis could be performed to see whether covariances introduced by these additional parameters have an impact on our conclusions.

4.6 Acknowledgments

D.A. and N.Y. acknowledge support from the NSF CAREER Grant PHY-1250636. K.Y. acknowledges support from JSPS Postdoctoral Fellowships for

Research Abroad and NSF grant PHY-1305682. Some calculations used the computer algebra-systems MAPLE, in combination with the GRTENSORII package [121].

BLACK HOLE CONTINUUM SPECTRA AS A TEST OF GENERAL RELATIVITY: QUADRATIC GRAVITY

Contribution of Authors and Co-Authors

Manuscript in Chapter 5

Author: Dimitry Ayzenberg

Contributions: Conceived and implemented the study design. Wrote first draft of the manuscript.

Co-Author: Dr. Nicolás Yunes

Contributions: Helped conceive the study design. Provided feedback of analysis and comments on drafts of the manuscript.

Manuscript Information Page

Dimitry Ayzenberg, Nicolás Yunes

Classical and Quantum Gravity

Status of Manuscript:

___Prepared for submission to a peer-reviewed journal

_x_Officially submitted to a peer-reviewed journal

___Accepted by a peer-reviewed journal

___Published in a peer-reviewed journal

Submitted to the Institute of Physics

Submitted January, 2017

Abstract

Observations of the continuum spectrum emitted by accretion disks around black holes allows us to infer their properties, including possibly whether black holes are described by the Kerr metric. Some modified gravity theories do not admit the Kerr metric as a solution, and thus, continuum spectrum observations could be used to constrain these theories. We here investigate whether current and next generation X-Ray observations of the black hole continuum spectrum can constrain such deviations from Einstein's theory, focusing on two well-motivated modified quadratic gravity theories: dynamical Chern-Simons gravity and Einstein-dilaton-Gauss-Bonnet gravity. We do so by determining whether the non-Kerr deviations in the continuum spectrum introduced by these theories are larger than the observational error intrinsic to the observations. We find that dynamical Chern-Simons gravity cannot be constrained better than current bounds with current or next generation continuum spectrum observations. Einstein-dilaton-Gauss-Bonnet gravity, however, may be constrained better than current bounds with next generation telescopes, as long as the systematic error inherent in the accretion disk modeling is decreased below the predicted observational error.

5.1 Introduction

The recent detections of gravitational waves from binary black hole (BH) mergers by advanced LIGO (aLIGO) [68,69] have ushered in the era of *extreme gravity* tests of General Relativity (GR) [47,67], i.e. probes that sample the non-linear and dynamical nature of the gravitational interaction. In the coming years, these two observations will be bolstered by further gravitational wave detections from aLIGO, aVirgo, and KAGRA [71] and pulsar timing arrays (PTAs) [72]. In the meantime, electromagnetic (EM) observations of accretion disks around BHs using new X-Ray telescopes and very long baseline interferometers (VLBIs) [16, 34, 35, 42, 135, 205] will also join the game. Unlike gravitational wave observations, EM ones do not directly probe the dynamical sector of the gravitational interaction, but instead, they detect the impact of a stationary source of strong gravity on radiation that attempts to escape from it.

These observations include, but are not limited to, the continuum spectrum of BH accretion disks, the BH "shadow", and the Kα iron line emitted from BH accretion disks [135, 206–208].

Continuum spectrum observations are of particular interest as the BH accretion disk spectrum is very sensitive to the properties of the BH spacetime. The continuum spectrum of thin disks is dominated by radiation originating near the inner radius of the accretion disk, which can be well approximated by the innermost stable circular orbit (ISCO) [16], i.e. the last stable orbit an accretion disk (test) particle can be in before plunging into the BH. The ISCO is independent of the accretion disk properties and depends only on the properties of the BH spacetime, e.g. the BH mass M and (the magnitude of) the spin angular momentum $|\vec{J}|$. Continuum spectrum observations are thus a useful tool for determining the properties of BHs and have been used to estimate the angular momentum of several BHs [8].

Black hole continuum spectrum observations could allow us, at least in principle, to test the *Kerr hypothesis*, i.e. that all isolated, stationary, and axisymmetric astrophysical (uncharged) BHs are described by the Kerr metric [136–141], which is completely determined by only two parameters (the mass and the angular momentum). The Kerr metric is a solution to the Einstein equations in vacuum, but it can also be a solution in certain modified gravity theories [173]. In this sense, verifying the Kerr hypothesis is a null test of General Relativity, but it does not necessarily rule out all modified gravity models. There are, however, modified theories of gravity that introduce violations to fundamental pillars of GR, and that, in particular, do not satisfy the Kerr hypothesis. In these cases, BH continuum spectrum observations can be used to place constraints on these theories.

Two such modified gravity theories that have also been well-studied are dynamical Chern-Simons (dCS) gravity [108] and Einstein-dilaton-Gauss-Bonnet (EdGB)

gravity [142]. Both theories modify the Einstein-Hilbert action by introducing a dynamical scalar field that couples to a curvature invariant, the Pontryagin invariant in the case of dCS gravity and the Gauss-Bonnet invariant in the case of EdGB gravity. These theories break parity invariance in the gravitational sector and the strong equivalence principle, both of which are pillars of Einstein's theory [60]. Black holes within these theories have been studied extensively and many numerical and approximate solutions have been found, although no exact solution is known for BHs that spin arbitrarily fast [85,86,107,143–150,187]. For the purpose of this work we will focus on a pair of purely analytic, approximate solutions, one for each theory. Both solutions are stationary and axisymmetric, and they represent a slowly-rotating BH to quadratic order in the ratio of spin angular momentum to BH mass squared [57,209].

An overarching goal of our research program is to determine the degree to which BH continuum spectrum observations can be used to constrain deviations from GR. A step in this direction and the primary goal of this paper is to consider constraints on dCS gravity and EdGB gravity. Both theories have been constrained with observations that are not in the extreme gravity regime [57,111,115], and thus, they are not very stringent. Given that EM observations are sensitive to strong-field physics, one could expect that they may lead to much more stringent constraints, if the modified gravity effects are not overwhelmed by observational error and modeling systematics. In this paper we will investigate this topic with continuum spectrum observations using both current and next generation X-Ray telescopes.

Whether continuum spectrum observations can be used to place constraints on modified gravity will depend on whether the induced deviations in the spectrum are *detectable*. As a proxy for detectability, we will here require that at the very least the modified gravity deviations should be larger than any other systematic, statistical, instrumental, and environmental error in the observations. Systematic error originates

from the approximate nature of the models we use to analyze the data, in particular the approximate nature of BH solutions in modified gravity and of the astrophysical models for accretion disks. The impact of using approximate, slowly-rotating BH solutions for continuum spectrum observations was studied recently [210], with results suggesting that the systematic error introduced is negligible, provided the BH is not close to maximally rotating. The impact of using approximate accretion disk models is currently unknown, because of their complexity and the large number of proposed models. In fact, there is much debate over which model(s) best describes continuum spectrum observations in GR [11, 171]. This source of systematic error is beyond the scope of this paper. Statistical, instrumental, and environmental errors will be collectively referred to as *observational errors*, and they affect the accuracy to which BH properties can be estimated by roughly 10% with current X-Ray telescopes [8]; next generation X-Ray telescopes will be able to estimate BH properties to 1% [34, 35, 170]

In order to determine whether continuum spectrum observations can be used to place constraints on modified gravity, we perform a parameter estimation study in which we treat the continuum spectrum of a Kerr BH as the *observation* or *injection* and the continuum spectrum of a BH in EdGB gravity or dCS gravity as the *model* we fit to the injection. The parameters we estimate are the BH mass, the BH spin angular momentum, and the inclination angle, i.e. the angle between the observer's line of sight and the BH's angular momentum. The parameter estimation study is done by minimizing the relative χ^2 over all parameters. We model the observational error using errors in the parameters that are representative of current and next generation continuum spectrum observations. Since the model is different from the observation, our parameter estimation will result in biased best-fit parameters that will differ from the true parameters of the signal. Continuum spectrum observations can then

be used to constrain EdGB and dCS gravity provided the difference between the biased parameter and the true parameters are larger than the observational errors.

The main results of this paper are that dCS gravity and EdGB gravity cannot be constrained better than current constraints using continuum spectrum observations with current X-Ray telescopes. Assuming a signal consistent with GR, the bias in the recovered BH parameters when analyzing the data with dCS gravity and EdGB gravity models is much smaller than the observational error with current telescopes. Using next generation telescopes, on the other hand, it may be possible to place better than current constraints on EdGB gravity, but not on dCS gravity. With a reduction in the observational error of an order of magnitude, the bias in parameter extraction with EdGB gravity models becomes significantly larger than the observational error for BHs of mass $M \lesssim 8M_{\odot}$. This is not, however, the case with dCS gravity models, for which the bias in parameter extraction remains well below the observational error. This is, in part, because non-spinning BHs are still described by the Schwarzschild metric in dCS gravity, with modifications only important very close to the BH's event horizon and always proportional to the spin. These results are summarized in Table 5.1.

	Current	Next Gen.
dCS	×	×
EdGB	×	✓

Table 5.1: Table summarizing main results of this paper, i.e. whether observations of black hole continuum spectra with current and next generation X-Ray telescopes can be used to place better than current constraints on dynamical Chern-Simons gravity and Einstein-dilaton-Gauss-Bonnet gravity. A checkmark, ✓, means better than current constraints can be placed $\forall\ M_{\rm BH} \lesssim 8M_{\odot}$, while a cross, ×, means better than current constraints cannot be placed.

As part of this investigation, we also obtain a set of secondary results. We calculate properties of EdGB and dCS gravity BH solutions that play an important role in the calculation of the spectrum, such as the conserved energy and angular momentum, the ISCO radius, and the gravitational redshift. More importantly, perhaps, we also show that test particles, i.e. particles with extremely weak self-gravity, follow geodesics in EdGB gravity, developing a proof that is similar to that employed previously in dCS gravity [94]. This proof allows one to continue to use the geodesic equation to solve for the motion of accretion disk particles in the background of a massive BH.

Our work extends previous work on BH electromagnetic observations in EdGB gravity and dCS gravity by studying the continuum spectrum of solutions in these theories that have not been studied in the past. Although a similar study had been carried out in dCS gravity before [211], this was only to linear-order in spin. DCS modifications that are quadratic in the spin enter the diagonal components of the metric, which could in principle have a larger effect on electromagnetic observables. The continuum spectrum in EdGB gravity had not been studied before, although other electromagnetic observables had been considered, such as the black hole shadow [212] and quasi-periodic oscillations [213]. Similar results to those in this work were found in the case of quasi-periodic oscillations, namely that next generation telescopes should be able to place better than current constraints on EdGB gravity. Showing that this result holds for multiple types of electromagnetic observations adds to the scientific case of next generation telescopes.

The remainder of this paper presents the details of the calculations that led us to the above conclusions. Section 5.2 briefly summarizes the quadratic gravity (QG) class of modified gravity theories of which dCS gravity and EdGB gravity are a part and the BH solutions this paper studies. Section 5.3 presents properties of the BH

solutions that are relevant to the continuum spectrum calculation. Section 5.4 details the continuum spectrum calculation, our statistical analysis methodology, and the results obtained. Section 5.5 concludes by summarizing our results and discussing implications. Throughout, we use the following conventions: the metric signature $(-,+,+,+)$; Latin letters in index lists stand for spacetime indices; parentheses and brackets in index lists for symmetrization and antisymmetrization, respectively, i.e. $A_{(ab)} = (A_{ab} - A_{ba})/2$ and $A_{[ab]} = (A_{ab} - A_{ba})/2$; geometric units with $G = c = 1$ (e.g. $1M_\odot$ becomes 1.477 km by multiplying by G/c^2 or 4.93×10^{-6} s by multiplying by G/c^3), except where otherwise noted.

5.2 Quadratic Gravity and BH Solutions

The action that describes the QG class of theories is defined by a modification to the Einstein-Hilbert action containing all possible quadratic, algebraic curvature scalars with running (i.e. nonconstant) couplings [85]

$$\begin{aligned} S \equiv \int d^4x\sqrt{-g}\{&\kappa R + \alpha_1 f_1(\vartheta) R^2 + \alpha_2 f_2(\vartheta) R_{ab}R^{ab} \\ &+ \alpha_3 f_3(\vartheta) R_{abcd}R^{abcd} + \alpha_4 f_4(\vartheta) R_{abcd}{}^*R^{abcd} \\ &- \frac{\beta}{2}\left[\nabla_a\vartheta\nabla^a\vartheta + 2V(\vartheta)\right] + \mathcal{L}_{\text{mat}}\}. \end{aligned} \tag{5.1}$$

Here, g stands for the determinant of the metric g_{ab}. R, R_{ab}, R_{abcd}, and ${}^*R_{abcd}$ are the Ricci scalar, Ricci tensor, and the Riemann tensor and its dual, respectively, with the latter defined as

$${}^*R^a{}_{bcd} = \frac{1}{2}\varepsilon_{cd}{}^{ef}R^a{}_{bef}\,, \tag{5.2}$$

and ε^{abcd} the Levi-Civita tensor. The quantity $\mathcal{L}_{\rm mat}$ is the external matter Lagrangian, ϑ is a field, $f_i(\vartheta)$ are functionals of this field, (α_i, β) are coupling constants, and $\kappa = 1/(16\pi)$.

We will focus on two specific theories within QG, EdGB gravity and dCS gravity. In EdGB gravity, $(\alpha_1, \alpha_2, \alpha_3, \alpha_4) = (\alpha_{\rm EdGB}, -4\alpha_{\rm EdGB}, \alpha_{\rm EdGB}, 0)$ and $(f_1, f_2, f_3, f_4) = (\vartheta, \vartheta, \vartheta, 0)$, where $\alpha_{\rm EdGB}$ is the EdGB gravity coupling constant and ϑ is the dilaton[1]. In dCS gravity, $(\alpha_1, \alpha_2, \alpha_3, \alpha_4) = (0, 0, 0, \alpha_{\rm dCS}/4)$ and $(f_1, f_2, f_3, f_4) = (0, 0, 0, \vartheta)$, where $\alpha_{\rm dCS}$ is the dCS gravity coupling parameter and ϑ is the dCS (axion like) field. The strongest constraint on EdGB gravity comes from low-mass X-Ray binary observations, $\sqrt{|\alpha_{\rm EdGB}|} < 1.9 \times 10^5$cm [111]. The strongest constraint on dCS gravity comes from Solar System [115] and tabletop experiments [57], $\sqrt{|\alpha_{\rm dCS}|} < 10^{13}$cm.

Let us now consider BH solutions in these theories. In GR, the solution for an isolated, stationary, axisymmetric, and uncharged BH is the Kerr metric. The line element associated with this metric in Boyer-Lindquist coordinates (t, r, θ, ϕ) is given by

$$\begin{aligned} ds^2_{\rm K} = &-\left(1 - \frac{2Mr}{\Sigma_{\rm K}}\right) dt^2 - \frac{4Mar\sin^2\theta}{\Sigma_{\rm K}} dt d\phi + \frac{\Sigma_{\rm K}}{\Delta_{\rm K}} dr^2 \\ &+ \Sigma_{\rm K} d\theta^2 + \left(r^2 + a^2 + \frac{2Ma^2 r \sin^2\theta}{\Sigma_{\rm K}}\right) \sin^2\theta d\phi^2, \end{aligned} \tag{5.3}$$

[1]In EdGB gravity, the functionals of the dilaton field are actually given by $(f_1, f_2, f_3, f_4) = (e^\vartheta, e^\vartheta, e^\vartheta, 0)$. For the BH solution we study in this work we assume ϑ is at the minimum of its potential, $V(\vartheta)$, and then Taylor expand about small perturbations from the minimum, $f_i(\vartheta) = f_i(0) + f_i'(0)\vartheta + \mathcal{O}(\vartheta^2)$ where $f_i(0)$ and $f_i'(0)$ are constants. The ϑ-independent term leads to a theory with a minimally coupled field, i.e. the field does not interact with the curvature invariants. The Guass-Bonnet invariant, $R_{\rm GB} = R^2 - 4R_{ab}R^{ab} + R_{abcd}R^{abcd}$, is a topological invariant, and thus, the $f_i(0)$ term does not modify the field equations. The $f_i(0)$ term is then irrelevant and we neglect it, instead focusing on the $f_i'(0)$ term, which can be modeled by letting $f_i(\vartheta) = c_i\vartheta$. We reabsorb the constant c_i into the coupling parameter $\alpha_{\rm EdGB}$, and then, the functionals are given by $(f_1, f_2, f_3, f_4) = (\vartheta, \vartheta, \vartheta, 0)$.

with $\Delta_{\rm K} \equiv r^2 - 2Mr + a^2$ and $\Sigma_{\rm K} \equiv r^2 + a^2\cos^2\theta$. Here M is the mass of the BH and $a \equiv J/M$ is the Kerr spin parameter, where $J := |\vec{J}|$ is the magnitude of the BH spin angular momentum.

For EdGB gravity and dCS gravity we will focus on the approximate, stationary, and axisymmetric solutions that represent slowly-rotating BHs to second order in the spin [57, 209]. These solutions take the form

$$g_{ab}^{{\rm QG},\chi^0} = g_{ab}^{\rm K} + \zeta\left[g_{ab}^{[0,1]} + \chi\, g_{ab}^{[1,1]} + \chi^2 g_{ab}^{[2,1]}\right], \tag{5.4}$$

where $g_{ab}^{\rm K}$ is the Kerr metric and $g_{ab}^{[x,y]}$ are the metric deformations due to EdGB gravity or dCS gravity at each order in spin and are given in E for completeness. Here $\chi = a/M = \vec{J}/M^2$ is the dimensionless spin parameter and $\zeta = 16\pi\alpha^2/M^4$ is the dimensionless coupling parameter, where we have set $\beta = 1$.

Due to the slow-rotation and small-coupling ($\zeta << 1$) expansions used to find these BH solutions in EdGB gravity and dCS gravity, they contain spurious features that would not appear in an exact solution. An example of such a spurious feature is that these solutions contain a divergence at $r = 2M$, which is unrelated to any physical property of the solutions (see e.g. [187]). To eliminate such spurious features one can perform a resummation, i.e. replace terms in the metric that, if expanded in small rotation, would produce higher order terms in χ, such as $r \to \Sigma_{\rm K}^{1/2}$. In principle, there are an infinite number of ways to resum the metric and, since the exact solution of a rotating BH is not known in EdGB gravity and dCS gravity, it is unknown which choice of resummation is the correct one to make. For simplicity, our choice of resummation throughout this work is to treat the slowly-rotating solutions as *exact*, i.e. to not expand in χ and ζ when computing observables, recognizing that the results presented may be different with other choices of resummation when χ is

sufficiently large. An analysis done in GR comparing the Kerr spectrum to a spectrum from a slowly-rotating expansion of Kerr suggests this choice of resummation is accurate up to $\chi \approx 0.9$ [210].

5.3 Properties of the dCS and EdGB BH Solutions

BH solutions in dCS and EdGB gravity were discussed in detail in [57, 209]. We here discuss the properties of these BHs that are related to continuum spectrum observations, summarizing results from [57, 209] and presenting new results when necessary.

5.3.1 Test particle motion

In order to calculate the continuum spectrum of an accretion disk orbiting a black hole it is first necessary to determine the motion of test particles, i.e. massive particles with extremely weak self-gravity. In GR, test particles follow geodesics, and the same was proven to be true in dCS gravity [94]. We here prove that test particles follow geodesics in EdGB gravity.

We begin from the action of a test particle moving along a worldline $x^a = z^a(\lambda)$, where λ parameterizes the trajectory. The action is given by [214]

$$S_{\rm mat} = -m \int_\gamma d\lambda \sqrt{-g_{ab}(z) \frac{dz^a}{d\lambda} \frac{dz^b}{d\lambda}}, \tag{5.5}$$

where m is the mass of the test particle and $dz^a/d\lambda$ is the tangent to the worldline γ. By varying $S_{\rm mat}$ with respect to the metric we can find the contribution to the matter stress-energy tensor from this test particle. Using that the proper time τ is related to λ via $d\tau = d\lambda \sqrt{-g_{ab}(z) \frac{dz^a}{d\lambda} \frac{dz^b}{d\lambda}}$ and that the particle four-velocity $u^a = dz^a/d\tau$ obeys

$g_{ab}u^a u^b = -1$, the matter stress-energy tensor of the test particle can be written as

$$T^{ab}_{\rm mat}(x^c) = m\int \frac{d\tau}{\sqrt{-\mathbf{g}}} u^a u^b \delta^{(4)}[x^c - z^c(\tau)], \tag{5.6}$$

where $\mathbf{g}$ denotes the metric determinant and $\delta^{(4)}$ is the four-dimensional Dirac density defined by $\int d^4x\sqrt{-\mathbf{g}}\ \delta^{(4)}(x^c) = 1$. One can easily show that the divergence of $T^{ab}_{\rm mat}$ is given by

$$\nabla_b T^{ab}_{\rm mat} = m\int \frac{d\tau}{\sqrt{-\mathbf{g}}} \frac{d^2 z^a}{d\tau^2} \delta^{(4)}[\mathbf{x} - \mathbf{z}(\tau)]. \tag{5.7}$$

The field equations of EdGB gravity with $V(\vartheta) = 0$ and $\beta = 1$ are given by [209]

$$G_{ab} + 16\pi\alpha_{\rm EdGB}\mathcal{D}^{(\vartheta)}_{ab} - 8\pi T^{(\vartheta)}_{ab} = 8\pi T^{\rm mat}_{ab}, \tag{5.8}$$

where

$$T^{(\vartheta)}_{ab} = \nabla_a\vartheta\nabla_b\vartheta - \frac{1}{2}g_{ab}\nabla_c\vartheta\nabla^c\vartheta, \tag{5.9}$$

is the stress-energy tensor of the scalar field and

$$\begin{aligned}\mathcal{D}^{(\vartheta)}_{ab} \equiv& -2R\nabla_a\nabla_b\vartheta + 2(g_{ab}R - 2R_{ab})\nabla^c\nabla_c\vartheta \\ &+ 8R_{c(a}\nabla^c\nabla_{b)}\vartheta - 4g_{ab}R^{cd}\nabla_c\nabla_d\vartheta + 4R_{acbd}\nabla^c\nabla^d\vartheta.\end{aligned} \tag{5.10}$$

The scalar field equation is given by

$$\Box\vartheta = -\alpha_{\rm EdGB}\left(R^2 - 4R_{ab}R^{ab} + R_{abcd}R^{abcd}\right) = -\alpha R_{\rm GB}. \tag{5.11}$$

For test particles to follow geodesics, the divergence of $T^{\rm mat}_{ab}$ must vanish, which means that the divergence of the second and third terms on the left-hand side of Eq. 5.8 must cancel. Taking the divergence of Eq. 5.8, we then find that test particles

follow geodesics if

$$\nabla_b \mathcal{D}^{ab} = -\frac{1}{2}(\nabla^a \vartheta) R_{\rm GB}, \tag{5.12}$$

where we have used that the divergence of $T^{ab}_{(\vartheta)}$ is given by

$$\nabla_b T^{ab}_{(\vartheta)} = (\nabla^a \vartheta)(\Box \vartheta) = -\alpha_{\rm EdGB}(\nabla^a \vartheta) R_{\rm GB}. \tag{5.13}$$

Let us then evaluate the left-hand side of Eq. 5.12. Taking the divergence of Eq. 5.10 we have

$$\begin{aligned}
\nabla_b \mathcal{D}^{ab} &= 4R\nabla^{[a}\nabla^{b]}\nabla_b\vartheta - 8R^{bc}\nabla^{[a}\nabla^{c]}\nabla_b\vartheta \\
&\quad - 8R^{ab}\nabla_{[b}\nabla_{c]}\nabla^c\vartheta - 8\nabla^{[a}R^{c]b}\nabla_b\nabla_c\vartheta \\
&\quad - 4R^{abcd}\nabla_d\nabla_c\nabla_b\vartheta - 4\nabla_d R^{abcd}\nabla_c\nabla_b\vartheta.
\end{aligned} \tag{5.14}$$

Applying the Bianchi identities and the commutation of covariant derivatives gives

$$\begin{aligned}
\nabla_b \mathcal{D}^{ab} &= -2RR^{ab}\nabla_b\vartheta + 4R^{ac}R_{bc}\nabla^b\vartheta \\
&\quad + 4R_{cd}R^{acbd}\nabla_b\vartheta + 4R^{acde}R_{becd}\nabla^b\vartheta.
\end{aligned} \tag{5.15}$$

Using the definition of the Weyl tensor, $W_{abcd} \equiv R_{abcd} - (g_{a[c}R_{d]b} - g_{b[c}R_{d]a}) + 1/3Rg_{a[c}g_{d]b}$, we replace the Riemann tensor to get

$$\begin{aligned}
\nabla_b \mathcal{D}^{ab} &= -\frac{1}{3}R^2\nabla^a\vartheta + R_{bc}R^{bc}\nabla^a\vartheta \\
&\quad - 4W^{acde}W_{bcde}\nabla^b\vartheta + 4W^{acde}W_{bdce}\nabla^b\vartheta.
\end{aligned} \tag{5.16}$$

Applying the identities $W^{acde}W_{bcde} = 1/4 g^a_b W^{cdef}W_{cdef}$ and $W^{acde}W_{bdce} = 1/8 g^a_b W^{cdef}W_{cdef}$ gives

$$\nabla_b \mathcal{D}^{ab} = (\nabla^a \vartheta)(-\frac{1}{3}R^2 + R_{bc}R^{bc} - \frac{1}{2}W_{bcde}W^{bcde}). \tag{5.17}$$

Finally, using the definition of the Weyl tensor we find that the divergence of the stress-energy tensor of the scalar field is given by

$$\nabla_b \mathcal{D}^{ab} = -\frac{1}{2}(\nabla^a \vartheta)(R^2 - 4R_{bc}R^{bc} + R_{abcd}R^{abcd}) = -\frac{1}{2}(\nabla^a \vartheta)R_{\rm GB}. \tag{5.18}$$

Thus, Eq. 5.12 is satisfied, proving that test particles must follow geodesics in EdGB gravity

$$\frac{d^2 z^a}{d\tau^2} = 0. \tag{5.19}$$

5.3.2 Conserved Quantities

All three BH solutions considered within this work are stationary and axisymmetric, and thus, each possesses a timelike and an azimuthal Killing vector, which in turn implies the existence of two conserved quantities: the specific energy E and the z-component of the specific angular momentum L_z. In the dCS and the EdGB cases, these Killing vectors are approximate, i.e. they solve the Killing equation to $\mathcal{O}(\zeta, \chi^2)$, so E and L_z are also approximately conserved.

The definitions of E and L_z and the normalization condition for the 4-velocity $u^a u_a = -1$ allow us to find the equations of motion for test particles. As discussed above, such particles follow geodesics of the metric in dCS gravity and EdGB gravity. From the definition of E and L_z we find

$$\dot{t} = \frac{E g_{\phi\phi} + L_z g_{t\phi}}{g^2_{t\phi} - g_{tt}g_{\phi\phi}}, \qquad \dot{\phi} = -\frac{E g_{t\phi} + L_z g_{tt}}{g^2_{t\phi} - g_{tt}g_{\phi\phi}}, \tag{5.20}$$

where the overhead dot represents a derivative with respect to the affine parameter (proper time for a massive particle). Substituting Eq. 5.20 into the normalization condition, we find

$$g_{rr}\dot{r}^2 + g_{\theta\theta}\dot{\theta}^2 = V_{\rm eff}(r, \theta; E, L_z), \tag{5.21}$$

where we parameterize the four velocity via $u^a = (\dot{t}, \dot{r}, \dot{\theta}, \dot{\phi})$ with overhead dots representing derivatives with respect to proper time, and where the effective potential is

$$V_{\rm eff} \equiv \frac{E^2 g_{\phi\phi} + 2EL_z g_{t\phi} + L_z^2 g_{tt}}{g_{t\phi}^2 - g_{tt}g_{\phi\phi}} - 1. \tag{5.22}$$

Restricting attention to equatorial and circular orbits, we can obtain explicit expressions for the energy and angular momentum as a function of the metric components. Using the stability and circularity conditions $V_{\rm eff} = 0$ and $\partial V_{\rm eff}/\partial r = 0$, and solving for E and L_z, we find

$$E = -\frac{g_{tt} + g_{t\phi}\Omega}{\sqrt{-(g_{tt} + 2g_{t\phi}\Omega + g_{\phi\phi}\Omega^2)}}, \tag{5.23}$$

$$L_z = \frac{g_{t\phi} + g_{\phi\phi}\Omega}{\sqrt{-(g_{tt} + 2g_{t\phi}\Omega + g_{\phi\phi}\Omega^2)}}, \tag{5.24}$$

where the angular velocity of equatorial circular geodesics is defined via

$$\Omega := \frac{d\phi}{dt} = \frac{-g_{t\phi,r} + \sqrt{(g_{t\phi,r})^2 - g_{tt,r}g_{\phi\phi,r}}}{g_{\phi\phi,r}}. \tag{5.25}$$

5.3.3 ISCO

The ISCO is the stable circular orbit that is closest to the BH event horizon. Any circular orbit inside the ISCO will thus be unstable and any test particle that finds itself there is expected to rapidly plunge and cross the event horizon. Because

of this many accretion disk models assume the inner radius of the disk is exactly at the ISCO. This assumption is motivated by physical arguments, simulations, and observational evidence [21–25] and it could, in principle be relaxed. We, however, will retain this assumption throughout this work and leave its relaxation to future studies.

Since the ISCO is a geometric property of BHs that plays a key role in the continuum spectrum of accretion disks, let us now calculate its location. The ISCO radius can be found by substituting Eq. 5.23 into Eq. 5.22, and then solving $\partial^2 V_{\rm eff}/\partial r^2 = 0$ for r. The ISCO radius for equatiorial geodesics in Kerr is

$$r_{\rm ISCO} = M\left\{3 + Z_2 \mp \left[(3 - Z_1)\,(3 + Z_1 + 2Z_2)\right]^{1/2}\right\}, \tag{5.26}$$

where

$$Z_1 = 1 + \left(1 - \chi^2\right)^{1/3}\left[(1+\chi)^{1/3} + (1-\chi)^{1/3}\right], \tag{5.27}$$

$$Z_2 = \left(3\chi^2 + Z_1^2\right)^{1/2}, \tag{5.28}$$

where the $\mp$ denotes whether the disk's angular momentum is in the same $(-)$ or the opposite $(+)$ direction as the BH's angular momentum.

The ISCO radius in the EdGB and dCS BH solutions when treated as exact must be solved for numerically as the solutions to $\partial^2 V_{\rm eff}/\partial r^2 = 0$ are not analytically tractable. Note that, when the solutions are treated as approximate, the ISCO radius can be found analytically by expanding in χ and ζ; the difference, however, is negligible in dCS gravity and at most $\sim 2\%$ in EdGB gravity for the ranges of χ and ζ that we consider. To remain consistent throughout this work we also compute

the ISCO radius in Kerr numerically instead of using the above analytic solution, ensuring that the numerical ISCO agrees with the analytic to within our numerical error. Figure 5.1 shows the ISCO radius as a function of dimensionless spin χ for Kerr, the EdGB gravity solution with $\sqrt{|\alpha_{\rm EdGB}|} = 1.9 \times 10^5$cm, and the dCS gravity solution with $\sqrt{|\alpha_{\rm dCS}|} = 2.33 \times 10^5$cm, for a BH with mass $M = 5M_\odot$. Observe that the ISCO location in EdGB BHs is significantly different from the ISCO in Kerr BHs, even in the non-spinning limit, while the deviation in dCS BHs is essentially negligible even at higher spins.

The amount of deviation in the ISCO radius between the Kerr solution and the solutions in EdGB gravity and dCS gravity is not an intrinsic property of the BH solutions. Non-spinning BHs in EdGB gravity are not given by the Schwarzschild metric, in contrast to non-spinning BHs in dCS gravity. Thus, the ISCO radius in the EdGB BH solution is different from GR even when $\chi = 0$, while the ISCO radius in the dCS BH case is the same as in GR. This also means that any modifications to the ISCO radius in rotating dCS BHs must arise from spin-dependent terms in the metric, which are subdominant relative to terms independent of spin for slowly-rotating BHs. The small modification to the ISCO radius in dCS gravity is also due to our choice of coupling constant. A larger coupling would increase the deviation from Kerr, but may violate the small-coupling approximation used in finding the solution studied here.

5.3.4 Gravitational Redshift

The gravitational redshift is a quantity that describes how much the frequency of photons changes as they travel out of the BH potential. We can define this quantity via

$$g \equiv \frac{E_o}{E_e} = \frac{(p_a u^a)_o}{(p_b u^b)_e}, \tag{5.29}$$

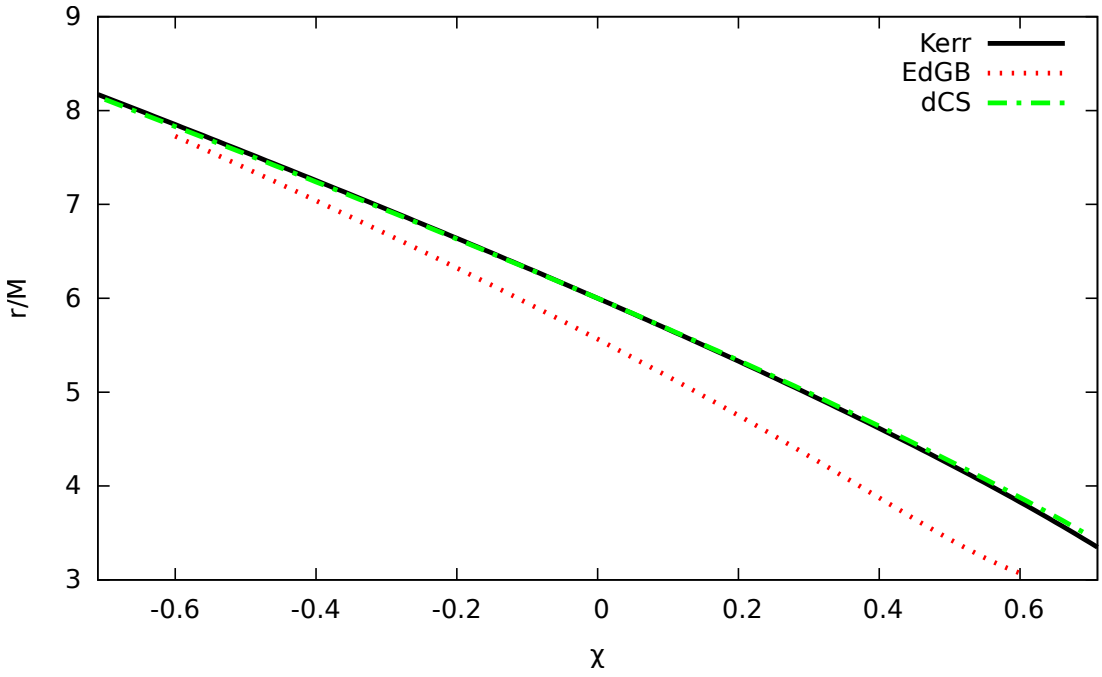

Figure 5.1: ISCO radius as a function of dimensionless spin χ for Kerr (black solid line), EdGB gravity with $\sqrt{|\alpha_{\rm EdGB}|} = 1.9 \times 10^5$cm (red dotted line), and dCS gravity with $\sqrt{|\alpha_{\rm dCS}|} = 2.33 \times 10^5$cm (green dashed-dotted line), for a BH mass $M = 5M_\odot$.

where p_a is the four-momentum of a photon traveling from the emitting material to the observer, and u_o^a and u_e^a are the four-velocities of the observer and the emitting material, respectively.

Let us now detail how to compute this redshift quantity explicitly in terms of components of the metric tensor by first focusing on the photon's four-momentum. The BH solutions we study are stationary and axisymmetric, so they are independent of the t and ϕ coordinates. Thus, the corresponding components of the four-momentum are conserved and we can write

$$p_a = (p_t, p_r, p_\theta, p_\phi) = (-E, p_r, p_\theta, L_z). \tag{5.30}$$

Let us now focus on the four-velocities of the observer and the emitting material. If we treat the observer as static, then $u_o^a = (1, 0, 0, 0)$. The four-velocity for material in a circular orbit on the equatorial plane is simply

$$u_e^a = u_e^t(1, 0, 0, \Omega), \tag{5.31}$$

where

$$u_e^t = \frac{1}{\sqrt{-(g_{tt} + 2g_{t\phi}\Omega + g_{\phi\phi}\Omega^2)}} \tag{5.32}$$

to enforce the timelike normalization condition.

With these quantities computed, we can now explicitly solve for the redshift factor. The numerator of Eq. 5.29 is simply $(p_a u^a)_o = -E$, while the denominator is $(p_a u^a)_e = -Eu_e^t + u_e^t \Omega L_z$, yielding the redshift factor

$$g = \frac{\sqrt{-(g_{tt} + 2g_{t\phi}\Omega + g_{\phi\phi}\Omega^2)}}{1 - \Omega\xi}, \tag{5.33}$$

where $\xi = L_z/E$.

The redshift factor depends on the ratio of the angular momentum and the energy, which although conserved are not directly measurable. We can recast the redshift factor, however, in terms of celestial coordinates α and β as follows. First, we place the observer at spatial infinity ($r = +\infty$) at an inclination angle ι between the observer's line of sight and the BH's angular momentum. We then define (α, β) as the Cartesian coordinates on the observer's plane of the sky, as measured from the observer's line of sight, i.e. measured in directions perpendicular and parallel to the rotation axis of the BH when projected onto the observer's plane of the sky, respectively. At large spatial distances, and using the fact that the BH metrics are asymptotically flat, the celestial coordinate α is given by

$$\alpha = \lim_{r\to\infty} -\frac{rp^\phi}{p^t} = \frac{-\xi}{\sin\iota}. \tag{5.34}$$

Neglecting light-bending[2], α can also be written as $\alpha = r\cos\phi$ where $\phi = 0$ is along the line of nodes, where the disk intersects the observer's plane of the sky. Then, solving for ξ one finds $\xi = -r\cos\phi\sin\iota$, and thus the redshift factor can be written as

$$g = \frac{\sqrt{-(g_{tt} + 2g_{t\phi}\Omega + g_{\phi\phi}\Omega^2)}}{1 + r\Omega\cos\phi\sin\iota}. \tag{5.35}$$

This expression depends only on the metric components, the angle ϕ and the material's angular velocity.

[2]There is no reason to assume the effect of light-bending is negligible compared to other relativistic effects, but incorporating its effects would require a general relativistic ray-tracing code and this is beyond the scope of this work.

5.4 Continuum Spectrum in dCS and EdGB BHs

We use the Novikov-Thorne accretion disk model [12], the standard general relativistic model for geometrically-thin and optically-thin accretion disks. The model assumes the disk is in the equatorial plane of the BH and the disk particles move on nearly geodesic circular orbits, i.e. geodesics except for a small radial momentum. With these assumptions, two of the equations that describe the time-averaged radial structure of the disk and are that are used for calculating the continuum spectrum are

$$\dot{M} = -2\pi\sqrt{-\mathbf{g}}\Sigma(r)u^r = \text{constant}, \tag{5.36}$$

$$\mathcal{F}(r) = \frac{\dot{M}}{4\pi\sqrt{-\mathbf{g}}}f(r), \tag{5.37}$$

where $\dot{M}$ and $\mathcal{F}$ are the time-averaged mass accretion rate and radially-dependent energy flux, respectively. In these equations, $\Sigma(r)$ is the surface density, u^r is the radial four-velocity of the disk particles, $\mathbf{g}$ is the determinant of the metric in the near equatorial plane in cylindrical coordinates, and the function $f(r)$ is defined by

$$f(r) = \frac{-\partial_r\Omega}{(E-\Omega L_z)^2}\int_{r_{\rm in}}^{r}(E-\Omega L_z)(\partial_{r'}L_z)dr'. \tag{5.38}$$

Here $r_{\rm in}$ is the inner radius of the accretion disk, which we choose to be the location of the ISCO.

The accretion rate $\dot{M}$ can be rewritten as $\dot{M} = L_{\rm bol}/\eta$, where $L_{\rm bol}$ is the bolometric luminosity and η is the radiative efficiency, the efficiency of conversion between rest-mass and EM energy. The radiative efficiency can be written as

$\eta = 1 - E(r_{\rm ISCO})$, by assuming the energy radiated by a particle falling into a BH is approximately equal to the binding energy of the ISCO [190]. The accretion rate is then given by

$$\dot{M} = \frac{L_{\rm bol}}{1 - E(r_{\rm ISCO})}, \tag{5.39}$$

and the radial energy flux of Eq. 5.37 can be rewritten as

$$\mathcal{F}(r) = \frac{L_{\rm bol}}{4\pi\sqrt{-\mathbf{g}}\left[1 - E(r_{\rm ISCO})\right]} \frac{-\partial_r \Omega}{\left(E - \Omega L_z\right)^2} \int_{r_{\rm in}}^{r} \left(E - \Omega L_z\right)\left(\partial_{r'} L_z\right) dr'. \tag{5.40}$$

Assuming the disk is in thermal equilibrium and modeling the radiation emitted by the disk as a black-body, we can compute its luminosity. This quantity is nothing but the integral of the spectral radiance given by Planck's law over the extent of the disk, namely

$$L(\nu) = \frac{8\pi h}{c^2} \cos\iota \int_{r_{\rm in}}^{r_{\rm out}} \int_0^{2\pi} \frac{\nu^3 \sqrt{-\mathbf{g}}}{\exp\left[h\nu / g k_{\rm B} T(r)\right] - 1} dr d\phi, \tag{5.41}$$

where g is the redshift found in Eq. 5.35, h is the Planck constant, $k_{\rm B}$ is the Boltzmann constant, ν is the observed frequency, $r_{\rm out}$ is the outer radius of the disk, and we have here restored the speed of light c. The quantity $T(r)$ is the temperature of the disk, which can be related to the radial energy flux using the Stefan-Boltzmann law

$$T(r) = \left(\frac{\mathcal{F}(r)}{\sigma}\right)^{1/4}, \tag{5.42}$$

where σ is the Stefan-Boltzmann constant.

The main observable we will be concerned with is the accretion disk luminosity, which as we can see depends on the metric in various ways. The luminosity $L(\nu)$ is given by Eq. 5.41, which depends on the metric via the determinant factor in its

integrand, the ISCO in the limits of integration, and also through the temperature $T(r)$. The latter is given in terms of the radial energy flux in Eq. 5.42, while the energy flux is given in Eq. 5.40. This flux clearly depends on the metric through its associated conserved quantities E and L_z, as well as the angular velocity Ω of test particles in a circular orbit. It stands to reason, then, that if the metric changes, for example if modified gravity theories do not allow the Kerr metric as a solution for BH spacetimes, then the luminosity of its associated accretion disk will also change.

5.4.1 Method

We wish to determine whether better-than-current constraints can be placed on EdGB gravity and dCS gravity using current and next generation continuum spectrum observations. Following the same prescription as [210], let us assume that the Kerr metric is the correct description of a BH spacetime and that the associated spectrum is our observation. We shall refer to the Kerr spectrum observation as the *injected synthetic signal* or *injection* for short. Further, we use the spectrum calculated with the EdGB gravity or dCS gravity metrics as our *model* and fit it to the injection.

When constructing both the injections and the models, the spectrum is calculated using Eq. 5.41, as explained in the previous subsection. The integrals are numerically evaluated using Simpson's rule with step sizes chosen to ensure numerical error is small. For the energy flux integration, we choose a radial step size of $\delta r = 0.1M$, with a much smaller step size of $\delta r = 10^{-4}M$ for $r \leq r_{\rm ISCO} + 2.5M$, as the energy flux changes rapidly near the ISCO radius. For the luminosity integration, we choose step sizes of $\delta r = M$ and $\delta\phi = 0.1$. A lengthy numerical investigation was performed to guarantee the numerical error is under control with these choices of step sizes.

The parameters of the spectrum model outlined in Sec. 5.4 are $\vec{\lambda} = (M, \chi, \iota, F_{\rm bol})$, i.e. the BH mass, its dimensionless spin $\chi = a/M$, the inclination angle, and the bolometric luminosity, respectively. The latter, $F_{\rm bol}$, should in principle be extracted from observations, but since we wish to focus on the impact of modified BH solutions rather than the properties of the accretion disk itself, we will fix $L_{\rm bol} = 1.2572 \times 10^{36}$ erg/s. This luminosity is also equal to 10% of the Eddington luminosity, $L_{\rm Edd} = 1.2572 \times 10^{38}\,(M/M_\odot)$erg/s for a $1M_\odot$ object. This leaves the mass m, the spin χ, and the inclination angle ι as the parameters of the spectrum model, for all of which we choose a flat prior over the following ranges. For the mass and inclination angle, we choose ranges that are representative of current BH continuum spectrum observations: $6M_\odot \leq M \leq 19M_\odot$ and $10^\circ \leq \iota \leq 80^\circ$. The spin range is limited by the region of validity for the slow-rotating EdGB gravity and dCS gravity solutions. For EdGB gravity we use the range $-0.6 \leq \chi \leq 0.6$ [209] and for dCS gravity we use the range $-0.7 \leq \chi \leq 0.7$ [106].

As we wish to compare the projected constraints we will obtain against current constraints on EdGB gravity and dCS gravity we fix the coupling constant α in each model, thus not including it as a parameter of the model. In the case of EdGB gravity we choose $\sqrt{|\alpha_{\rm EdGB}|} = 1.9 \times 10^5$cm, which saturates the current constraint [111]. For dCS gravity we choose $\sqrt{|\alpha_{\rm dCS}|} = 2.33 \times 10^5$cm, which gives a dimensionless coupling of $\zeta = 0.5$ for BH mass $M = 5M_\odot$, the smallest mass, and thus, the largest dimensionless coupling, used in our analysis. For coupling values larger than this, the small-coupling approximation used to construct the dCS BH solution would be violated.

We estimate parameters in the model by minimizing the relative χ^2 over all parameters. The reduced χ^2 is defined as

$$\chi^2_{\rm red} = \frac{\chi^2}{N} = \frac{1}{N}\sum_{i=1}^{N}\left[\frac{L_{\rm QG}(\nu_i, M, \chi, \iota) - L_{\rm K}(\nu_i, M^*, \chi^*, \iota^*)}{\sigma(\nu_i)}\right]^2, \tag{5.43}$$

where the summation is over N sampling frequencies $\nu_i \in (10^{15}, 10^{18})$Hz wth 10 samples per decade spaced logarithmically. This sampling choice is representative of that made in the observed spectra of BHs with estimated spins [24, 24, 192–197]. The quantity $L_{\rm QG}(\nu, M, \chi, \iota)$ is the spectrum model, which depends on the frequency ν and the model parameters (M, χ, ι), while $L_{\rm K}(\nu, M^*, \chi^*, \iota^*)$ is the injection, which depends on the frequency and the injected parameters (M^*, χ^*, ι^*). The values of model parameters that minimize the reduced χ^2 are the best-fit model parameters.

We model the standard deviation of the distribution, σ, via

$$\sigma(\nu_i) = \sigma_M(\nu_i) + \sigma_\chi(\nu_i) + \sigma_\iota(\nu_i), \tag{5.44}$$

where

$$\sigma_M(\nu_i) = \frac{|L_{\rm K}(\nu_i, M^* + \delta m, \chi^*, \iota^*) - L_{\rm K}(\nu_i, M^* - \delta m, \chi^*, \iota^*)|}{2}, \tag{5.45}$$

$$\sigma_\chi(\nu_i) = \frac{|L_{\rm K}(\nu_i, M^*, \chi^* + \delta\chi, \iota^*) - L_{\rm K}(\nu_i, M^*, \chi^* - \delta\chi, \iota^*)|}{2}, \tag{5.46}$$

$$\sigma_\iota(\nu_i) = \frac{|L_{\rm K}(\nu_i, M^*, \chi^*, \iota^* + \delta\iota) - L_{\rm K}(\nu_i, M^*, \chi^*, \iota^* - \delta\iota)|}{2}, \tag{5.47}$$

where M^*, χ^*, and ι^* are the injected mass, spin, and inclination angle of the Kerr spectrum, respectively. The quantities $\delta M, \delta\chi$, and $\delta\iota$ serve as a way

to represent the observational error in the observations. When considering the ability of current telescopes to place constraints on modified gravity, we choose $(\delta M, \delta\chi, \delta\iota) = (1M_\odot, 0.1, 1^\circ)$, which is comparable to or better than the error in current BH mass, spin, and inclination angle measurements for BHs in which the spins were measured using continuum spectrum observations [8]. When considering the ability of next generation telescopes to place constraints on modified theories, we reduce the observational error in the spin parameter by an order of magnitude, i.e. $\delta\chi = 0.01$ [34, 35, 170].

5.4.2 Results

We first wish to determine if better-than-current constraints can be placed on modified gravity theories with continuum spectrum observations using current telescopes. To do so we define the weighted deviation $\Delta_A = |A^* - A|/\sigma_A$ where $A = [M, \chi, \iota]$, i.e. the difference between the value of the injected parameter and the value of the best fit parameter weighted by the error in that parameter. When $\Delta_A > 1$, we expect the deviation in the continuum spectrum due to the modified gravity solution to be in principle detectable, i.e. larger than the observational error, and the modified theory may be constrained. However, if $\Delta_A < 1$ the deviation in the continuum spectrum is not detectable (not even in principle) and the modified theory cannot be constrained.

Figure 5.2 shows the weighted deviation for spin as a function of injected mass when averaged over the injected spin and inclination angle for EdGB gravity with current telescopes. The weighted deviation for mass and inclination angle, as well as that for mass as a function of injected spin and inclination angle, are approximately zero in the entire range explored, so we do not show them here. Although the weighted deviation is below unity for all parameters, and thus, the deviation due

to EdGB gravity is not detectable, the spin weighted deviation does increase as the BH mass decreases. This occurs because the deviation from GR is proportional to the dimensionless coupling ζ, which goes as $1/M^4$, thus deviations are larger in smaller mass BHs.

The weighted deviations for dCS gravity is also approximately zero, but for the full range of injected masses, spins, and inclination angles we considered. This means the deviation in the metric due to dCS gravity is not detectable with current telescopes at all. The deviation is so small in this case because Schwarzschild is already a solution in dCS gravity, and thus, the non-spinning part of the BH solution is not modified.

Let us now consider constraints one can place on modified gravity with next generation X-Ray telescopes. The results for dCS gravity are similar to those for current telescopes; the weighted deviations for mass, spin, and inclination angle are all approximately zero for the full range of injected masses, spins, and inclination angles considered. Thus, even with next generation telescopes, dCS gravity cannot be better constrained using these observations. In the EdGB case, however, the situation is slightly different. Figure 5.2 shows the weighted deviation for spin as a function of injected mass for EdGB gravity; all other weighted deviations remain below unity, and we thus do not show them here. As the weighted deviation for spin is significantly above 1 for low BH mass, next generation telescopes may be able to place better-than-current constraints on the EdGB gravity coupling constant with continuum spectrum observations of BHs provided $M \lesssim 8M_{\odot}$. As explained previously, deviations from GR are larger for smaller mass BHs because the deviations are proportional to $1/M^4$.

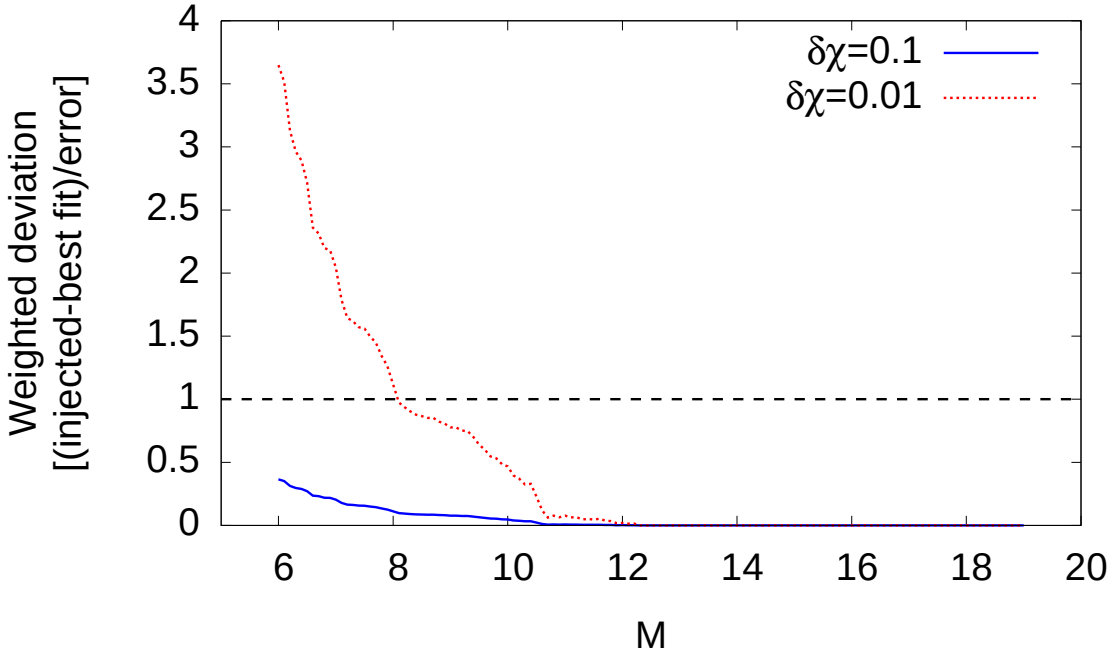

Figure 5.2: Weighted deviation for spin as a function of injected mass when averaged over injected spin and inclination angle for EdGB gravity with $\sqrt{|\alpha_{\rm EdGB}|} = 1.9 \times 10^5$cm, $\delta M = 1 M_\odot$, and $\delta\iota = 1^\circ$. To represent current telescopes we use $\delta\chi = 0.1$ (blue solid line) and to represent next generation telescopes we use $\delta\chi = 0.01$ (red dotted line). The black dashed line at a weighted deviation of 1 marks the boundary between a deviation being detectable (> 1) and not detectable (< 1), i.e. being able to place a constraint or not place a constraint on a modified theory, respectively.

5.5 Discussion

We have studied whether it is possible to place better-than-current constraints on coupling constants in modified gravity theories using BH continuum spectrum observations with both current and next generation X-Ray telescopes. We focused on EdGB gravity and dCS gravity, two theories within the broader class of quadratic gravity theories, as examples of well-motivated modified theories. The BHs were modeled using approximate solutions in EdGB gravity and dCS gravity that are quadratic in the angular momentum and linear in the coupling. We have found that dCS gravity cannot be constrained using continuum spectrum observations, both with current and next generation telescopes, as the modifications in the spectrum are much smaller than the sensitivity of the telescopes. In the EdGB gravity case, however, we find that although current telescopes cannot place better-than-current constraints on the coupling, next generation telescopes will be able to do so provided the BHs observed have a sufficiently small mass.

While our results show that the deviation due to EdGB gravity in the spin parameter extracted from the continuum spectrum is larger than the sensitivity of next generation telescopes, to actually place constraints on $\alpha_{\rm EdGB}$ a second, independent measurement of the spin parameter is required to break the degeneracy between the spin and the modified theory. Possible independent measurements include the Kα iron line emitted from accretion disks [208] or quasi-periodic oscillations observed in accretion disks [215]. An interesting extension of our work would be to determine if a constraint could still be placed on EdGB gravity with next generation telescopes when a second independent measurement, and the error associated with it, is taken into account.

Our analysis assumes the accretion disk and continuum spectrum are well understood and well modeled, i.e. the systematic error due to our lack of understanding of accretion disk physics is negligible. In reality this is currently not the case as there are numerous accretion disk models, analytic and numerical, that include different assumptions about the initial conditions and physics involved, and current observations of accretion disks are not able to distinguish between all the models [11, 216, 217]. The systematic error due to accretion disk model uncertainty is generally estimated to be on the order of the current observational error in continuum spectrum observations, i.e. $\sim 10\%$ error in the accuracy to which BH properties can be estimated [8]. Before constraints can be placed on modified gravity theories using continuum spectrum observations with next generation telescopes, as our analysis suggests is possible, the systematic error in the model must be brought down to similar levels as the observational error, i.e. $\sim 1\%$ error in the recovered BH parameters.

The approximate BH solutions in EdGB gravity and dCS gravity we studied in this work are of quadratic order in the spin angular momentum and linear order in the dimensionless coupling constant. Repeating the analysis done here with solutions that include higher orders in spin would allow this work to be extended to BHs with higher spins, eventually approaching the maximal spin limit. An extension of this sort that includes higher order in spin effects is particularly important for dCS gravity as the modifications to GR from dCS gravity are only present for rotating BHs. For EdGB gravity a solution that is fifth order in the spin and seventh order in the coupling parameter $\alpha_{\rm EdGB}$ was found in [178], and can be used to extend the work in this paper. For dCS gravity a higher order solution has not yet been found.

Other extensions of our work could be to relax some of the other assumptions that were made, in turn further verifying our conclusions. The effect of light-bending was neglected and could be taken into account with a ray-tracing algorithm. The

assumption that the inner radius of the accretion disk is at the ISCO is an important one, but it is not necessarily correct. The Novikov-Thorne model is a simple accretion disk model and real accretion disks are almost certainly more complex. Other accretion disk models with varying inner radii could be used to determine whether our results are independent of accretion disk model.

5.6 Acknowledgments

We thank Kent Yagi, Alejandro Cárdenas-Avendaño, and Andrew Sullivan for useful discussions. This work was supported by the NSF CAREER Grant PHY-1250636. Some calculations used the computer algebra-systems MAPLE, in combination with the GRTENSORII package [121].

CONCLUSION

With current and upcoming instruments reaching sensitivities high enough to test General Relativity near extreme gravitational objects, it is more important now than ever to attain a better understanding of modified gravity theories observationally and theoretically. In this dissertation I have presented four studies that attempted to contribute to just such an undertaking. These studies focused on two modified gravity theories within the wider class of theories known as quadratic gravity, dynamical Chern-Simons gravity and Einstein-dilaton-Gauss-Bonnet gravity, and on black hole electromagnetic observations as tests of GR.

Chapter 2 presented a linear stability analysis of QG, focusing on dCS gravity and EdGB gravity. Dispersion relations for linear perturbations within these theories were calculated and studied in BH backgrounds. The results show that on these backgrounds these theories are stable far from the BHs. This work was the first linear stability analysis in QG of all perturbation modes in generic backgrounds. Since this work new BH solutions have been found in dCS gravity [57] and EdGB gravity [178, 209] and a similar analysis can be done in those backgrounds. Furthermore, a full analysis was not done on the derived dispersion relations. The dispersion relations were found to be dependent on the amplitudes of the metric and scalar field perturbations. Due to this dependence, it is difficult to determine whether the scalar and gravitational waves will be generically stable, i.e. linearly stable on all backgrounds and in all cases, not just the limiting cases studied here. The far-field analysis that was carried out suggests that the waves should be stable, but it is possible that in this limit there are suppressed terms that would lead to instabilities. A more complete analysis that does not take the far-field limit may yield interesting results. Another extension would be to perform a stability analysis to higher order

in the perturbation as instabilities can be found at higher than linear order. Such a study could be carried out analytically or numerically if the mathematics becomes intractable.

In Chapter 3, a new approximate rotating BH solution up to quadratic order in spin in EdGB gravity was found. The properties of the new solution were then calculated and studied, such as the event horizon radius and the energy and angular momentum of orbiting particles. BH solutions in modified gravity theories are necessary for studying these theories with observations. Since this work, a new solution has been found, going to higher order in the spin and the coupling [178]. Current numerical solutions in EdGB gravity do not treat the theory as *effective*, so an obvious avenue of research would be to search for a numerical solution in the *effective field theory* approach. Recently, a BH solution was found in dCS gravity in the extremal limit [187], i.e. the maximum spin allowed for a BH. The same method could be used to find an extremal limit solution in EdGB gravity. Furthermore, one could perform a resummation of the higher order in spin solution found by [178] using the extremal limit solution, in principle finding a solution that is valid at all values of the spin.

Chapter 4 attempted to answer the question of how much systematic error is introduced into BH EM observations when using an approximate BH solution as the model. The EM observations of the continuum spectrum and BH shadow were analyzed and the Kerr solution was compared to a quadratic order in spin approximation of the Kerr solution. It was found that the systematic error introduced in these observations is negligible for small enough spins when compared to the current levels of observational error. As the Kerr solution is not the correct solution for a rotating BH in many modified gravity theories, this result may not necessarily apply in those theories. Since exact solutions may not exist in those other theories, one

cannot compare analytic solutions in the same way, but it may be possible to compare approximate analytic solutions to numerical solutions. One could also compare low-order approximate solutions to much higher order approximate ones, using the latter as a proxy for exact solutions.

Finally, in Chapter 5, the question of whether it is possible to place better-than-current constraints on dCS gravity and EdGB gravity using the BH continuum spectrum observation was studied. In the case of dCS gravity, better-than-current constraints cannot be placed primarily because there are no corrections to the non-spinning part of the BH solution. This leads to an overall smaller modification to the continuum spectrum from GR. In the case of EdGB gravity, using next generation X-Ray telescopes it may be possible to place better-than-current constraints using continuum spectrum observations of BHs with masses less than about 8 solar masses. This final work can be expanded upon by using more realistic models for the accretion disk and continuum spectrum, as the models used here are the simplest models that incorporate the relavent physics. This study can also be applied to BH shadows, and has been for a linear-in-spin BH solution in dCS gravity [211] and for a numerical spinning BH solution in EdGB gravity [218]. New work could study shadows using the spinning BH solutions used in Chapter 5.

REFERENCES CITED

[1] Einstein A 1915 *Sitzungsberichte der Königlich Preußischen Akademie der Wissenschaften (Berlin), Seite 844-847.*

[2] Schwarzschild K 1916 *Abh. Konigl. Preuss. Akad. Wissenschaften Jahre 1906,92, Berlin,1907* **1916**

[3] Eddington A S 1924 *Nature* **113** 192

[4] Lemaître G 1933 *Annales de la Société Scientifique de Bruxelles* **53**

[5] Finkelstein D 1958 *Physical Review* **110** 965–967

[6] Kerr R P 1963 *Physical Review Letters* **11** 237–238

[7] Kristian J, Brucato R, Visvanathan N, Lanning H and Sandage A 1971 *Astrophys. J. Lett.* **168** L91

[8] Miller M C and Miller J M 2015 *Phys. Rep.* **548** 1–34 (*Preprint* 1408.4145)

[9] Volonteri M 2010 *A&A Rev.* **18** 279–315 (*Preprint* 1003.4404)

[10] Greene J E 2012 *Nature Communications* **3** 1304 (*Preprint* 1211.7082)

[11] Abramowicz M A and Fragile P C 2013 *Living Reviews in Relativity* **16** URL http://www.livingreviews.org/lrr-2013-1

[12] Novikov I D and Thorne K S 1973 Astrophysics of black holes. *Black Holes* ed Dewitt C and Dewitt B S pp 343–450

[13] Van Oss R F, Van Den Oord G H J and Kuperus M 1993 *Accretion Disk Flares in Energetic Radiation Fields* (Dordrecht: Springer Netherlands) pp 217–218 ISBN 978-94-011-0772-3 URL http://dx.doi.org/10.1007/978-94-011-0772-3_38

[14] Williams G and Maletesta K 2002 *Astronom. J.* **123** 1095–1105

[15] Gies D R 2008 Binaries in Massive Star Formation *Massive Star Formation: Observations Confront Theory* (*Astronomical Society of the Pacific Conference Series* vol 387) ed Beuther H, Linz H and Henning T p 93

[16] Bambi C 2015 *ArXiv e-prints* (*Preprint* 1509.03884)

[17] Nixon C and Salvesen G 2014 *Mon. Not. Roy. Astron. Soc.* **437** 3994–3999 (*Preprint* 1311.2930)

[18] Cabanac C, Fender R P, Dunn R J H and Körding E G 2009 *MNRAS* **396** 1415–1440 (*Preprint* 0904.0701)

[19] Kazanas D, Fukumura K, Behar E, ContopouLos I and Shrader C 2012 *Astronomical Review* **7** 92–123 (*Preprint* http://dx.doi.org/10.1080/21672857.2012.11519707) URL http://dx.doi.org/10.1080/21672857.2012.11519707

[20] Frank J, King A and Raine D J 2002 *Accretion Power in Astrophysics: Third Edition*

[21] Reynolds C S and Fabian A C 2008 *Astrophys. J.* **675** 1048–1056 (*Preprint* 0711.4158)

[22] Shafee R, McKinney J C, Narayan R, Tchekhovskoy A, Gammie C F and McClintock J E 2008 *Astrophys. J.* **687** L25–L28 (*Preprint* 0808.2860)

[23] Penna R F, McKinney J C, Narayan R, Tchekhovskoy A, Shafee R and McClintock J E 2010 *MNRAS* **408** 752–782 (*Preprint* 1003.0966)

[24] Gou L, McClintock J E, Liu J, Narayan R, Steiner J F, Remillard R A, Orosz J A, Davis S W, Ebisawa K and Schlegel E M 2009 *Astrophys. J.* **701** 1076–1090 (*Preprint* 0901.0920)

[25] Steiner J F, McClintock J E, Remillard R A, Gou L, Yamada S and Narayan R 2010 *ApJ Letters* **718** L117–L121 (*Preprint* 1006.5729)

[26] Zhu Y, Davis S W, Narayan R, Kulkarni A K, Penna R F and McClintock J E 2012 *MNRAS* **424** 2504–2521 (*Preprint* 1202.1530)

[27] Beloborodov A M 1999 *ASP Conf. Ser.* **161** 295 (*Preprint* astro-ph/9901108)

[28] Schnittman J D, Krolik J H and Noble S C 2016 *Astrophys. J.* **819** 48 (*Preprint* 1512.00729)

[29] Contopoulos I and Papadopoulos D B 2012 *MNRAS* **425** 147–152 (*Preprint* 1205.6597)

[30] Bromley B C, Miller W A and Pariev V I 1998 *Nature* **391** 54

[31] Krolik J H and Hawley J F 2002 *Astrophys. J.* **573** 754 (*Preprint* astro-ph/0203289)

[32] Johannsen T 2013 *Phys. Rev.* **D87** 124010 (*Preprint* 1304.8106)

[33] Medeiros L, Chan C k, zel F, Psaltis D, Kim J, Marrone D and Sdowski A 2016 (*Preprint* 1610.03505)

[34] Zhang S N *et al.* (eXTP) 2016 eXTP – enhanced X-ray Timing and Polarimetry Mission *Proceedings, SPIE Astronomical Telescopes + Instrumentation 2016 : Millimeter, Submillimeter, and Far-Infrared Detectors and*

Instrumentation for Astronomy VIII: Edinburgh, United Kingdom, June 28-July 1, 2016 (*Preprint* 1607.08823) URL https://inspirehep.net/record/1478578/files/arXiv:1607.08823.pdf

[35] Takahashi T, Mitsuda K, Kelley R, Fabian A, Mushotzky R, Ohashi T, Petre R and on behalf of the ASTRO-H Science Working Group 2014 *ArXiv e-prints* (*Preprint* 1412.2351)

[36] Harrison T E, Howell S B, Szkody P and Cordova F A 2007 *The Astronomical Journal* **133** 162 URL http://stacks.iop.org/1538-3881/133/i=1/a=162

[37] Johannsen T 2015 (*Preprint* 1512.03818)

[38] Walsh J L, Barth A J, Ho L C and Sarzi M 2013 *Astrophys. J.* **770** 86 (*Preprint* 1304.7273)

[39] Thomas J, Ma C P, McConnell N J, Greene J E, Blakeslee J P and Janish R 2016 *Nature* **532** 340–342 (*Preprint* 1604.01400)

[40] Doeleman S, Agol E, Backer D, Baganoff F, Bower G C, Broderick A, Fabian A, Fish V, Gammie C, Ho P, Honman M, Krichbaum T, Loeb A, Marrone D, Reid M, Rogers A, Shapiro I, Strittmatter P, Tilanus R, Weintroub J, Whitney A, Wright M and Ziurys L 2009 Imaging an Event Horizon: submm-VLBI of a Super Massive Black Hole *astro2010: The Astronomy and Astrophysics Decadal Survey* (*Astronomy* vol 2010) (*Preprint* 0906.3899)

[41] Felli M and Spencer R E 1989 *Very Long Baseline Interferometry: Techniques and Applications* (Springer Netherlands)

[42] Psaltis D 2008 *Living Reviews in Relativity* **11** URL http://www.livingreviews.org/lrr-2008-9

[43] Oppenheimer J R and Snyder H 1939 *Physical Review* **56** 455–459

[44] Friedman A 1999 *General Relativity and Gravitation* **31** 1991–2000 ISSN 1572-9532 URL http://dx.doi.org/10.1023/A:1026751225741

[45] Yunes N and Siemens X 2013 (*Preprint* 1304.3473)

[46] Clifton T, Ferreira P G, Padilla A and Skordis C 2012 *Phys. Rept.* **513** 1–189 (*Preprint* 1106.2476)

[47] Yunes N, Yagi K and Pretorius F 2016 *Phys. Rev.* **D94** 084002 (*Preprint* 1603.08955)

[48] Yunes N and Siemens X 2013 *Living Reviews in Relativity* **16** URL http://www.livingreviews.org/lrr-2013-9

[49] Brans C 2010 *Einstein Online* **4**

[50] Hinterbichler K 2012 *Rev. Mod. Phys.* **84** 671–710 (*Preprint* 1105.3735)

[51] Yagi K, Stein L C and Yunes N 2016 *Phys. Rev.* **D93** 024010 (*Preprint* 1510.02152)

[52] Alexander S H S and Gates Jr S J 2006 *J. Cosm. Astropart. Phys.* **6** 018 (*Preprint* arXiv:hep-th/0409014)

[53] Gates S J, Ketov S V and Yunes N 2009 *Phys. Rev. D* **80**(6) 065003 URL http://link.aps.org/doi/10.1103/PhysRevD.80.065003

[54] Weinberg S 2008 *Phys. Rev. D* **77**(12) 123541 URL http://link.aps.org/doi/10.1103/PhysRevD.77.123541

[55] Taveras V and Yunes N 2008 *Phys. Rev. D* **78**(6) 064070 URL http://link.aps.org/doi/10.1103/PhysRevD.78.064070

[56] Mercuri S and Taveras V 2009 *Phys. Rev. D* **80**(10) 104007 URL http://link.aps.org/doi/10.1103/PhysRevD.80.104007

[57] Yagi K, Yunes N and Tanaka T 2012 *Phys.Rev.* **D86** 044037 (*Preprint* 1206.6130)

[58] Dyda S, Flanagan E E and Kamionkowski M 2012 *Phys.Rev.* **D86** 124031 (*Preprint* 1208.4871)

[59] Motohashi H and Suyama T 2011 *Phys. Rev. D* **84**(8) 084041 URL http://link.aps.org/doi/10.1103/PhysRevD.84.084041

[60] Will C M 2014 *Living Rev. Rel.* **17** 4 (*Preprint* 1403.7377)

[61] Damour T and Schaefer G 1991 *Physical Review Letters* **66** 2549–2552

[62] Lorimer D R and Freire P C C 2005 *ASP Conf. Ser.* **328** 19 (*Preprint* astro-ph/0404270)

[63] Freire P C C, Kramer M and Wex N 2012 *Class. Quant. Grav.* **29** 184007 (*Preprint* 1205.3751)

[64] Gonzalez M E, Stairs I H, Ferdman R D, Freire P C C, Nice D J, Demorest P B, Ransom S M, Kramer M, Camilo F, Hobbs G, Manchester R N and Lyne A G 2011 *Astrophys. J.* **743** 102 (*Preprint* 1109.5638)

[65] Yagi K, Stein L C, Yunes N and Tanaka T 2013 *Phys. Rev.* **D87** 084058 [Erratum: Phys. Rev.D93,no.8,089909(2016)] (*Preprint* 1302.1918)

[66] Vasúth M, Keresztes Z, Mihály A and Gergely L A 2003 *Phys. Rev. D* **68**(12) 124006 URL https://link.aps.org/doi/10.1103/PhysRevD.68.124006

[67] Abbott B P *et al.* (Virgo, LIGO Scientific) 2016 *Phys. Rev. Lett.* **116** 221101 (*Preprint* 1602.03841)

[68] Abbott B P *et al.* (Virgo, LIGO Scientific) 2016 *Phys. Rev. Lett.* **116** 061102 (*Preprint* 1602.03837)

[69] Abbott B P *et al.* (Virgo, LIGO Scientific) 2016 *Phys. Rev. Lett.* **116** 241103 (*Preprint* 1606.04855)

[70] Acernese F *et al.* (VIRGO) 2015 *Class. Quant. Grav.* **32** 024001 (*Preprint* 1408.3978)

[71] Aso Y, Michimura Y, Somiya K, Ando M, Miyakawa O, Sekiguchi T, Tatsumi D and Yamamoto H (The KAGRA Collaboration) 2013 *Phys. Rev. D* **88**(4) 043007 URL http://link.aps.org/doi/10.1103/PhysRevD.88.043007

[72] Stairs I H 2003 *Living Reviews in Relativity* **6** URL http://www.livingreviews.org/lrr-2003-5

[73] Gendreau K C, Arzoumanian Z and Okajima T 2012 The Neutron star Interior Composition ExploreR (NICER): an Explorer mission of opportunity for soft x-ray timing spectroscopy *Space Telescopes and Instrumentation 2012: Ultraviolet to Gamma Ray* (*Proc. SPIE* vol 8443) p 844313

[74] Lorimer D R 2008 *Living Reviews in Relativity* **11** 8 ISSN 1433-8351 URL http://dx.doi.org/10.12942/lrr-2008-8

[75] Yunes N and Pretorius F 2009 *Phys. Rev. D* **80**(12) 122003 URL http://link.aps.org/doi/10.1103/PhysRevD.80.122003

[76] Koyama K 2016 *Rept. Prog. Phys.* **79** 046902 (*Preprint* 1504.04623)

[77] Psaltis D, Ozel F, Chan C K and Marrone D P 2015 *Astrophys. J.* **814** 115 (*Preprint* 1411.1454)

[78] Pani P, Cardoso V and Gualtieri L 2011 *Phys. Rev.* **D83** 104048 (*Preprint* 1104.1183)

[79] Yagi K, Stein L C, Yunes N and Tanaka T 2012 *Phys.Rev.* **D85** 064022 (*Preprint* 1110.5950)

[80] Cardoso V and Gualtieri L 2009 *Phys.Rev.* **D80** 064008 (*Preprint* 0907.5008)

[81] Molina C, Pani P, Cardoso V and Gualtieri L 2010 *Phys. Rev. D* **81**(12) 124021 URL http://link.aps.org/doi/10.1103/PhysRevD.81.124021

[82] Garfinkle D, Pretorius F and Yunes N 2010 *Phys. Rev. D* **82**(4) 041501 URL http://link.aps.org/doi/10.1103/PhysRevD.82.041501

[83] Motohashi H and Suyama T 2012 *Phys.Rev.* **D85** 044054 (*Preprint* 1110.6241)

[84] Jackiw R and Pi S Y 2003 *Phys. Rev.* **D68** 104012 (*Preprint* gr-qc/0308071)

[85] Yunes N and Stein L C 2011 *Phys. Rev. D* **83**(10) 104002 URL http://link.aps.org/doi/10.1103/PhysRevD.83.104002

[86] Pani P, Macedo C F, Crispino L C and Cardoso V 2011 *Phys.Rev.* **D84** 087501 (*Preprint* 1109.3996)

[87] Will C M 1993 *Theory and Experiment in Gravitational Physics*

[88] Eardley D M, Lee D L, Lightman A P, Wagoner R V and Will C M 1973 *Phys. Rev. Lett.* **30**(18) 884–886 URL http://link.aps.org/doi/10.1103/PhysRevLett.30.884

[89] Will C M and Yunes N 2004 *Classical and Quantum Gravity* **21** 4367–4381 (*Preprint* arXiv:gr-qc/0403100)

[90] Berti E, Buonanno A and Will C M 2005 *Phys. Rev. D* **71**(8) 084025 URL http://link.aps.org/doi/10.1103/PhysRevD.71.084025

[91] Jones D I 2005 *Astrophys. J., Letters* **618** L115–L118 (*Preprint* arXiv:gr-qc/0411123)

[92] Alexander S, Finn L S and Yunes N 2008 *Phys. Rev. D* **78**(6) 066005 URL http://link.aps.org/doi/10.1103/PhysRevD.78.066005

[93] Arun K G and Will C M 2009 *Classical and Quantum Gravity* **26** 155002 (*Preprint* 0904.1190)

[94] Sopuerta C F and Yunes N 2009 *Phys. Rev. D* **80**(6) 064006 URL http://link.aps.org/doi/10.1103/PhysRevD.80.064006

[95] Schutz B F, Centrella J, Cutler C and Hughes S A 2009 Will Einstein Have the Last Word on Gravity? *astro2010: The Astronomy and Astrophysics Decadal Survey* (*ArXiv Astrophysics e-prints* vol 2010) p 265 (*Preprint* 0903.0100)

[96] Yunes N, Pretorius F and Spergel D 2010 *Phys. Rev. D* **81**(6) 064018 URL http://link.aps.org/doi/10.1103/PhysRevD.81.064018

[97] Alves M, Miranda O and de Araujo J 2009 *Physics Letters B* **679** 401 – 406 ISSN 0370-2693 URL http://www.sciencedirect.com/science/article/pii/S0370269309009198

[98] Amaro-Seoane P, Schutz B and Sopuerta C F 2010 *ArXiv e-prints* (*Preprint* 1009.1402)

[99] Mishra C K, Arun K G, Iyer B R and Sathyaprakash B S 2010 *Phys. Rev. D* **82**(6) 064010 URL http://link.aps.org/doi/10.1103/PhysRevD.82.064010

[100] Yunes N, O'Shaughnessy R, Owen B J and Alexander S 2010 *Phys. Rev. D* **82**(6) 064017 URL http://link.aps.org/doi/10.1103/PhysRevD.82.064017

[101] Stein L C and Yunes N 2011 *Phys. Rev. D* **83**(6) 064038 URL http://link.aps.org/doi/10.1103/PhysRevD.83.064038

[102] Tinto M and Alves M E d S 2010 *Phys. Rev. D* **82**(12) 122003 URL http://link.aps.org/doi/10.1103/PhysRevD.82.122003

[103] Del Pozzo W, Veitch J and Vecchio A 2011 *Phys. Rev. D* **83**(8) 082002 URL http://link.aps.org/doi/10.1103/PhysRevD.83.082002

[104] Yagi K and Tanaka T 2010 *Phys.Rev.* **D81** 064008 (*Preprint* 0906.4269)

[105] Yagi K and Tanaka T 2010 *Prog.Theor.Phys.* **123** 1069–1078 (*Preprint* 0908.3283)

[106] Yagi K, Yunes N and Tanaka T 2012 *Phys. Rev. Lett.* **109** 251105 [Erratum: Phys. Rev. Lett.116,no.16,169902(2016)] (*Preprint* 1208.5102)

[107] Yunes N and Pretorius F 2009 *Phys. Rev.* **D79** 084043 (*Preprint* 0902.4669)

[108] Alexander S and Yunes N 2009 *Phys. Rept.* **480** 1–55

[109] Konno K, Matsuyama T and Tanda S 2009 *Prog.Theor.Phys.* **122** 561–568 (*Preprint* 0902.4767)

[110] Isaacson R A 1967 *Phys.Rev.* **166** 1263–1271

[111] Yagi K 2012 *Phys.Rev.* **D86** 081504 (*Preprint* 1204.4524)

[112] Amendola L, Charmousis C and Davis S C 2007 *JCAP* **0710** 004 (*Preprint* 0704.0175)

[113] Amaro-Seoane P, Aoudia S, Babak S, Binetruy P, Berti E *et al.* 2012 (*Preprint* 1201.3621)

[114] Seto N, Kawamura S and Nakamura T 2001 *Phys.Rev.Lett.* **87** 221103 (*Preprint* astro-ph/0108011)

[115] Ali-Haimoud Y and Chen Y 2011 *Phys.Rev.* **D84** 124033 (*Preprint* 1110.5329)

[116] Hansen D and Yunes N 2013 *Phys.Rev.* **D88** 104020 (*Preprint* 1308.6631)

[117] Wald R M 1984 *General Relativity* (The University of Chicago Press)

[118] Garfinkle D private communication

[119] Stephani H, Kramer D, MacCallum M, Hoenselaers C and Herlt E 2003 *Exact solutions of Einstein's field equations* (Cambridge: Cambridge University Press)

[120] Thorne K S *Lectures presented at the Second Latin-American Symposium on Relativity and Gravitation, Caracas, Venezuela, December 8-13, 1975* URL http://www.its.caltech.edu/~kip/scripts/PubScans/II-68.pdf

[121] GRTensorII this is a package which runs within Maple but distinct from packages distributed with Maple. It is distributed freely on the World-Wide-Web from the address: http://grtensor.org

[122] Gillessen S, Eisenhauer F, Trippe S, Alexander T, Genzel R, Martins F and Ott T 2009 *Astrophys.J.* **692** 1075–1109 (*Preprint* 0810.4674)

[123] Ghez A, Salim S, Weinberg N, Lu J, Do T *et al.* 2008 *Astrophys.J.* **689** 1044–1062 (*Preprint* 0808.2870)

[124] Kendrew S, Hippler S, Brandner W, Clenet Y, Deen C *et al.* 2012 *Proc. SPIE* **8446** 84467W–84467W–9 URL http://dx.doi.org/10.1117/12.926558

[125] Gillessen S, Eisenhauer F, Perrin G, Brandner W, Straubmeier C *et al.* 2010 (*Preprint* 1007.1612)

[126] Woillez J, Akeson R, Colavita M, Eisner J, Ghez A *et al.* 2010 *Proc.SPIE Int.Soc.Opt.Eng.* **7734** 773412 (*Preprint* 1208.3272)

[127] Stone J M, Eisner J, Monnier J, Woillez J, Wizinowich P *et al.* 2012 *Astrophys.J.* **754** 151 (*Preprint* 1206.1364)

[128] Bartko H, Gillessen S, Rabien S, Thiel M, Grater A *et al.* 2010 (*Preprint* 1007.1765)

[129] Eisner J, Akeson R, Colavita M, Ghez A, Graham J *et al.* 2010 *Proc.SPIE Int.Soc.Opt.Eng.* **7734** 773411 (*Preprint* 1008.4335)

[130] Pott J U, Woillez J, Akeson R L, Colavita M M, Eisner J A *et al.* 2009 *New Astron.Rev.* **53** 363–372 (*Preprint* 0811.2264)

[131] Broderick A E, Fish V L, Doeleman S S and Loeb A 2009 *Astrophys. J.* **697** 45–54 (*Preprint* 0809.4490)

[132] Broderick A E, Fish V L, Doeleman S S and Loeb A 2011 *Astrophys. J.* **735** 110 (*Preprint* 1011.2770)

[133] Broderick A E, Loeb A and Reid M J 2011 *Astrophys.J.* **735** 57 (*Preprint* 1104.3146)

[134] Fish V L, Doeleman S S, Beaudoin C, Blundell R, Bolin D E *et al.* 2011 *Astrophys.J.* **727** L36 (*Preprint* 1011.2472)

[135] Fish V L and Doeleman S S 2009 *IAU Symp.* **261** 271–276 (*Preprint* 0906.4040)

[136] Robinson D C 1975 *Physical Review Letters* **34** 905

[137] Israel W 1967 *Physical Review* **164** 1776–1779

[138] Israel W 1968 *Communications in Mathematical Physics* **8** 245–260

[139] Hawking S W 1971 *Physical Review Letters* **26** 1344–1346

[140] Hawking S W 1972 *Communications in Mathematical Physics* **25** 152–166

[141] Carter B 1971 *Physical Review Letters* **26** 331–333

[142] Moura F and Schiappa R 2007 *Class.Quant.Grav.* **24** 361–386 (*Preprint* hep-th/0605001)

[143] Kleihaus B, Kunz J and Radu E 2011 *Phys.Rev.Lett.* **106** 151104 (*Preprint* 1101.2868)

[144] Torii T, Yajima H and Maeda K i 1997 *Phys.Rev.* **D55** 739–753 (*Preprint* gr-qc/9606034)

[145] Kanti P, Mavromatos N, Rizos J, Tamvakis K and Winstanley E 1996 *Phys.Rev.* **D54** 5049–5058 (*Preprint* hep-th/9511071)

[146] Alexeev S and Pomazanov M 1997 *Phys.Rev.* **D55** 2110–2118 (*Preprint* hep-th/9605106)

[147] Campbell B A, Kaloper N, Madden R and Olive K A 1993 *Nucl.Phys.* **B399** 137–168 (*Preprint* hep-th/9301129)

[148] Campbell B A, Kaloper N and Olive K A 1992 *Phys.Lett.* **B285** 199–205

[149] Campbell B A, Duncan M J, Kaloper N and Olive K A 1990 *Phys.Lett.* **B251** 34–38

[150] Campbell B A, Duncan M J, Kaloper N and Olive K A 1991 *Nucl.Phys.* **B351** 778–792

[151] Zerilli F J 1970 *Phys. Rev. D* **2**(10) 2141–2160 URL `http://link.aps.org/doi/10.1103/PhysRevD.2.2141`

[152] Sago N, Nakano H and Sasaki M 2003 *Phys.Rev.* **D67** 104017 (*Preprint* `gr-qc/0208060`)

[153] Zerilli F J 1970 *Phys. Rev. Lett.* **24**(13) 737–738 URL `http://link.aps.org/doi/10.1103/PhysRevLett.24.737`

[154] Poisson E 2004 *A relativist's toolkit: the mathematics of black-hole mechanics* (Cambridge, UK: Cambridge Univ. Pr.)

[155] Thorne K S 1980 *Rev. Mod. Phys.* **52**(2) 299–339 URL `http://link.aps.org/doi/10.1103/RevModPhys.52.299`

[156] Campanelli M, Lousto C O and Zlochower Y 2009 *Phys.Rev.* **D79** 084012 (*Preprint* `0811.3006`)

[157] Bardeen J M, Press W H and Teukolsky S A 1972 *Astrophys. J.* **178** 347–370

[158] Niedermaier M and Reuter M 2006 *Living Reviews in Relativity* **9** URL `http://www.livingreviews.org/lrr-2006-5`

[159] Gair J R, Li C and Mandel I 2008 *Phys.Rev.* **D77** 024035 (*Preprint* `0708.0628`)

[160] Bambi C and Barausse E 2011 *Phys.Rev.* **D84** 084034 (*Preprint* 1108.4740)

[161] Sopuerta C F and Yunes N 2011 *Phys.Rev.* **D84** 124060 (*Preprint* 1109.0572)

[162] Canizares P, Gair J R and Sopuerta C F 2012 *Phys.Rev.* **D86** 044010 (*Preprint* 1205.1253)

[163] Falcke H and Markoff S 2013 *Class.Quant.Grav.* **30** 244003 (*Preprint* 1311.1841)

[164] Chen S and Jing J 2012 *Phys.Rev.* **D85** 124029 (*Preprint* 1204.2468)

[165] Johannsen T and Psaltis D 2010 *Astrophys. J.* **718** 446–454 (*Preprint* 1005.1931)

[166] Akiyama K, Lu R S, Fish V L, Doeleman S S, Broderick A E, Dexter J, Hada K, Kino M, Nagai H, Honma M, Johnson M D, Algaba J C, Asada K, Brinkerink C, Blundell R, Bower G C, Cappallo R, Crew G B, Dexter M, Dzib S A, Freund R, Friberg P, Gurwell M, Ho P T P, Inoue M, Krichbaum T P, Loinard L, MacMahon D, Marrone D P, Moran J M, Nakamura M, Nagar N M, Ortiz-Leon G, Plambeck R, Pradel N, Primiani R A, Rogers A E E, Roy A L, SooHoo J, Tavares J L, Tilanus R P J, Titus M, Wagner J, Weintroub J, Yamaguchi P, Young K H, Zensus A and Ziurys L M 2015 *Astrophys. J.* **807** 150 (*Preprint* 1505.03545)

[167] Broderick A E, Narayan R, Kormendy J, Perlman E S, Rieke M J and Doeleman S S 2015 *Astrophys. J.* **805** 179 (*Preprint* 1503.03873)

[168] Gwinn C R, Kovalev Y Y, Johnson M D and Soglasnov V A 2014 *Astrophys. J.* **794** L14 (*Preprint* 1409.0530)

[169] Doeleman S S, Weintroub J, Rogers A E E, Plambeck R, Freund R, Tilanus R P J, Friberg P, Ziurys L M, Moran J M, Corey B, Young K H, Smythe D L, Titus M, Marrone D P, Cappallo R J, Bock D C J, Bower G C, Chamberlin R, Davis G R, Krichbaum T P, Lamb J, Maness H, Niell A E, Roy A, Strittmatter P, Werthimer D, Whitney A R and Woody D 2008 *Nature* **455** 78–80 (*Preprint* 0809.2442)

[170] Miller J M, Mineshige S, Kubota A, Yamada S, Aharonian F, Done C, Kawai N, Hayashida K, Reis R, Mizuno T, Noda H, Ueda Y, Shidatsu M and for the ASTRO-H Science Working Group 2014 *ArXiv e-prints* (*Preprint* 1412.1173)

[171] Lasota J P 2015 (*Preprint* 1505.02172)

[172] Claudel C M, Virbhadra K S and Ellis G F R 2001 *J. Math. Phys.* **42** 818–838 (*Preprint* gr-qc/0005050)

[173] Psaltis D, Perrodin D, Dienes K R and Mocioiu I 2008 *Phys. Rev. Lett.* **100** 091101 [Phys. Rev. Lett.100,119902(2008)] (*Preprint* 0710.4564)

[174] Kleihaus B, Kunz J and Mojica S 2014 *Phys. Rev.* **D90** 061501 (*Preprint* 1407.6884)

[175] Kleihaus B, Kunz J, Mojica S and Radu E 2016 *Phys. Rev. D* **93**(4) 044047 URL http://link.aps.org/doi/10.1103/PhysRevD.93.044047

[176] Pani P and Cardoso V 2009 *Phys. Rev.* **D79** 084031 (*Preprint* 0902.1569)

[177] Ayzenberg D and Yunes N 2014 *Phys. Rev. D* **90** 044066 (*Preprint* 1405.2133)

[178] Maselli A, Pani P, Gualtieri L and Ferrari V 2015 *Phys. Rev.* **D92** 083014 (*Preprint* 1507.00680)

[179] Maselli A, Silva H O, Minamitsuji M and Berti E 2015 *Phys. Rev.* **D92** 104049 (*Preprint* 1508.03044)

[180] Wang A 2013 *Physical Review Letters* **110** 091101 (*Preprint* 1212.1876)

[181] Barausse E and Sotiriou T P 2013 *Phys. Rev. D* **87** 087504 (*Preprint* 1212.1334)

[182] Hendi S H 2010 *Progress of Theoretical Physics* **124** 493–502 (*Preprint* 1008.0544)

[183] Barausse E, Sotiriou T P and Vega I 2016 *Phys. Rev. D* **93**(4) 044044 URL http://link.aps.org/doi/10.1103/PhysRevD.93.044044

[184] Smith T L, Erickcek A L, Caldwell R R and Kamionkowski M 2008 *Phys. Rev.* **D77** 024015 (*Preprint* 0708.0001)

[185] Konno K and Takahashi R 2014 *Phys. Rev.* **D90** 064011 (*Preprint* 1406.0957)

[186] Stein L C 2014 *Phys. Rev.* **D90** 044061 (*Preprint* 1407.2350)

[187] McNees R, Stein L C and Yunes N 2016 *Class. Quant. Grav.* **33** 235013 (*Preprint* 1512.05453)

[188] Yazadjiev S 2000 *Gen. Rel. Grav.* **32** 2345–2352 (*Preprint* gr-qc/9907092)

[189] Moore C J and Gair J R 2015 *Phys. Rev.* **D92** 024039 (*Preprint* 1507.02998)

[190] Misner C W, Thorne K S and Wheeler J A 1973 *Gravitation*

[191] Bambi C and Barausse E 2011 *Astrophys. J.* **731** 121 (*Preprint* 1012.2007)

[192] Liu J, McClintock J E, Narayan R, Davis S W and Orosz J A 2008 *ApJ Letters* **679** L37–L40 (*Preprint* 0803.1834)

[193] Steiner J F, McClintock J E, Orosz J A, Remillard R A, Bailyn C D, Kolehmainen M and Straub O 2014 *ApJ Letters* **793** L29 (*Preprint* 1402.0148)

[194] Gou L, McClintock J E, Steiner J F, Narayan R, Cantrell A G, Bailyn C D and Orosz J A 2010 *ApJ Letters* **718** L122–L126 (*Preprint* 1002.2211)

[195] Morningstar W R, Miller J M, Reis R C and Ebisawa K 2014 *ApJ Letters* **784** L18 (*Preprint* 1401.1794)

[196] Shafee R, McClintock J E, Narayan R, Davis S W, Li L X and Remillard R A 2006 *ApJ Letters* **636** L113–L116 (*Preprint* astro-ph/0508302)

[197] Steiner J F, Reis R C, McClintock J E, Narayan R, Remillard R A, Orosz J A, Gou L, Fabian A C and Torres M A P 2011 *MNRAS* **416** 941–958 (*Preprint* 1010.1013)

[198] Tsukamoto N, Li Z and Bambi C 2014 *JCAP* **1406** 043 (*Preprint* 1403.0371)

[199] Abdujabbarov A A, Rezzolla L and Ahmedov B J 2015 *Mon. Not. Roy. Astron. Soc.* **454** 2423 (*Preprint* 1503.09054)

[200] Chan C k, Psaltis D and Özel F 2013 *Astrophys. J.* **777** 13 (*Preprint* 1303.5057)

[201] Doeleman S S, Fish V L, Schenck D E, Beaudoin C, Blundell R, Bower G C, Broderick A E, Chamberlin R, Freund R, Friberg P, Gurwell M A, Ho P T P, Honma M, Inoue M, Krichbaum T P, Lamb J, Loeb A, Lonsdale C, Marrone D P, Moran J M, Oyama T, Plambeck R, Primiani R A, Rogers A E E, Smythe D L, SooHoo J, Strittmatter P, Tilanus R P J, Titus M, Weintroub J, Wright M, Young K H and Ziurys L M 2012 *Science* **338** 355–358 (*Preprint* http://www.sciencemag.org/content/338/6105/355.full.pdf)

[202] Doeleman S S, Fish V L, Broderick A E, Loeb A and Rogers A E E 2009 *Astrophys. J.* **695** 59–74 (*Preprint* 0809.3424)

[203] Babichev E and Fabbri A 2014 *Phys. Rev.* **D90** 084019 (*Preprint* 1406.6096)

[204] Xu Y D 2011 *Astrophys. J.* **729** 10 (*Preprint* 1101.0507)

[205] Goddi C *et al.* 2016 BlackHoleCam: fundamental physics of the Galactic center (*Preprint* 1606.08879) URL https://inspirehep.net/record/1472928/files/arXiv:1606.08879.pdf

[206] Zhang S N, Cui W and Chen W 1997 *The Astrophysical Journal Letters* **482** L155 URL http://stacks.iop.org/1538-4357/482/i=2/a=L155

[207] Falcke H, Melia F and Agol E 2000 *Astrophys. J. Lett.* **528** L13–L16 (*Preprint* astro-ph/9912263)

[208] Bambi C, Cardenas-Avendano A, Dauser T, Garcia J A and Nampalliwar S 2016 (*Preprint* 1607.00596)

[209] Ayzenberg D and Yunes N 2014 *Phys. Rev.* **D90** 044066 [Erratum: Phys. Rev.D91,no.6,069905(2015)] (*Preprint* 1405.2133)

[210] Ayzenberg D, Yagi K and Yunes N 2016 *Class. Quant. Grav.* **33** 105006 (*Preprint* 1601.06088)

[211] Vincent F H 2013 *Class. Quant. Grav.* **31** 025010 (*Preprint* 1311.3251)

[212] Cunha P V P, Herdeiro C A R, Kleihaus B, Kunz J and Radu E 2017 *ArXiv e-prints* (*Preprint* 1701.00079)

[213] Maselli A, Gualtieri L, Pani P, Stella L and Ferrari V 2015 *Astrophys. J.* **801** 115 (*Preprint* 1412.3473)

[214] Poisson E 2004 *Living Reviews in Relativity* **7** URL `http://www.livingreviews.org/lrr-2004-6`

[215] Motta S E 2016 *Astron. Nachr.* **337** 398 (*Preprint* `1603.07885`)

[216] Davis S W, Done C and Blaes O M 2006 *Astrophys. J.* **647** 525–538 (*Preprint* `astro-ph/0602245`)

[217] Maccarone T J 2014 *Space Sci. Rev.* **183** 101–120 (*Preprint* `1312.1438`)

[218] Cunha P V P, Herdeiro C A R, Kleihaus B, Kunz J and Radu E 2017 *Phys. Lett.* **B768** 373–379 (*Preprint* `1701.00079`)

APPENDICES

APPENDIX A

WEYL-RIEMANN IDENTITY

Here we show that

$$\bar{W}^{ac}\bar{W}_{ac} = \bar{S}^{ac}\bar{S}_{ac} + \mathcal{O}(\xi'). \tag{A.1}$$

Using the definition of $\bar{W}^{ac}$ and $\bar{S}^{ac}$ in Eq. (2.38) we have

$$\bar{W}^{ac}\bar{W}_{ac} = \bar{C}_{abcd}\bar{C}^{aecf}k^b k^d k_e k_f, \tag{A.2}$$

$$\bar{S}^{ac}\bar{S}_{ac} = \frac{1}{4}\epsilon_{cdef}\epsilon^{chij}\bar{C}^{abef}\bar{C}_{agij}k_b k^d k^g k_h. \tag{A.3}$$

Contracting the Levi-Civita tensors

$$\begin{aligned} 4\bar{S}^{ac}\bar{S}_{ac} &= -6\delta^d_{[h}\delta^i_e\delta^j_{f]}\bar{C}_{agij}\bar{C}^{abef}k_b k^d k^g k_h \\ &= 2\bar{C}^{abij}\bar{C}_{agij}k_b k^g k^h k_h + 2\bar{C}^{abjh}\bar{C}_{agij}k_b k^i k^g k_h + 2\bar{C}^{abhi}\bar{C}_{agij}k_b k^j k^g k_h \\ &= 2\bar{C}^{abij}\bar{C}_{agij}k_b k^g k^h k_h - 4W^{ab}W_{ab}. \end{aligned} \tag{A.4}$$

Notice that the first term contains the term $k^a k_a$, which vanishes in GR because of the $\mathcal{O}(\epsilon, \xi'^0)$ perturbed Einstein equations. Thus, $k^a k_a = 0 + \mathcal{O}(\xi')$. Therefore, the first term can be ignored to leading order in ξ' and we find

$$\bar{W}^{ac}\bar{W}_{ac} = \bar{S}^{ac}\bar{S}_{ac} + \mathcal{O}(\xi'). \tag{A.5}$$

APPENDIX B

TENSOR HARMONICS

In this paper, we used the following tensor spherical harmonics to decompose the metric perturbation and the source term [151, 152]

$$a_{ab}^{\ell 0(0)} = \begin{pmatrix} Y_{\ell 0} & 0 & 0 & 0 \\ 0 & 0 & 0 & 0 \\ 0 & 0 & 0 & 0 \\ 0 & 0 & 0 & 0 \end{pmatrix}, \tag{B.1}$$

$$a_{ab}^{\ell 0} = \begin{pmatrix} 0 & 0 & 0 & 0 \\ 0 & Y_{\ell 0} & 0 & 0 \\ 0 & 0 & 0 & 0 \\ 0 & 0 & 0 & 0 \end{pmatrix}, \tag{B.2}$$

$$b_{ab}^{\ell 0} = \frac{r}{\sqrt{2\ell(\ell+1)}} \begin{pmatrix} 0 & 0 & 0 & 0 \\ 0 & 0 & \frac{\partial}{\partial\theta} Y_{\ell 0} & 0 \\ 0 & \frac{\partial}{\partial\theta} Y_{\ell 0} & 0 & 0 \\ 0 & 0 & 0 & 0 \end{pmatrix}, \tag{B.3}$$

$$g_{ab}^{\ell 0} = \frac{r^2}{\sqrt{2}} \begin{pmatrix} 0 & 0 & 0 & 0 \\ 0 & 0 & 0 & 0 \\ 0 & 0 & Y_{\ell 0} & 0 \\ 0 & 0 & 0 & \sin^2\theta Y_{\ell 0} \end{pmatrix}, \tag{B.4}$$

$$f^{\ell 0}_{ab} = \frac{r^2}{\sqrt{2\ell(\ell+1)(\ell-1)(\ell+2)}} \begin{pmatrix} 0 & 0 & 0 & 0 \\ 0 & 0 & 0 & 0 \\ 0 & 0 & W_{\ell 0} & 0 \\ 0 & 0 & 0 & -\sin^2\theta W_{\ell 0} \end{pmatrix}, \tag{B.5}$$

where $Y^{\ell 0}$ are the $m = 0$ spherical harmonics and $W^{\ell 0}$ are given by

$$W^{\ell 0} \equiv \left(\frac{d^2}{d\theta^2} - \cot\theta \frac{d}{d\theta} \right) Y^{\ell 0}. \tag{B.6}$$

The coefficients of the source after a tensor spherical harmonics decomposition are

$$\begin{aligned} A^{(0)}_{00}(r) = &- 24\sqrt{\pi}\zeta \frac{M^4}{r^6}\frac{\chi^2}{f^2}\left(1 - \frac{101}{18}\frac{M}{r} + \frac{25M^2}{r^2} - \frac{877}{18}\frac{M^3}{r^3} - \frac{1022}{15}\frac{M^4}{r^4} - \frac{2224}{9}\frac{M^5}{r^5}\right. \\ &\left. + \frac{107786}{45}\frac{M^6}{r^6} - \frac{53452}{15}\frac{M^7}{r^7} - \frac{208}{45}\frac{M^8}{r^8} + \frac{5920}{3}\frac{M^9}{r^9}\right), \end{aligned} \tag{B.7}$$

$$\begin{aligned} A^{(0)}_{20}(r) = &- \frac{44\sqrt{5\pi}}{15}\zeta \frac{M^5}{r^7}\chi^2\left(1 + \frac{7737}{110}\frac{M}{r} - \frac{4201}{55}\frac{M^2}{r^2} + \frac{1047}{11}\frac{M^3}{r^3} - \frac{22086}{11}\frac{M^4}{r^4}\right. \\ &\left. + \frac{194424}{55}\frac{M^5}{r^5} - \frac{8880}{11}\frac{M^6}{r^6}\right), \end{aligned} \tag{B.8}$$

$$\begin{aligned} A_{00}(r) = &- 2\sqrt{\pi}\zeta \frac{M^2}{r^4}\frac{\chi^2}{f^4}\left(1 - \frac{4M}{r} + \frac{16}{3}\frac{M^2}{r^2} + \frac{40}{3}\frac{M^3}{r^3} - \frac{236}{3}\frac{M^4}{r^4} + \frac{482}{3}\frac{M^5}{r^5} + \frac{13672}{15}\frac{M^6}{r^6}\right. \\ &\left. - \frac{6416}{3}\frac{M^7}{r^7} - \frac{15288}{5}\frac{M^8}{r^8} + \frac{13808}{5}\frac{M^9}{r^9} + \frac{84928}{5}\frac{M^{10}}{r^{10}} - \frac{18560M^{11}}{r^{11}}\right), \end{aligned} \tag{B.9}$$

$$\begin{aligned} A_{20}(r) = &- \frac{236\sqrt{5\pi}}{75}\zeta \frac{M^4}{r^6}\frac{\chi^2}{f^2}\left(1 + \frac{163}{59}\frac{M}{r} - \frac{2913}{118}\frac{M^2}{r^2} + \frac{3183}{59}\frac{M^3}{r^3} - \frac{4587}{59}\frac{M^4}{r^4}\right. \\ &\left. + \frac{25798}{59}\frac{M^5}{r^5} - \frac{59448}{59}\frac{M^6}{r^6} + \frac{34800}{59}\frac{M^7}{r^7}\right), \end{aligned} \tag{B.10}$$

$$B_{20}(r) = \frac{92\sqrt{15\pi}}{75}\zeta\frac{M^4}{r^6}\frac{\chi^2}{f}\left(1+\frac{153}{46}\frac{M}{r}-\frac{651}{23}\frac{M^2}{r^2}-\frac{513}{23}\frac{M^3}{r^3}-\frac{1682}{23}\frac{M^4}{r^4} + \frac{33704}{69}\frac{M^5}{r^5}-\frac{2000}{23}\frac{M^6}{r^6}\right), \tag{B.11}$$

$$G^{(s)}_{00}(r) = \frac{56\sqrt{2\pi}}{3}\zeta\frac{M^4}{r^6}\frac{\chi^2}{f}\left(1-\frac{5}{4}\frac{M}{r}+\frac{333}{28}\frac{M^2}{r^2}+\frac{157}{14}\frac{M^3}{r^3}-\frac{969}{70}\frac{M^4}{r^4}-\frac{1807}{5}\frac{M^5}{r^5} + \frac{2068}{5}\frac{M^6}{r^6}+\frac{1320}{7}\frac{M^7}{r^7}\right), \tag{B.12}$$

$$G^{(s)}_{20}(r) = \frac{2\sqrt{10\pi}}{15}\zeta\frac{M^4}{r^6}\chi^2\left(1-\frac{15M}{r}-\frac{4963}{5}\frac{M^2}{r^2}-\frac{1164M^3}{r^3} -\frac{2910M^4}{r^4}+\frac{96528}{5}\frac{M^5}{r^5}-\frac{2640M^6}{r^6}\right), \tag{B.13}$$

$$F_{20}(r) = -\frac{4\sqrt{15\pi}}{15}\zeta\frac{M^4}{r^6}\chi^2\left(1+\frac{8M}{r}+\frac{809}{5}\frac{M^2}{r^2}-\frac{358}{5}\frac{M^3}{r^3}+\frac{1386}{5}\frac{M^4}{r^4} -\frac{25888}{15}\frac{M^5}{r^5}+\frac{2160M^6}{r^6}\right). \tag{B.14}$$

Substituting these source terms into Eqs. (3.25)-(3.29), we obtain a set of ordinary differential equations for H_{000}, H_{200}, K_{00}, H_{020}, H_{220}, and K_{20}, which we solve to find

$$H^{00}_0(r) = \frac{\sqrt{\pi}}{3}\zeta\frac{M^3}{r^3}\frac{\chi^2}{f}\left(1+\frac{14M}{r}+\frac{52}{5}\frac{M^2}{r^2}+\frac{1358}{15}\frac{M^3}{r^3}+\frac{652}{3}\frac{M^4}{r^4}+\frac{1204}{5}\frac{M^5}{r^5} -\frac{1792}{3}\frac{M^6}{r^6}-\frac{1120}{3}\frac{M^7}{r^7}\right), \tag{B.15}$$

$$H_2^{00}(r) =\sqrt{\pi}\zeta\frac{M^2}{r^2}\frac{\chi^2}{f^2}\left(1-\frac{M}{r}+\frac{10M^2}{r^2}-\frac{12M^3}{r^3}+\frac{218}{3}\frac{M^4}{r^4}+\frac{128}{3}\frac{M^5}{r^5}-\frac{724}{15}\frac{M^6}{r^6}\right.$$
$$\left.-\frac{22664}{15}\frac{M^7}{r^7}+\frac{25312}{15}\frac{M^8}{r^8}+\frac{1600}{3}\frac{M^9}{r^9}\right), \tag{B.16}$$

$$K_{00}(r) =0, \tag{B.17}$$

$$H_0^{20}(r) =-\frac{17852\sqrt{5\pi}}{13125}\zeta\frac{M^3}{r^3}\frac{\chi^2}{f}\left(1+\frac{M}{r}+\frac{27479}{31241}\frac{M^2}{r^2}-\frac{2186945}{187446}\frac{M^3}{r^3}-\frac{448285}{31241}\frac{M^4}{r^4}\right.$$
$$\left.-\frac{78975}{4463}\frac{M^5}{r^5}+\frac{1229650}{13389}\frac{M^6}{r^6}+\frac{303800}{13389}\frac{M^7}{r^7}-\frac{210000}{4463}\frac{M^8}{r^8}\right), \tag{B.18}$$

$$H_2^{20}(r) =-\frac{17852\sqrt{5\pi}}{13125}\zeta\frac{M^3}{r^3}\frac{\chi^2}{f}\left(1+\frac{3588}{4463}\frac{M}{r}-\frac{9271}{31241}\frac{M^2}{r^2}-\frac{7545095}{187446}\frac{M^3}{r^3}+\frac{1972315}{31241}\frac{M^4}{r^4}\right.$$
$$\left.-\frac{446825}{4463}\frac{M^5}{r^5}+\frac{7215350}{13389}\frac{M^6}{r^6}-\frac{4809000}{4463}\frac{M^7}{r^7}+\frac{3570000}{4463}\frac{M^8}{r^8}\right), \tag{B.19}$$

$$K_{20}(r) =-\frac{8926\sqrt{10\pi}}{13125}\zeta\frac{M^3}{r^3}\chi^2\left(1+\frac{10370}{4463}\frac{M}{r}+\frac{266911}{62482}\frac{M^2}{r^2}+\frac{63365}{13389}\frac{M^3}{r^3}\right.$$
$$\left.-\frac{309275}{31241}\frac{M^4}{r^4}-\frac{81350}{4463}\frac{M^5}{r^5}-\frac{443800}{13389}\frac{M^6}{r^6}+\frac{210000}{4463}\frac{M^7}{r^7}\right). \tag{B.20}$$

These solutions are then used to reconstruct the metric perturbation, as presented in the main text.

APPENDIX C

HIGH-ORDER SCALAR FIELD

In this section, we present the scalar field to $\mathcal{O}(\chi^8)$. Let us decompose the field as in Eq. 3.11, where $\vartheta^{(0,1)}$ was already presented in Eq. 3.12 and $\vartheta^{(2,1)}$ was given in Eq. 3.17. Let us further define $\tilde{r} = r/M$ and $\tilde{\vartheta}^{(m,n)} = \vartheta^{(m,n)}/(\alpha/\beta)$. The nonvanishing, higher order pieces are then

$$\begin{aligned}\tilde{\vartheta}^{(4,1)} =& -\frac{2}{35\bar{r}^5} - \frac{1}{7\bar{r}^4} - \frac{3}{14\bar{r}^3} - \frac{1}{4\bar{r}^2} - \frac{1}{4\bar{r}} + \left(\frac{360}{7\bar{r}^7} + \frac{110}{7\bar{r}^6} + \frac{22}{7\bar{r}^5}\right)\cos^4(\theta) \\ &+ \left(\frac{4}{7\bar{r}^6} + \frac{24}{35\bar{r}^5} + \frac{3}{7\bar{r}^4} + \frac{1}{7\bar{r}^3}\right)\cos^2(\theta)\,, \end{aligned} \tag{C.1}$$

$$\begin{aligned}\tilde{\vartheta}^{(6,1)} =& -\frac{5}{252\bar{r}^6} - \frac{5}{84\bar{r}^5} - \frac{5}{48\bar{r}^4} - \frac{5}{36\bar{r}^3} - \frac{5}{32\bar{r}^2} - \frac{5}{32\bar{r}} \\ &+ \left(-\frac{896}{9\bar{r}^9} - \frac{70}{3\bar{r}^8} - \frac{10}{3\bar{r}^7}\right)\cos^6(\theta) + \left(-\frac{5}{6\bar{r}^8} - \frac{5}{7\bar{r}^7} - \frac{25}{84\bar{r}^6} - \frac{5}{84\bar{r}^5}\right)\cos^4(\theta) \\ &+ \left(\frac{1}{7\bar{r}^7} + \frac{5}{21\bar{r}^6} + \frac{3}{14\bar{r}^5} + \frac{1}{8\bar{r}^4} + \frac{1}{24\bar{r}^3}\right)\cos^2(\theta)\,, \end{aligned} \tag{C.2}$$

$$\begin{aligned}\tilde{\vartheta}^{(8,1)} =& -\frac{1}{132\bar{r}^7} - \frac{7}{264\bar{r}^6} - \frac{7}{132\bar{r}^5} - \frac{7}{88\bar{r}^4} - \frac{35}{352\bar{r}^3} - \frac{7}{64\bar{r}^2} - \frac{7}{64\bar{r}} \\ &+ \left(\frac{1800}{11\bar{r}^{11}} + \frac{342}{11\bar{r}^{10}} + \frac{38}{11\bar{r}^9}\right)\cos^8(\theta) + \left(\frac{56}{55\bar{r}^{10}} + \frac{112}{165\bar{r}^9} + \frac{7}{33\bar{r}^8} + \frac{1}{33\bar{r}^7}\right)\cos^6(\theta) \\ &+ \left(-\frac{2}{11\bar{r}^9} - \frac{5}{22\bar{r}^8} - \frac{45}{308\bar{r}^7} - \frac{5}{88\bar{r}^6} - \frac{1}{88\bar{r}^5}\right)\cos^4(\theta) \\ &+ \left(\frac{1}{22\bar{r}^8} + \frac{15}{154\bar{r}^7} + \frac{5}{44\bar{r}^6} + \frac{1}{11\bar{r}^5} + \frac{9}{176\bar{r}^4} + \frac{3}{176\bar{r}^3}\right)\cos^2(\theta)\,. \end{aligned} \tag{C.3}$$

In deriving these expressions, we have required that the scalar field be asymptotically flat (at spatial infinity) and regular at the Kerr event horizon.

APPENDIX D

BH SHADOW IN THE KERR SPACETIME

The boundary of the BH shadow is described by the separatrix between the photon geodesics that make it out to spatial infinity and those that fall into the BH event horizon [172]. The construction of the BH shadow thus requires the solution to the null-geodesic equations, which can be derived, for example, through the Hamilton-Jacobi equation. For generic spacetimes, the null geodesic equations cannot be solved through separation of variables and must thus be treated numerically. For separable spacetimes, however, like that described by the Kerr metric in Boyer-Lindquist coordinates, the separatrix between outgoing and ingoing null geodesics can be found analytically. We here show how this is done in the Kerr spacetime in Boyer-Lindquist coordinates.

We begin with the Hamilton-Jacobi equation

$$\frac{\partial S}{\partial \lambda} = \frac{1}{2} g^{ab} \frac{\partial S}{\partial x^a} \frac{\partial S}{\partial x^b}, \tag{D.1}$$

where S is the Jacobi action, λ is the affine parameter, and x^a are generalized coordinates. If we assume separability and note that we only care about null geodesics, the Jacobi action can be written as

$$S = -Et + L_z \phi + S_r(r) + S_\theta(\theta). \tag{D.2}$$

Inserting this ansatz into Eq. D.1, we find the partial differential equation

$$2\frac{\partial S}{\partial \lambda} = 0 = g^{tt} E^2 - 2 g^{t\phi} E L_z + g^{\phi\phi} L_z^2 + g^{rr} \left(\frac{dS_r}{dr} \right)^2 + g^{\theta\theta} \left(\frac{dS_\theta}{d\theta} \right)^2, \tag{D.3}$$

which through separation of variables becomes

$$\Delta_{\rm K} \left(\frac{dS_r}{dr} \right)^2 = \frac{1}{\Delta_{\rm K}} \left[E \left(r^2 + a^2 \right) - a L_z \right]^2 - (L_z - aE)^2 - \mathcal{Q}, \tag{D.4}$$

$$\left(\frac{dS_\theta}{d\theta}\right)^2 = \mathcal{Q} + \cos^2\theta\left[a^2E^2 - \frac{L_z^2}{\sin^2\theta}\right], \tag{D.5}$$

where $\mathcal{Q}$ is the Carter constant.

The null-geodesic equations for the $r(\lambda)$ and $\theta(\lambda)$ components of the null trajectories can be found by noting that $dS/dr = p_r = g_{rr}(dr/d\lambda)$ and $dS/d\theta = p_\theta = g_{\theta\theta}(d\theta/d\lambda)$. The equations are then simply

$$\Sigma_{\text{K}}\frac{dr}{d\lambda} = \pm\sqrt{\mathcal{R}}, \tag{D.6}$$

$$\Sigma_{\text{K}}\frac{d\theta}{d\lambda} = \pm\sqrt{\Theta}\,, \tag{D.7}$$

where we have defined the two functions

$$\mathcal{R}(r) \equiv \left[E\left(r^2+a^2\right) - aL_z\right]^2 - \Delta_{\text{K}}\left[\mathcal{Q} + (L_z - aE)^2\right], \tag{D.8}$$

$$\Theta(\theta) \equiv \mathcal{Q} + \cos^2\theta\left[a^2E^2 - \frac{L_z^2}{\sin^2\theta}\right]. \tag{D.9}$$

Unstable spherical photon orbits are defined by the conditions

$$\mathcal{R} = 0, \quad \frac{d\mathcal{R}}{dr} = 0, \tag{D.10}$$

$$\Theta \geq 0. \tag{D.11}$$

For simplicity, we define the conserved quantities $\xi \equiv L_z/E$ and $\eta \equiv Q/E^2$, and solve for each using Eq. D.8 and Eq. D.10 to find

$$\xi_{\rm sph} = \frac{r_{\rm sph}^2 + a^2}{a} - \frac{2\Delta_{\rm K} r_{\rm sph}}{a\left(r_{\rm sph} - M\right)}, \tag{D.12}$$

$$\eta_{\rm sph} = -\frac{r_{\rm sph}^3\left[r_{\rm sph}\left(r_{\rm sph} - 3M\right)^2 - 4a^2 M\right]}{a^2\left(r_{\rm sph} - M\right)^2}, \tag{D.13}$$

where $r_{\rm sph}$ is the constant radius of the unstable spherical orbits. This radius is constrained by the condition in Eq. D.11, which we can simplify by rewriting Θ in terms of ξ and η as

$$\frac{\Theta}{E^2} = \mathcal{J} - \left(a\sin\theta - \xi\csc\theta\right)^2, \tag{D.14}$$

where

$$\mathcal{J} = \eta + \left(a - \xi\right)^2. \tag{D.15}$$

Therefore, the $\Theta \geq 0$ condition for unstable spherical orbits implies the necessary (but not sufficient) condition $\mathcal{J} \geq 0$. Substituting Eqs. D.12 and D.13 into the above gives the condition

$$\mathcal{J} = \frac{4r_{\rm sph}^2\Delta_{\rm K}}{\left(r_{\rm sph} - M\right)^2} \geq 0, \tag{D.16}$$

which reduces simply to $\Delta_{\rm K} \geq 0$ or $r_{\rm sph} \geq M + \sqrt{M^2 - a^2}$, which is the Kerr horizon radius.

The BH shadow boundary is defined as the sky projection of the photon sphere as observed at spatial infinity. The conserved parameters ξ and η can be related to

the celestial coordinates of the observer at infinity via

$$\alpha = \lim_{r\to\infty} \frac{-rp^{(\phi)}}{p^{(t)}} = -\frac{\xi_{\rm sph}}{\sin\iota}, \tag{D.17}$$

$$\beta = \lim_{r\to\infty} \frac{rp^{(\theta)}}{p^{(t)}} = \left(\eta_{\rm sph} + a^2\cos^2\iota - \xi_{\rm sph}^2\cot^2\iota\right)^{1/2}. \tag{D.18}$$

The separatrix between ingoing and outgoing photon geodesics, what we call the boundary of the BH shadow, can then be constructed by plotting (α, β) by varying $r_{\rm sph}$ from $r = M + \sqrt{M^2 - a^2}$ to $r = 4.5M$; the latter is the photon sphere radius for a Schwarzschild BH and also the largest radius for which closed photon orbits are possible for all values of spin.

APPENDIX E

BH SOLUTIONS IN EDGB GRAVITY AND DCS GRAVITY

We here provide the metric modifications to the Kerr solution due to EdGB gravity and dCS gravity.

In EdGB gravity the only nonvanishing terms are

$$g_{tt}^{[0,1]} = -\frac{M^3}{r^4}\left[1+\frac{26M}{r}+\frac{66}{5}\frac{M^2}{r^2}+\frac{96}{5}\frac{M^3}{r^3}-\frac{80M^4}{r^4}\right], \tag{E.1}$$

$$g_{rr}^{[0,1]} = -\frac{M^2}{r^2 f^2}\left[1+\frac{M}{r}+\frac{52}{3}\frac{M^2}{r^2}+\frac{2M^3}{r^3}+\frac{16}{5}\frac{M^4}{r^4}-\frac{368}{3}\frac{M^5}{r^5}\right], \tag{E.2}$$

$$g_{t\phi}^{[1,1]} = \frac{3}{5}\frac{M^4\sin^2\theta}{r^3}\left[1+\frac{140}{9}\frac{M}{r}+\frac{10M^2}{r^2}+\frac{16M^3}{r^3}-\frac{400}{9}\frac{M^4}{r^4}\right], \tag{E.3}$$

$$\begin{aligned} g_{tt}^{[2,1]} = &-\frac{4463}{2625}\frac{M^3}{r^3}\left[\left(1+\frac{M}{r}+\frac{27479}{31241}\frac{M^2}{r^2}-\frac{2275145}{187446}\frac{M^3}{r^3}-\frac{2030855}{93723}\frac{M^4}{r^4}\right.\right.\\ &\left.-\frac{99975}{4463}\frac{M^5}{r^5}+\frac{1128850}{13389}\frac{M^6}{r^6}+\frac{194600}{4463}\frac{M^7}{r^7}-\frac{210000}{4463}\frac{M^8}{r^8}\right)\left(3\cos^2\theta-1\right)\\ &-\frac{875}{8926}\left(1+\frac{14M}{r}+\frac{52}{5}\frac{M^2}{r^2}+\frac{1214}{15}\frac{M^3}{r^3}+\frac{68M^4}{r^4}+\frac{724}{5}\frac{M^5}{r^5}-\frac{11264}{15}\frac{M^6}{r^6}\right.\\ &\left.\left.+\frac{160}{3}\frac{M^7}{r^7}\right)\right], \end{aligned} \tag{E.4}$$

$$\begin{aligned} g_{rr}^{[2,1]} = &-\frac{M^3}{r^3 f^3}\left[\frac{4463}{2625}\left(1-\frac{5338}{4463}\frac{M}{r}-\frac{59503}{31241}\frac{M^2}{r^2}-\frac{7433843}{187446}\frac{M^3}{r^3}+\frac{13462040}{93723}\frac{M^4}{r^4}\right.\right.\\ &-\frac{7072405}{31241}\frac{M^5}{r^5}+\frac{9896300}{13389}\frac{M^6}{r^6}-\frac{28857700}{13389}\frac{M^7}{r^7}+\frac{13188000}{4463}\frac{M^8}{r^8}\\ &\left.-\frac{7140000}{4463}\frac{M^9}{r^9}\right)\left(3\cos^2\theta-1\right)-\frac{r}{2M}\left(1-\frac{M}{r}+\frac{10M^2}{r^2}-\frac{12M^3}{r^3}+\frac{218}{3}\frac{M^4}{r^4}\right.\\ &\left.\left.+\frac{128}{3}\frac{M^5}{r^5}-\frac{724}{15}\frac{M^6}{r^6}-\frac{22664}{15}\frac{M^7}{r^7}+\frac{25312}{15}\frac{M^8}{r^8}+\frac{1600}{3}\frac{M^9}{r^9}\right)\right], \end{aligned} \tag{E.5}$$

$$g_{\theta\theta}^{[2,1]} = -\frac{4463}{2625}\frac{M^3}{r}\left(1+\frac{10370}{4463}\frac{M}{r}+\frac{266911}{62482}\frac{M^2}{r^2}+\frac{63365}{13389}\frac{M^3}{r^3}-\frac{309275}{31241}\frac{M^4}{r^4}\right.$$

$$-\frac{81350}{4463}\frac{M^5}{r^5}-\frac{443800}{13389}\frac{M^6}{r^6}+\frac{210000}{4463}\frac{M^7}{r^7}\Bigg)\left(3\cos^2\theta-1\right), \tag{E.6}$$

$$g^{[2,1]}_{\phi\phi}=g^{[2,1]}_{\theta\theta}\sin^2\theta, \tag{E.7}$$

where $f=1-2M/r$.

In dCS gravity the only nonvanishing terms are

$$g^{[1,1]}_{t\phi}=\frac{5}{8}\frac{M^5}{r^4}\left(1+\frac{12}{7}\frac{M}{r}+\frac{27}{10}\frac{M^2}{r^2}\right)\sin^2\theta, \tag{E.8}$$

$$\begin{aligned} g^{[2,1]}_{tt}=&\frac{M^3}{r^3}\Bigg[\frac{201}{1792}\Bigg(1+\frac{M}{r}+\frac{4474}{4221}\frac{M^2}{r^2}-\frac{2060}{469}\frac{M^3}{r^3}+\frac{1500}{469}\frac{M^4}{r^4}-\frac{2140}{201}\frac{M^5}{r^5}\\ &+\frac{9256}{201}\frac{M^6}{r^6}-\frac{5376}{67}\frac{M^7}{r^7}\Bigg)\left(3\cos^2\theta-1\right)\\ &-\frac{5}{384}\frac{M^2}{r^2}\left(1+\frac{100M}{r}+\frac{194M^2}{r^2}+\frac{2220}{7}\frac{M^3}{r^3}-\frac{1512}{5}\frac{M^4}{r^4}\right)\Bigg], \end{aligned} \tag{E.9}$$

$$\begin{aligned} g^{[2,1]}_{rr}=&\frac{M^3}{r^3f^2}\Bigg[\frac{201}{1792}f\Bigg(1+\frac{1459}{603}\frac{M}{r}+\frac{20000}{4221}\frac{M^2}{r^2}+\frac{51580}{1407}\frac{M^3}{r^3}-\frac{7580}{201}\frac{M^4}{r^4}\\ &-\frac{22492}{201}\frac{M^5}{r^5}-\frac{40320}{67}\frac{M^6}{r^6}\Bigg)\left(3\cos^2\theta-1\right)\\ &-\frac{25}{384}\frac{M}{r}\left(1+\frac{3M}{r}+\frac{322}{5}\frac{M^2}{r^2}+\frac{198}{5}\frac{M^3}{r^3}+\frac{6276}{175}\frac{M^4}{r^4}-\frac{17496}{25}\frac{M^5}{r^5}\right)\Bigg], \end{aligned} \tag{E.10}$$

$$\begin{aligned} g^{[2,1]}_{\theta\theta}=&\frac{201}{1792}\frac{M^3}{r}\Bigg(1+\frac{1420}{603}\frac{M}{r}+\frac{18908}{4221}\frac{M^2}{r^2}+\frac{1480}{603}\frac{M^3}{r^3}+\frac{22460}{1407}\frac{M^4}{r^4}\\ &+\frac{3848}{201}\frac{M^5}{r^5}+\frac{5376}{67}\frac{M^6}{r^6}\Bigg)\left(3\cos^2\theta-1\right), \end{aligned} \tag{E.11}$$

$$g^{[2,1]}_{\phi\phi}=\sin^2\theta g^{[2,1]}_{\theta\theta}. \tag{E.12}$$